REPORT DOCUMENTATION PAGE

Form Approved OMB No. 0704-0188

1. REPORT DATE *(DD-MM-YYYY)*	2. REPORT TYPE	3. DATES COVERED *(From – To)*
28-02-2001	Final Report	21 April 2000 - 23-Apr-01

4. TITLE AND SUBTITLE

Studies of intensive X, gamma and optic emissions in runaway breakdown process

5a. CONTRACT NUMBER
F61775-00-WE040

5b. GRANT NUMBER

5c. PROGRAM ELEMENT NUMBER

6. AUTHOR(S)

Dr. Alexander Viktorovich Gurevich

5d. PROJECT NUMBER

5d. TASK NUMBER

5e. WORK UNIT NUMBER

7. PERFORMING ORGANIZATION NAME(S) AND ADDRESS(ES)

P. N. Lebedev Physical Institute
Leninsky pr.,53
Moscow 117924
Russia

8. PERFORMING ORGANIZATION REPORT NUMBER

N/A

9. SPONSORING/MONITORING AGENCY NAME(S) AND ADDRESS(ES)

EOARD
PSC 802 BOX 14
FPO 09499-0014

10. SPONSOR/MONITOR'S ACRONYM(S)

11. SPONSOR/MONITOR'S REPORT NUMBER(S)
SPC 00-4040

12. DISTRIBUTION/AVAILABILITY STATEMENT

Approved for public release; distribution is unlimited.

13. SUPPLEMENTARY NOTES

14. ABSTRACT

This report results from a contract tasking P. N. Lebedev Physical Institute as follows: The contractor will investigate electromagnetic emission generated by suprathermal runaway electrons. The investigation of "runaway breakdown" will be in both atmospheric and in laboratory experiments. It has been established that runaway breakdown is accompanied by a strong optic, X and gamma ray emissions. The contractor will address the following advanced problems in this proposal: (i) Investigate runaway breakdown process in stationary electric field. (ii) Investigate runaway breakdown phenomena in laboratory installation in conditions of cyclotron resonance.
(iii) Investigate the influence of combined effects of runaway breakdown and cosmic rays on lightning processes in thunderstorm atmosphere.

15. SUBJECT TERMS
EOARD, Atmospherics, Atmospheric Emission

16. SECURITY CLASSIFICATION OF:			17. LIMITATION OF ABSTRACT	18, NUMBER OF PAGES	19a. NAME OF RESPONSIBLE PERSON
a. REPORT	b. ABSTRACT	c. THIS PAGE			David M. Burns, Lt Col, USAF
UNCLAS	UNCLAS	UNCLAS	UL	82	19b. TELEPHONE NUMBER *(Include area code)* +44 (0)20 7514 4955

Grant SPC 00-4040

Final Report

Studies of Intensive X, γ and Optic Emission in Runaway Breakdown Process

This work is driven by intersection of two lines of activities in studying of the electromagnetic emission generated by the suprathermal electrons. We have addressed the following advanced problems in the grant proposal:

1. Theoretical investigation of runaway breakdown process in stationary electric field.
2. Investigation of runaway breakdown phenomena in laboratory installation in conditions of cyclotron resonance.
3. Investigation of an influence of combined effects of runaway breakdown and cosmic rays on lightning processes in thunderstorm atmosphere.

The main new rezults obtained in this work can be summarized as follows:

1. The full kinetic theory of a new physical phenomenon, runaway breakdown, is developed. The theory takes into account both ionization and bremsstrahlung processes. The kinetic equation is fully formulated and solved. The distribution function and avalanche rate are determined. The electron–positron pairs generation is studied. The possibility to observe e^+e^- annihilation line during intensive high altitude discharges in atmosphere is predicted.
2. Kinetic theory of runaway breakdown in inhomogeneous thunderstorm electric field is develped. The main kinetic equation, boundary and initial conditions are formulated. Its solution describing the electron space distribution and energy spectrum is obtained. Spectrum of X-ray emission is calculated. It has quite a specific form: a sharp maximum at energies 50 – 60 keV and a rapid fall both to the smaller and higher energies. These results of the theory are in a good agreement with observations. The intensity of the emission is growing effectively with maximal electric field E_m and sharply falling down with the distance from the point z where $E(z)=E_m$. The strong growth of electrical conductivity in the layer ΔZ near this point is predicted.
3. The microwave electron cyclotron resonance discgarge in air is sstudied in a magnetic mirror trap. The obtained experimental data demonstrate a rapid growth of the number of fast electrons with a wide energy spectrum (1–300 keV). The discharge begins with the strong X-ray emission, followed by the syncrotron emission at second and third cyclotron harmonics. The optic emission from a low energy energy part of electron spectrum (<100 eV) has a delay up to 80 ms with respect to the X-ray emission.
4. The intensive X-ray emission during thunderstorms was studied at the height 3340 m above sea level by the specially established widely spread system of a large number (about 600) SI5G counters. For the first time the short-time (1—5 min) bursts of X-ray emission were observed. The bursts are highly correlated at the wide space region (about 0.5 km). The main component of X-ray emission in bursts has the energy 50—80 keV. The observed bursts could be attributed to the bremsstrahlung determinated by the runaway breakdown (RB) effect in the thundercloud electric field. Ground based observations of RB open a wide opportunities for the studies of fundamental processes in thunderstorms.

The following papers with the results of the investigations are published and prepared for publication:

1. Gurevich A.V., H.C. Carlson, Yu.V.Medvedev and K.P.Zybin "Generation of electron - positron pairs in runaway breakdown", Phys.Lett A **275** (2000) 101-108.
2. Sergeichev K.F., I.A.Sychov "Pecularities of ICR air breakdown in mirror magnetic trap." Prepared for publication in Radophysics.
3. Chubenko A.P., Antonova V.P., Kryukov S.Yu., Piskal V.V., Ptitsyn M.O., Shepetov A.L., Vildanova L.I., Zybin K.P., Gurevich A.V. "Intensive X-ray Emission Bursts During Thunderstorm", Phys.Lett A **275** (2000) 90-100.
4. Gurevich A.V., H.C. Carlson, Yu.V. Medvedev, K.P. Zybin "Kinetic theory of runaway breakdown in inhomogeneous thunderstorm electric field" Accepted for publication in Phys.Lett A.

1. Theoretical investigation of runaway breakdown process in stationary electric field

1.1 Abstract

The full kinetic theory of runaway breakdown for electrons at high energy range is developed. The theory takes into account both ionization and bremsstrahlung processes. The electron–positron pairs generation is studied. The possibility to observe e^+e^- annihilation line during intensive discharges in atmosphere is predicted.

1.2 Introduction

Runaway breakdown is a new phenomena determined by the effect of constant electric field at high energy ($\varepsilon \geq 100$ Kev) electrons [1]. Its physical mechanism is deeply related to the Coulomb character of neutral molecules ionization by high energy electrons: collisional crossection σ in nonrelativistic region drops rapidly with energy increase $\sigma \propto 1/\varepsilon^2$. Thus fast electrons in the presence of electric field $E > E_c$ (E_c – critical field) are able to become runaways: in other words they can be accelerated by the electric field. Accelerated electrons produce a number of low energy electrons by ionization of neutral molecules. In addition, a small number of high energy electrons may be generated. These electrons become runaways also if their energy exceeds critical value $\varepsilon_c \sim mc^2(E_c/E)$. Being accelerated, they produce another generation of fast runaway electrons and the process is ongoing, i.e. as a result an avalanche of runaway electrons starts. Exactly this process is called "runaway breakdown". It is determined by multiplication and acceleration of fast electrons. The exponential growth of the runaway electrons number characterizes the development of the avalanche and absorption of electromagnetic energy by discharge.

The kinetic theory of runaway breakdown was developed previously [2-5]. In these papers electrons with not very high energies ($\varepsilon \leq 5$ MeV) were considered. The goal of the present work to provide the full kinetic description of runaway breakdown effect for high energies also. We will demonstrate that at high energies the main role in runaway breakdown process is played not by ionization Coulomb collisions, but by much more stronger bremsstrahlung effect. The structure of electron distribution function at high energies would be determined. The role of energy distribution of initial fast electrons triggering the runaway avalanche will be examined in details. The generation of electron - positron pairs during runaway breakdown will be studied as well. It would be demonstrated, that the last process is quite effective what allows to predict the possibility to observe e^+e^- annihilation γ-line during powerfull atmospheric discharges.

1.3 Kinetic theory of runaway breakdown at high energies

At high energies to describe the runaway breakdown it is necessary in addition to ionization effect take into account bremsstrahlung processes for electrons, additional ionization by high energy photons and Compton effect for photons. To estimate the influence of all these processes let us first discuss kinetic equations for electrons and photons in a simple "τ" approximation

$$\frac{dn_{ph}}{dx} = -\frac{n_{ph}}{l_c} + \frac{n_e}{l_{br}} \qquad (1)$$

$$\frac{dn_e}{dx} = -\frac{n_e}{l_I} + \frac{n_{ph}}{l_c} \qquad (2)$$

$$\frac{1}{l_c} \approx \pi N_m r_0^2 \frac{1}{\gamma} \ln(2\gamma) \qquad \frac{1}{l_I} \approx 2\pi N_m Z r_0^2 mc^2 \ln\left[\frac{\gamma^2 (mc^2)^2}{I^2(Z)}\right] \qquad (3)$$

$$\frac{1}{l_{br}} \approx 4\pi\alpha Z^2 r_0^2 \ln(2\gamma)$$

Here n_e and n_{ph} – number densities of electrons and photons, N_m and Z – number density of molecules and full charge of their nucleas, $\alpha = e^2/\hbar c$ is a fine structure constant, $r_0 = e^2/mc^2$ – classical radius of electron. The first term in (1) describes the absorbtion of photons because of Compton effect, l_c is Compton absorption length, the second term in (1) describes the photon generation due to bremsstrahlung (l_{br} is the length of generation of photon). The first term in (2) describes the ionization of neutral moleculas by fast electrons (l_I – ionization length, $I(Z)$=13.5 Z eV), and the second one by photons.

Let us first compare the ionization and Compton terms (3). Analyzing the equations (1) and (2) it is possible to show, that in conditions

$$\gamma \ln^2(2\gamma) << (\pi/\alpha Z) \ln^2[2^{1/2} mc^2/I(Z)] \qquad (4)$$

the avalanche is determined mostly by ionization process. In this work condition (4) is supposed to be fulfilled always.

The full kinetic equation describing the runaway breakdown process takes inconditions

(4) the following form [6].

$$\frac{\partial f}{\partial t} = \mathrm{e}\,\mathrm{E}\left\{\mu\frac{\partial f}{\partial p} + \frac{1-\mu^2}{p}\frac{\partial f}{\partial \mu}\right\} = St(f) + S_I(f)$$

$$St(f) = \frac{1}{p^2}\frac{\partial}{\partial p}\left(p^2\left(F_D + F_{br}\right)f(p,\mu)\right) + \upsilon(p)\frac{\partial}{\partial \mu}\left[\left(1-\mu^2\right)\frac{\partial f(p,\mu)}{\partial \mu}\right] \qquad (5)$$

$$\mathrm{F_D} = \frac{4\pi Z e^4 N_m}{mc^2}\frac{\gamma^2}{\gamma^2 - 1}a \qquad \upsilon(p) = \mathrm{F_D}\frac{\xi}{4\gamma p} \qquad \xi = \sum_{i=1}\frac{Z_i^2}{Z} \qquad a \approx 11$$

$$S_I = N_m v \frac{2\pi Z c^4}{mc^2}\int_{\varepsilon}^{\infty}\frac{\gamma'^2}{\gamma^2 - 1}\left[\frac{1}{\varepsilon^2} + \frac{1}{\left(W + mc^2\right)^2}\right]\int\frac{d\phi}{2\pi}\int f(W,\mu',\phi)\delta(\mu_1 - \mu_0)d\mu_1 dW$$

$$\mu' = \frac{\mu\mu_1 \pm (1-\mu_1^2)^{1/2}\sin\phi\sqrt{\mu_1^2 - \mu^2 + (1-\mu_1^2)\sin^2\phi}}{\mu_1^2 + (1-\mu_1^2)\sin^2\phi}$$

$$\mu_0 = \left[\varepsilon(W + 2mc^2)/W(\varepsilon + 2mc^2)\right]^{1/2}$$

Here $f(p,\mu,t)$ is the electron distribution function, p – electron momentum, E – electric field, $\mu = (\boldsymbol{E}\,\boldsymbol{p})/(E\,p)$ – cosine of pitch angle. The integral St describes collision of fast electrons with atomic electrons and nucleus. F_D and F_{br} is friction forces of electron determining energy losses due to ionization and bremsstrahlung:

$$F_{br} = \left\langle \frac{d\varepsilon}{dt} \right\rangle = -4\alpha N_m Z_i^2 \frac{e^4}{m^2 c^4} \varepsilon v \{\ln(2\gamma) - 1/3\} \qquad (6)$$

Here Z_i is nucleus charge.

The second term in (5) describes pitch angle scattering of runaway electrons. Term S_I describes appearance of a new born runaway electrons, γ – Lorentz factor of electron, ε and W – kinetic energy of fast electron $\varepsilon = mc^2(\gamma - 1)$, $W = mc^2(\gamma - 1)$.

At Fig.1.1 the full friction force is demonstrated. One can see, that the ionization plays the main role at low energies $\varepsilon \leq 5$ MeV. At $\varepsilon \geq 5$ MeV the dominant role belongs to bremsstrahlung force. The basic relation of the theory which determines the runaway boundaries $eE = F$ now has two roots. The first root $\gamma = \gamma_1$ determines as usual critical electron energy ε_c [1]. The runaway region lays between γ_1 and γ_2 . The second root is determined mainly by bremsstrahlung force. The runaway boundaries energies $\varepsilon_c = mc^2(\gamma_1 - 1)$ and $\varepsilon_{c2} = mc^2(\gamma_2 - 1)$ depend on relation E/E_c

$$\varepsilon_c \approx mc^2 \frac{E_c}{E} \qquad \varepsilon_{c2} \approx mc^2 \frac{\pi a}{\alpha Z_i \ln(2\gamma_2)} \frac{E}{E_c} \qquad E > E_c \qquad (7)$$

where

$$E_c = \frac{F_{\min}}{e} = \frac{4\pi Z_i e^3}{mc^2} a \qquad (8)$$

F_{min} is the minimal drag force of electrons [1]. One can see from (7), that the width of runaway region

$$\Delta\varepsilon_r = \varepsilon_{c2} - \varepsilon_c \approx \varepsilon_{c2} \approx mc^2 \frac{\pi a}{\alpha Z_i \ln(2\gamma_2)} \frac{E}{E_c}$$

The highest energy ε_{c2} which can be reached by runaway electron is growing with E/E_c approximately linearly: at $E/E_c = 5$ it reaches the value *430 MeV*, *at* $E/E_c = 10$ – the value *850 MeV*. This values are fully determined by bremsstrahlung force. We note, that in previous papers the term (6) was omitted. It means that kinetic theory was considered in [1] for low energy diapason $\varepsilon << \varepsilon_{c2}$ only.

Analyzing collision integral we see that pitch angle scattering due to relativistic growth of electron mass with energy increase falls down more efficient than drag force. So, it could be neglected if conditions

$$\frac{\xi}{4\gamma} << 1 \qquad (9)$$

are fulfilled. At such conditions pitch angle scattering is not significant and due to this the distribution function becomes strongly directed along electric field (see [7]). Thus one can consider one dimensional – integrated over angles distribution function.

$$f_0(\gamma) = \frac{1}{2} \int_{-1}^{1} f(\gamma, \mu) d\mu$$

Introducing dimensionless variables γt^*,

$$\gamma = \sqrt{\left(\frac{p}{mc}\right)^2 + 1}, \qquad t^* = \frac{t}{t_0}, \qquad t_0 = \frac{m^2 c^3}{4\pi e^4 Z N_m a} \qquad (10)$$

we finaly obtain:

$$\frac{\partial}{\partial\gamma}\left\{\left[\left(\gamma^2-1\right)\left(\phi_D+\kappa_{br}\right)-\delta_E\right]f_0\right\}=\gamma\sqrt{\gamma^2-1}\frac{\partial f_0}{\partial t}-S_I(f_0) \qquad (11)$$

$$\phi_D=\frac{1}{a}\frac{\gamma^2}{\gamma^2-1}\left[8.4+\frac{1}{2}\ln(\gamma^2-1)+\frac{1}{2}\ln(\gamma-1)-0.347\left(\frac{2}{\gamma}-\frac{1}{\gamma^2}\right)+\frac{1}{2\gamma^2}+\frac{(\gamma-1)^2}{16\gamma^2}\right]$$

Here $\delta_E=E/E_c$ is electric field parameter, function φ_D:
determines dimensionless ionization losses and:

$$\kappa_{br}=\frac{\alpha Z\gamma}{\pi a}\left(\ln(2\gamma)-\frac{1}{3}\right)$$

– bremsstrahlung losses.
The ionization term takes a simple form:

$$S_I=N_m v\frac{2\pi Ze^4}{mc^2}\int_{\varepsilon}^{\infty}\frac{\gamma'^2}{\gamma^2-1}\left\{\frac{1}{\varepsilon^2}+\frac{1}{\left(W+mc^2\right)^2}\right\}f_0(W)dW \qquad (12)$$

Thus in a high energy range due to relativistic growth of the electron mass its scattering by atomic neucleus is weak enough and the distribution function of energetic electrons became strongly alongated along electric field. It allows to use kinetic equation in a more simple form (11), (12).

1.4 Time development of distribution function

The threshold field for runaway breakdown E_c is usually much less than for conventional breakdown E_t. As an example for air and for hydogenium $E_c/E_{th} \sim 0.1$. On the other hand to excite runaway breakdown one needs fast electrons with energies $\varepsilon > \varepsilon_c$. That determines an important difference between runaway and conventional breakdown. How the time development of distribution function depends on the existance of fast electrons or more generally on initial function $f_0(\gamma)$? The problem was studied numerically. The numerical soutions were obtained in runaway region ($\gamma < \gamma_{c2}$) by predictor – corrector and Crank – Nickolson methods with boundary condition $f(\gamma_{c2})=0$. Both methods demonstrates identical results. To determine the dependance of runaway process on the energy of seed electrons the initial function $f_0(\gamma)$ was taken usually close to delta function $f_0(\gamma) \propto \delta(\gamma-\gamma^*)$.

Results of numerical calculations of equation (11) are demonstrated at the Fig.1.2 – Fig.1.5. We see from Fig.1.2, that at $\gamma^* < \gamma_1$ (or $\varepsilon^* < \varepsilon$) independing on the value of electric field ($E > E_c$), the initial distribution function dissapears in time and initial number density of electrons N_e falls down exponentially. So, without seed fast electrons runaway breakdown does not exist.

On the contrary, if $\gamma^* > \gamma_1$ the runaway breakdown is effectively developing. Its main features seen from Fig.1.3: independently on the value γ^* the distribution function at low energies develops very fast to its quasistationary state

$$f(\gamma,t)=F_0(\gamma)\, e^{\lambda t} \qquad (13)$$

The typical time of this process

$$t_1 \sim \lambda^{-1} \qquad (14)$$

At the high energy range ($\gamma \geq \gamma^*$) the establishing of quasistationary solution is much more slow and takes time

$$t_2 \sim (\gamma_2-\gamma^*)/(\delta_E-1) \qquad \delta_E > 1.2 \qquad (15)$$

Note that the time t_2 is diminishing with the growth of γ^* and at $\gamma^* \geq \gamma_2$ its became an order of t_1.

The established asympthotic solution takes the exponential form (13) quite analogous to the conventional breakdown. It is natural, because runaway breakdown is described by linear equation. Stationary asympthotic distribution function $F_0(\gamma)$ is shown at Fig.1.4. for different values of parameter δ_E. One can see, that function F_0 falls down monotonically with γ, sharply increasing at small energies $\varepsilon = mc^2(\gamma-1)$ and disappearing at the second runaway boundary $F_0(\gamma_2) = 0$. The behaviour of asympthotic solution F_0 could be studied analytically. The analytical analysis of equation (5) shows that ionization integral and friction term are most essential at small energies. The balance of these terms gives asymptotics at $\varepsilon \to 0$

$$f \propto \varepsilon^{-1+1/a}.$$

In intermediate energy range $\gamma_1 << \gamma << \gamma_2$ the distribution function falls down exponentially

$$f \propto \exp\left\{-\frac{\lambda}{\delta_E}u\right\} \qquad u = \sqrt{1-\frac{1}{\gamma^2}}$$

To determine cutoff the distribution function near right stationary point γ_2 we can neglect the ionization term. Expanding friction force near this point we can find the solution

$$f \propto \left(1-\frac{q}{\delta_E}\mu p\right)^{\frac{\lambda}{q}-3} \qquad 1-\frac{q}{\delta_E}\mu p > 0 \qquad p = mc\gamma$$

Here $q = \left.\frac{dF_D}{d\gamma}\right|_{\gamma=\gamma_2}$. These results are in agreement with numerical simulation.

1.5 The avalanche rate

One of the most important parameter of breakdown is the avalanche rate. The increasing of number density of electrons N(t) is shown for different beam energies γ^* at Fig.1.5. We see that the asympthotic solution demonstrates exponential growth with parameter λ:

$$N(t) = N_0 e^{\lambda t}$$

We investigated the dependence of avalanche rate λ on dimensionless electric field δ . The results are shown at Fig.1.6. For high enough values of δ this behavior is well fitted by the law:

$$\lambda = 0.064\ \delta^{3/2} \qquad (16)$$

Note that as seen from Fig.1.5. the asympthotic time behaviour of electron density does not depend on on the initial distribution function (if $\gamma^* > \gamma_c$) in agreement with (13). Some small difference in $N(t)$ is seen in the begining of the process at time scale of the order of t_1 (14). We see, that the full time of establishment of distribution function (15) is not significant — electron density growth is going with the same avalanche rate from the very begining. It means that the avalanche process practically does not depend on the established distribution function $F_0(\gamma)$ in the whole breakdown region. The dominant role is played by its initial part in the vicinity of the left stationary point — the first root γ_1. In

other words, only the region near critical energy ε_c determines the avalanche rate. This fact is in agreement with qualitative theory [1].

Basing on this analysis we can estimate analytically the avalanche rate. Really, near left stationary point it is possible to consider nonrelativistic approximation. In this approximation the kinetic equation (5) is reduced to the form:

$$\frac{\partial f_0}{\partial t} = \delta_E \frac{1}{u^2}\frac{\partial}{\partial u}\left(u^2 f_0\right) = \frac{1}{u^2}\frac{\partial f}{\partial u} + \frac{1}{au^5}\int_u^\infty f_0(w)wdw, \qquad w = \sqrt{1-\frac{1}{\gamma^2}} \tag{17}$$

There is an important property of the equation (17) – it allower to eliminate the electric field δ_E. Introducing variables

$$\tau = 2t\delta_E^{3/2}, \qquad v = u\sqrt{\delta_E}$$

one can find

$$\frac{\partial f_0}{\partial \tau} + \frac{1}{v^2}\frac{\partial}{\partial v}\left(v^2 f_0\right) = \frac{1}{v^2}\frac{\partial f}{\partial v} + \frac{1}{av^5}\int_v^\infty f_0(w)wdw \tag{18}$$

Searching exponential solution of equation (18) $f_0 = fe^{2\tau\sigma/a}$ we reduce it to the form:

$$(1-y)\Phi'' - \left(\frac{\sigma}{a}\sqrt{y}+1\right)\Phi' - \frac{\Phi}{4ay^2} = 0 \tag{19}$$

Here $\Phi = \int_u^\infty f(w)wdw$, and variable $y = v^2 = u^2\delta_E$.

Note, that parameter a determined by (5) could be cosidered in equation (19) as a large parameter. For $a \to \infty$ we have from (19)

$$(1-y)\Phi'' - \Phi' = 0 \qquad \Phi = C_0\ln(y-1) + C_1$$

This solution is not valid for $y \to \infty$ and $y \to 1$. To match this solution let us return to the finite big values of parameter a and use an expanding variables introducing z as $y = a^2 z$.
The equation (19) takes the form:

$$\frac{1}{a^2}(1-a^2 z)\Phi_{zz} - (\sigma\sqrt{z}+1)\Phi_z - \frac{\Phi}{4a^3z^2} = 0$$

For $a \to \infty$ its solution is

$$\Phi_z = A_0\frac{e^{-2\sigma z}}{z}$$

Using a procedure of matching solution [8] we find "combined" solution which is good with exponential accuracy everywhere except the vicinity of point $y=1$:

$$\Phi_y = \frac{e^{-2\sigma\sqrt{y}/a}}{y-1} \tag{20}$$

In the vicinity of $y=1$, introducing x: $y = 1 + x\,a^{-1}$ we find the solution

$$\Phi = e^{-\frac{x}{4}}$$

It means that solution (20) is cut at $u_*^2 = 1 + 4/a$. As we shall see below this cutting defines the avalanche rate with logarithmic accuracy. Integrating (18) from u_* to ∞, one can find:

$$\sigma\ln\left(\frac{a^3}{16\sigma^2}\right) = \frac{1}{2}\ln\left[\frac{a}{2}\left(1+\frac{2}{a}+\sqrt{1+\frac{4}{a}}\right)\right] + \left(1+\frac{4}{a}\right)^{-\frac{1}{2}} + O\left(\sigma/a\right) \tag{21}$$

This algebraic equation defines parameter $\lambda=2\sigma\delta^{3/2}/a$. For $a=11$ the solution of (21) gives

$$\lambda \approx 0.055\ \delta^{3/2}$$

This result is in a good agreement with numerical calculations (16). More than that it is in agreement with previous numerical solution of kinetic equation in the low energy limit [2-5] and with approximate qualitative theory [1]. The reason of this agreement is in the fact that main role in ranaway breakdown process plays the low energy runaway boundary ε_c.

1.6 e^+ e^- generation

The distribution function of runaway electrons falls down rather slow (see(20)). It means that fast electrons generates intensive flux of X and γ photons due to bremsstrahlung process. The high energy photons can generate electron - positron pairs.

The process of X and γ generation by fast electrons in neutral gas is well known. The total number of photons could be estimated using emissivity q_γ [9]

$$\frac{dN_\gamma}{dt}=\frac{q_\gamma}{\varepsilon}cN_mN_\varepsilon \qquad q_\gamma \approx 4Z^2\alpha r_0\varepsilon$$

Here N_e – the number density of fast electrons which generate bremsstrahlung emission and N_m – density of neutrals.

The crossection of $e^\pm$ generation is quite analogous to Bethe and Heitler bremsstrahlung crossection [9]

$$d\sigma=-\frac{Z^2\alpha r_0}{2\pi}\frac{m^2p_+p_-d\varepsilon}{\omega^3q^4}\sin\theta_+d\theta_+\sin\theta_-d\theta_-d\phi\times D \qquad (22)$$

$$D=\frac{p_+^2}{\kappa_+^2}(4\varepsilon_-^2-q^2)\sin\theta_+ +\frac{p_-^2}{\kappa_-^2}(4\varepsilon_+^2-q^2)\sin\theta_- -\frac{2\omega^2}{\kappa_+\kappa_-}(p_+^2\sin^2\theta_+ + p_-^2\sin^2\theta_-)-$$

$$-\frac{2p_+p_-}{\kappa_+\kappa_-}(2\varepsilon_+^2+2\varepsilon_-^2q^2)\sin\theta_+\sin\theta_-\cos\phi$$

Here

$$\kappa_\pm=\varepsilon_\pm-p_\pm\cos\theta_\pm, \qquad q^2=(\boldsymbol{p}_+ +\boldsymbol{p}_- -\boldsymbol{k})^2, \qquad \varepsilon_+ +\varepsilon_-=\omega$$

Integrating this crossection we can estimate the $e^\pm$ production

$$\frac{dN_{e\pm}}{dt}=\sigma_\pm cN_mN_\gamma \qquad \sigma_\pm \approx \frac{22}{9}Z^2\alpha r_0$$

Taking into account that N_e grows exponentially with t, we find:

$$\frac{N_{e\pm}}{N_\gamma}\approx\frac{7}{9}\frac{N_\gamma}{N_e} \qquad (23)$$

This relation determines the number of generated e^+e^- pairs.

To estimate the emission intensity of the e^+e^- annihilation line intensity generated during thunderstorm it is natural to compare with the results of observations γ - burst from high altitude lightning at "Compton" observatory. According to Fishman et al [10] and Nemiroff et al. [11] the flux of gamma quants in energy diapason 300 ÷ 1000 KeV observed by BATSE at the heights 500 km was of the order of 100 photons/cm^{2}s. Using relation (23) and taking into account that $N_\gamma/N_e \sim \alpha \sim 10^{-2}$ one can estimate the flux of photons from e^+e^- annihilation at the distance 100 km from the source as 20 photons/cm^{2}s. Taking into account that the width of unihilation line is narrow one can suppose that the γ-quants generated during thunderstorm could be detected in experiments.

1.7 References

[1] A.V.Gurevich, G.M.Milikh and R.Roussel-Dupre Phys.Lett.A **165** (1992), 463 – 468.

[2] R.A.Roussel - Dupre, A.V.Gurevich, T. Tunnell, G.M.Milikh Phys.Rev.E **v.49**, N3, 1994 (2257 – 2271)

[3] N.G.Lehtinen, T.E.Bell V.P.Pasko, U.S. Inan GRL **24**, 2639, 1997

[4] L.P.Babich, I.M.Kutsyk, E.N.Donskoy, A.Yu.Kondratiev Phys.Lett.A **245**, 460, 1998

[5] E.Symbalisty, R.Roussel - Dupre, L.Babich, I.Kutsyk, E.Donskoy, A.Kudryavtsev EOS Trans. AGU, **46**, 4760, 1997

[6] A.V.Gurevich R.A.Roussel - Dupré and K.P.Zybin Phys.Lett.A Phys.Lett.A **237**, 240, 1998.

[7] A.V.Gurevich Sov.Phys. JETP **12**, 904, 1961.

[8] A.H.Najfe Introduction to Perturbation Techniques, Wiley-Interscience Publication NY 1980.

[9] L.D.Landau, E.M.Lifshits Quantum Electrodynamics Moscow Nauka 1980.

[10] J.Fishman et al. Science, **264**, 1313,1994.

[11] J.Nemiroff, J.Bounell, J.Norris JGR, **102**, 9659, 1997.

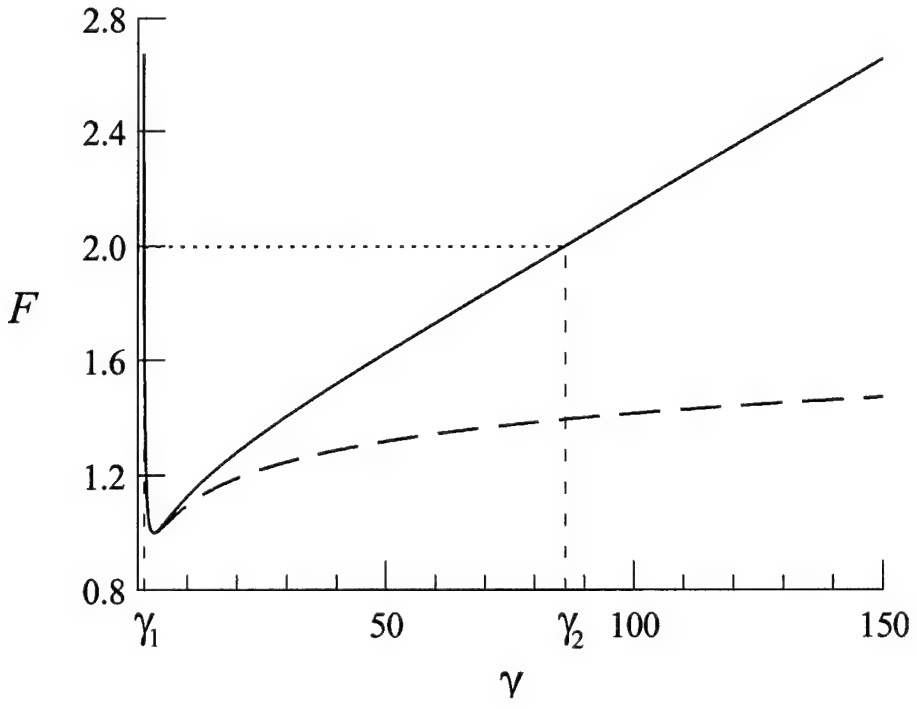

Figure 1.1 Dependence of the full friction force F on γ (solid curve). The dashed curev presents the friction force without accounting bremsstrahlung.

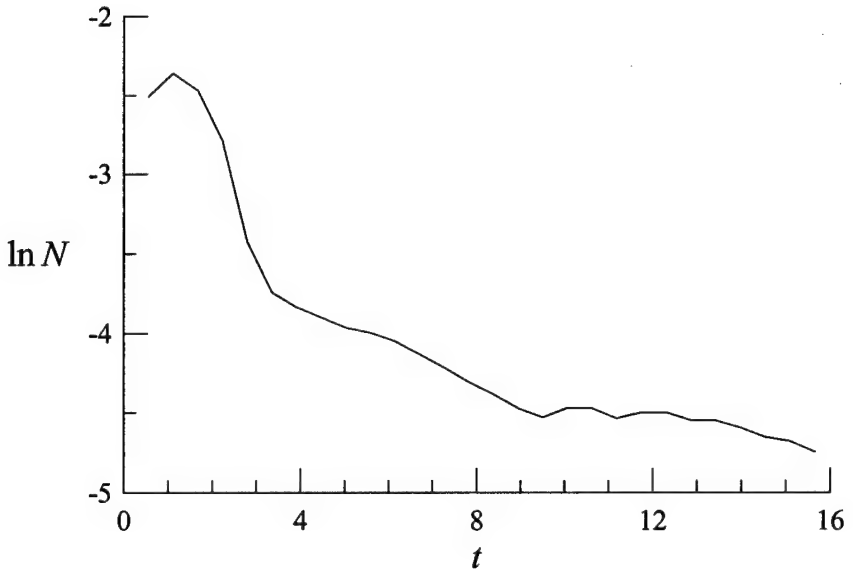

Figure 1.2 Logarithm of the full number of electrons N as a function of time in the case of $\gamma_b<\gamma_1$.

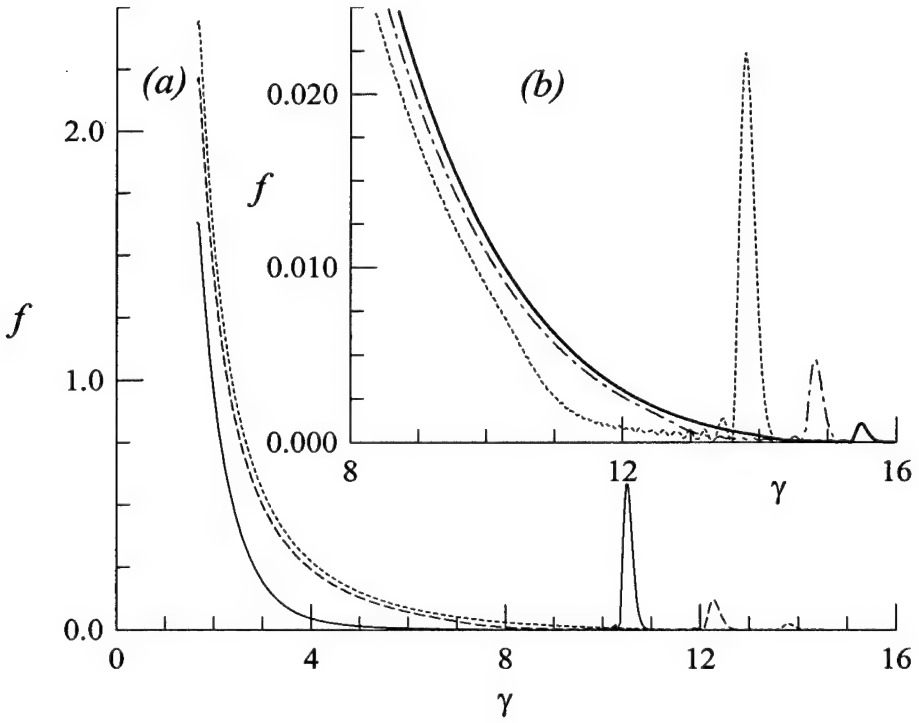

Figure 1.3 Distribution function $f(\gamma)$ at t=5.6 (solid), 28 (dashed), 56 (dotted), 84 (dot-dashed) and 112 (double solid) in the case of γ_b=10, δ=1.21.

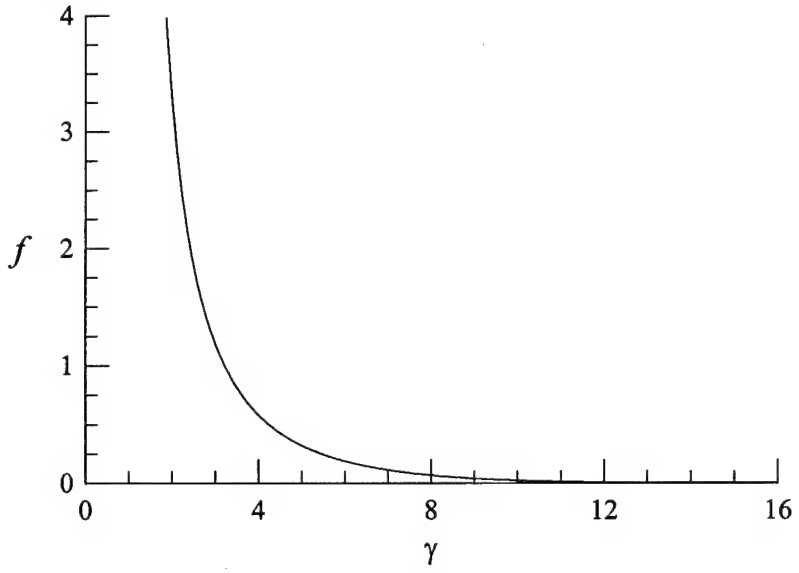

Figure 1.4 Stationary distibution function $f(\gamma)\exp(-\lambda t)$.

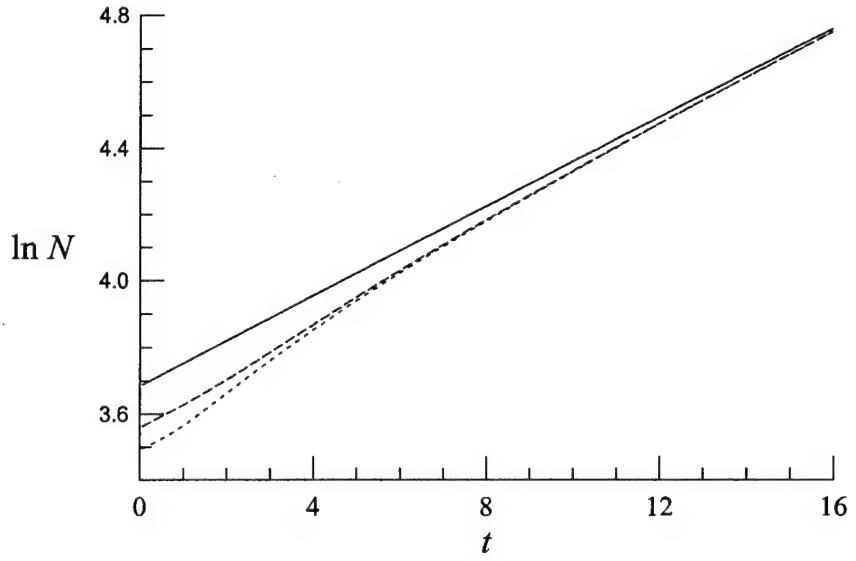

Figure 1.5 Logarithm of the full number of electrons N as a function of time for different positions of the beam of seed electrons $\gamma_b = 5$ (dotted), 10 (dashed) and 15 (solid)

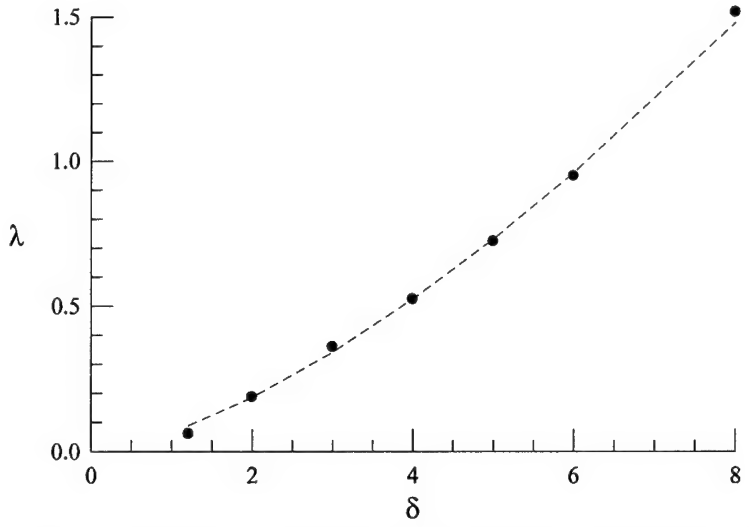

Figure 1.6 Dependence of λ on δ (symbols) in comparision with the fitting curve $\lambda=0.0654\delta^{3/2}$ (dashed curve)

2. Kinetic theory of runaway breakdown in inhomogeneous thundercloud electric field

2.1 Introduction

Multiple observations at balloons and airplanes of electric field and X-ray emission inside thunderclouds revealed a definite agreement with the predictions of runaway breakdown (RB) theory [1]:

1. Maximal values of observed in thunderclouds electric field $|E|_m$ are close to RB critical field E_c [1,2],

$$E_c \approx 200 \frac{N_m(z)}{N_m(0)} \ \frac{\text{kV}}{\text{m}} \qquad (1)$$

Here $N_m(0)$ the density of molecules at the sea level ($N_m(0)=2.7\times 10^{19}\ cm^{-3}$), and $N_m(z)$ – the same density at the given height z.

2. The observed values of $|E_m|$ fall down exponentially with the height z in accordance with formulae (1) [2,3].

3. The definite correlation of lightning activity with the regions, where electric field $|E|$ is close to E_c is seen [3].

4. At the same region X-ray bursts – strong increase of X-ray emission during one minute time intervals are observed [4-6].

Note that the structure of electric fields in thunderstorm atmosphere is strongly inhomogeneous. The thunderclouds have a layered structures [3] what means, that the main field inhomogeniety is always along the height z

$$E=E(z)$$

It is of importance, that not only the value of electric field $|E(z)| \sim E_c$, but the scale of field ingomogeniety L affect strongly the RB process – L should be much larger than the runaway avalanche length l_a

$$L >> l_a \qquad (2)$$

l_a is of the order 70 – 100 m inside thunderclouds and condition (2) is usually fulfilled there. The goal of the present paper is to develop a kinetic theory of RB in inhomogeneous thunderstorm electric field. The main kinetic equation, boundary and initial conditions are formulated in section 2. Its solution, presented in section 3 describes the electron space distribution and energy spectrum. Spectrum of X-ray emission is calculated in section 4. It has quite a specific form: a sharp maximum at energies 50 – 60 keV and a rapid fall both to the smaller and higher energies. The intensity of the emission is growing effectively with parameter E_m/E_c and falling down sharply with the distance near the point z where $E(z)=E_c$. Note that the role of thunderstorm cloud inhomogeniety was discussed in a simplified form previously in [7-9]

2.2 Kinetic equation in inhomogeneous electric field

Fast electrons generated during RB process in nonuniform electric field at stationary conditions ($\partial/\partial t = 0$) are described by kinetic equation [10]:

$$v\mu\frac{\partial f}{\partial z}+\frac{e}{m}E(z)\left\{\mu\frac{\partial f}{\partial \mathrm{v}}+\frac{(1-\mu^2)}{\mathrm{v}}\frac{\partial f}{\partial \mu}\right\}=\frac{1}{\mathrm{v}^2}\frac{\partial}{\partial \mathrm{v}}\left(\mathrm{v}^2F_D f\right) \qquad (3)$$

$$\frac{\nu_\mu}{\mathrm{v}^3}\frac{\partial}{\partial\mu}\left\{(1-\mu^2)\frac{\partial f}{\partial\mu}\right\}+S_I$$

Here $f=f(v,\mu,z)$ – is the electron distribution function, μ – is a cosine of an angle between direction of electric field **E** and velocity **v**, F_D – friction force due to ionization,

$$F_D=\frac{Q\Lambda}{\mathrm{v}^2} \qquad Q=4\pi N_m Z\left(\frac{\mathrm{e}^2}{m}\right)^2$$

Λ – Bethe's logarithm, ν_μ is angle frequency scattering parameter

$$\nu_\mu=Q\Lambda\xi \qquad \xi=\sum_{i=1}\frac{Z_i^2}{4Z}$$

where ξ– effective charge of molecules, Z_i – the charge of every moleculae component: $Z=\sum_i Z_i$.

The term S_I is ionization integral [11]. Concrete form of S_I will be presented later.

Electric field in a real atmospheric conditions increase inside thunderstorm cloud up to maximum value E_m and then decrease. In our calculations we choose it in a parabolic form:

$$E(z)=E_m\left(1-\frac{z^2}{L^2}\right) \qquad -L<z<L \qquad (4)$$

Here L is a scale of thunderstorm electric field.

According to the theory of runaway breakdown process the distribution function of fast electrons could be considered approximately as strongly directed along electric field [10]. Integrating (3) over pitch angles $d\mu$ we find a kinetic equation for distribution function $f(\gamma,z)$ of fast electrons

$$(\gamma^2-1)\frac{\partial f}{\partial z}=\frac{\partial f}{\partial\gamma}\left\{(\gamma^2-1)[\Phi_D(\gamma)-E(z)]f\right\}+S_I+q_{sr}(\gamma) \qquad (4)$$

where Φ_D is normalized relativistic friction force [10], $E(z)=\delta(1-a_l^2z^2)$ – electric field normalized on critical electric field $\delta = E_m/E_c$. Height z – normalized on ionization length l_a and parameter $a_l=l_a/L$, $q_{cr}(\gamma)$ is the source of cosmic ray secondaries generated at the given height z in atmosphere by the flux of cosmic rays [12].

Ionization integral according to [10,11] is determined by formulae:

$$S_I=\frac{1}{2}\int_1^\infty y^2 f(y,z)\left[\frac{1}{(\gamma-1)^2}+\frac{1}{y^2}\right]dy \qquad (5)$$

To solve the equation (5), (6) it is necessary to formulate initial and boundary conditions for distribution function. As is well known runaway breakdown take place in the presence of seed energetic electrons only. In the thunderclouds the role of seed fast electrons is played by the cosmic ray secondaries. So, the initial function $f_0(\gamma)$ is the energy distribution of cosmic rays secondaries. It is determined by solution of equation (\ref{fgam}) in the absence of the z – transport term ($\partial f/\partial z$) and electric field $E(z)$. The same function $f_0(\gamma)$ determines the boundary condition at the initial point $z=a_l^{-1}$. The natural boundary condition in energy space is $f(\gamma)\to 0$, if $\gamma\to\infty$.

Below we will describe the results of solution of equation (5), (6) for the given initial and boundary conditions.

2.3 Distribution function of electrons

The solution of equation (5),(6) was studied analytically and numerically. The results are presented at Fig.2.1 – Fig.2.4. At Fig. 2.1 the dependence of distribution function $f(\gamma)$ on the height z is demonstrated. One can see that the growth of electric field $E(z)$ is accompanied by the significant growth of distribution function $f(\gamma)$. It reaches maximal value at z=2.5 and after that f begin to diminish with z. The dependence F on γ at γ<2 is quite well described by analytical formulas [10]. The dependence of distribution function on maximum electric field E_m is shown at Fig. 2.2. The avalanche type growth of f and acceleration of electrons at $E_m/E_c>1$ is seen. The same avalanche process is demonstrated at Fig.2.3 for the number density N of runaway electrons. Note that at E=0 the number density N_0 describes the background cosmic ray secondaries. To eliminate this background which is not connected with RB process we normalized N on N_0. At $E_m>E_c$ an avalanche growth of N with z is clearly seen. Its sharp cut off coincides with the points z where $E(z)$ becomes less than E_c. The growth of the maximal avalanche value N_{max} on E_m/E_c shown at Fig. 2.4 is of a sharp exponential form. In the same time the point z_{max}, where $N(z)$ reaches its maximum value, moves in z direction with E_m/E_c rather smoothly, reaching for example z=2.6 l_a at E_m/E_c =1.2 (Fig. 2.4).

2.4 X-ray emission: energy spectrum and space distribution

High energy electrons passing through the neutral gas generate X-rays due to bremsstrahlung process. The bremsstrahlung intensity and spectra is determined by electron distribution function $f(\varepsilon, z)$:

$$J_\nu = N_m \int \sigma_\nu(\varepsilon) v f(\varepsilon, z) d\varepsilon = \sigma_b N_m j_\nu \qquad (7)$$

where v is the velocity of electrons, $\sigma_\nu(\varepsilon)$ the cross-section of the production of photons in the frequency range $d\nu$ by incident electron of energy ε and σ_b=16/3·$Z^2\alpha$ a_0^2, $a_0=e^2/mc^2$. Using expression for cross-section [13], one can find flux of photons j_ν:

$$j_\nu = \frac{1}{\nu}\int_1^\infty \gamma^2 \ln\left\{\frac{\sqrt{\gamma^2-1}+\sqrt{\gamma^2-1-2\nu\gamma^2}}{\sqrt{\gamma^2-1}-\sqrt{\gamma^2-1-2\nu\gamma^2}}\right\} f(\gamma, z) d\gamma \qquad \nu = \frac{\varepsilon_\nu}{mc^2} \qquad (8)$$

The expression (7) describes the source of bremsstrahlung photons at given point z. The dependence of the flux j_ν on the energy of X - ray quants ε_ν for distribution function $f(\gamma, z)$ at E_m/E_c=1.05 is shown on Fig. 2.5 for different space positions z. One can see from the figure that flux j_ν as a function z is initially growing with z, but at z=1.375 reaches maximal value and then falls down. All the changes of j_ν are fully determined by distribution function of runaway electrons and its dependence on the electric field $E(z)$.

The bremsstrahlung photons propagating through the neutral gas loose their energy due to Compton effect and disappear due to photoionization. The kinetic equation for photon distribution function $I(\nu,z)$, describing these processes could be presented in a form:

$$\frac{cl_T}{3l_a^2}\frac{\partial^2 I}{\partial z^2} + \frac{c}{l_T}\frac{\partial}{\partial \nu}\left(\nu^2 I\right) - c\sigma_{ph} I + J_\nu = 0 \qquad (9)$$

Here z is as previously normalized on the ionization length l_a determined by RB process, $l_T=1/N_e\sigma_T$ is Thompson scattering length, and σ_{ph}– photoionization cross-section.

The solution of diffusion equation (9) with the source (7), (8) is

$$I(\nu,z) = \frac{l_T}{c\sqrt{2\pi D}}\int_\nu^\infty \frac{d\nu_0}{\nu^2}\int_{-\infty}^{\infty} dz_0 \sqrt{\frac{\nu_0\nu}{\nu_0-\nu}}\exp\left\{-\frac{\nu_0\nu(z-z_0)^2}{4D(\nu_0-\nu)} - \frac{2\sigma_0}{9\sigma_T}\left(\nu_0^{-3/2}-\nu^{-3/2}\right)\right\} J_{\nu_0}(z_0) \qquad (10)$$

Here $D= l_T^2/3l_a^2$ and we take into account that for a considered energy range ε_ν> 20keV the photoionization crossection could be chosen in a form [15]:

$$\sigma_{ph} = 2^8 \frac{\pi}{3} \alpha a_0^2 Z^5 \left(\frac{\varepsilon_0}{mc^2} \right)^{7/2} \nu^{7/2} = \sigma_0 \nu^{-7/2}$$

Here as usually $\alpha = e^2/c = 1/137$ and $a_0 = e^2/mc^2$.

The solution (10) is shown on Fig. 2.6, 2.7 for various spatial locations z. At Fig. 2.6 the spectrum of X-ray emission I(ν) for various values z is presented. One can see, that the spectrum has very stable form, practically not depending on position z. It always has the distinct maximum at the energies $\varepsilon_\nu \approx 50 - 60$ keV and rapidly falls down both to the smaller (due to photoionization) and higher (due to Compton losses) values of ε_ν. Note that this result practically does not depend on the value of maximal electric field E_m. From the Fig. 2.7 it is seen that the maximal intensity I_{max} of emission is growing exponentially with electric field E_m. The position of emission maximum z_{max} is moving slowly in the direction of electron motion.

The obtained results are in a very good agreement with all observations of X-ray spectrum during thunderstorm at airplanes [4], balloons [5,6] and in the mountains experiments [6]. The observations always show a clear maximum at the energies ~ 60KeV and rapid fall of the spectrum both to 30 KeV and 100 KeV. One can conclude from the comparison with the present theory that in all these experiments the runaway avalanche effect inside thundercloud was observed.

We note also, that the effective growth of the number of runaway electrons at $E_m/E_c \sim 1 \div 1.2$ demonstrated at Fig. 2.3 lead to a much stronger growth of the number of low energy electrons due to ionization of air molecules. These electrons rapidly loose through collisions with molecules their energy and become thermal one [15]. Due to attachment of the thermal electrons to molecules O_2 and H_2O in a 100 ns time scale the plasma of positive and negative ions is formed. The ion density in this plasma layer is growing very effectively due to runaway breakdown process and in a time scale of the order 10 s a highly conducting layer could be generated. The creation of this layer can affect significantly the distribution of the electric charge and lead to destabilization of thunderstorm cloud which manifests itself eneration of lightning. The process of generation highly conducting region due to runaway breakdown was discussed in details in the previous papers [1,7,8].

2.5 Conclusion

Presented here theoretical study of runaway breakdown process in inhomogeneous thundercloud electric field has revealed two significant features of X-ray emission generated by runaway electrons:

1. The emission spectrum has well defined maximum located at $\varepsilon_\nu \approx 50 \div 60$KeV. The spectrum falls down rapidly both to the low energies ($\varepsilon_\nu \sim 30$)KeV and to the higher energies ($\varepsilon_\nu \sim 100 \div 150$KeV). This statement practically does not depend on z position, where the spectrum is observed.

2. The intensity of X- ray emission is diminished effectively with the distance from z_{max} – position of electric field maximum $E_m = E(z_{max})$, where runaway breakdown conditions are fulfilled $E_m \rho E_c(z_{max})$. At the distance about 1 km from z_{max} the maximal intensity of emission falls down more than an order of magnitude. Taking into account, that according to multiple observations of the thunderstorm electric field z_{max} is located at the heights 4 kmβ z_{max} β 8 km [2,3], we deduce, that the X-ray emission generated by runaway avalanche could be observed at the heights z ρ 3km only.

Both these statements are in agreement with the existing observations [4]-[6], [16,17]. They can serve to a definite indication for searching of runaway breakdown effect in the thunderstorm atmosphere.

2.6 References

[1] A.V.Gurevich, G.M.Milikh, R.A.Roussel-Dupre Phys.Lett. **A165**, 463, (1992).
[2] T.Marshall, M.McCarty, W.Rust JGR **100**, 7097 (1996)
[3] D.R.MacGormann, W.D.Rust The Electric Nature of Storms, Oxford Univ. Press, N.Y. 1998
[4] M.McCarthy, G.Parks GRL **12**, 383, (1985)
[5] K.B.Eack, W.H.Beasley, W.D.Rust, T.C.Marshall, M.Stolzenberg, J.Geophys.Res. **101**, 29637, (1996)
[6] A.Chubenko et al, Phys.Lett.A **275**, 90, (2000)
[7] A.V.Gurevich, G.M.Milikh, J.Valdivia Phys.Lett.A **231**, 402, (1997)
[8] A.V.Gurevich, G.M.Milikh Phys.Lett.A **262**, 457, (1989)
[9] E.M.Symbalisty, R.Roussel - Dupre, V.Yakimuk IEEE Trans. Plasma Sci. **26**, 1575, 1998
[10] A.V.Gurevich, H.Carlson, Yu.V.Medvedev, K.P.Zybin Phys.Lett.A **275**, 101, (2000)
[11] A.V.Gurevich, R.Roussel- Dupre, K.P.Zybin Phys.Lett.A **237**, 240, (1998)
[12] S.Z.Belenkij, The Theory of Extensive Atmospheric Showers, Moscow, Nauka 1956
[13] L.D.Landau, E.M.Lifshits "Quantum Mechanics", Pergamon, 1958, §121.
[14] L.D.Landau, E.M.Lifshits "Relativistic Quantum Mechanics" Pergamon, 1973, §82.
[15] A.V.Gurevich, N.D.Borisov, G.M.Milikh Physics of Microwave Discharge , Gordon and Beach, 1997
[16] D.M.Suszcynsky, R.Roussel-Dupre, G.E.Shaw J.Geophys.Res. **101**, 23505 (1996)
[17] M.Brunetti, S.Cechini, M.Galli, G.Giovanni, A.Paglarini Geophys.Res.Lett. **27**, 1599 (2000)

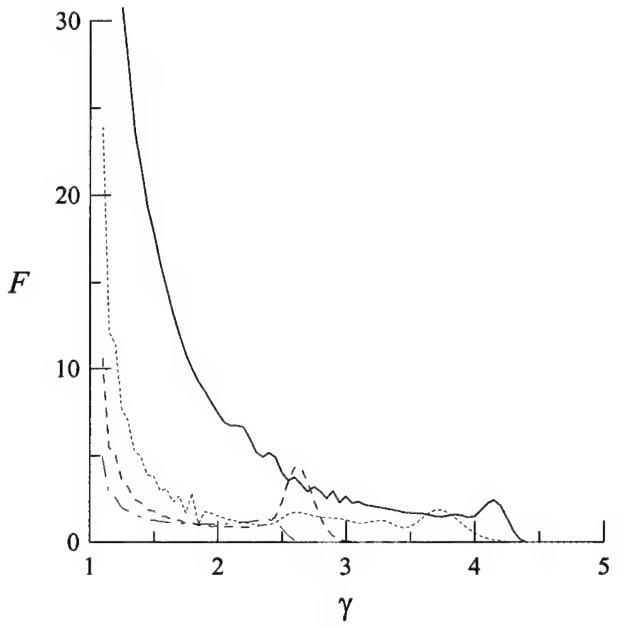

Fig.2.1. The distribution function $F(\gamma)$ calculated for different spatial positions z. z=-2 – dashed-dotted line, z=-1 – dashed, z=0 – dotted and z=2.5 – solid lines. Parameter E_m/E_c=1.1

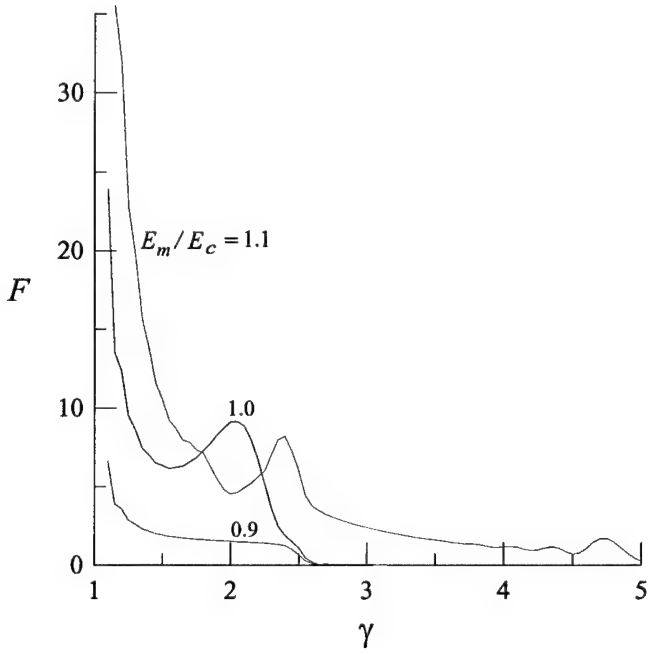

Fig.2.2. The electron distribution function $F(\gamma,z_{max})$ calculated for different values E_m/E_c.

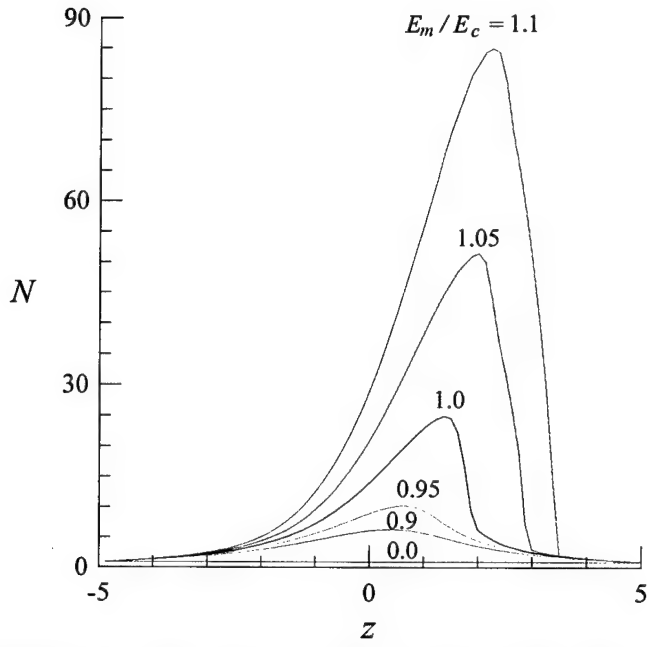

Fig.2.3. The dependence of number runaway electrons N on z for different values E_m/E_c.

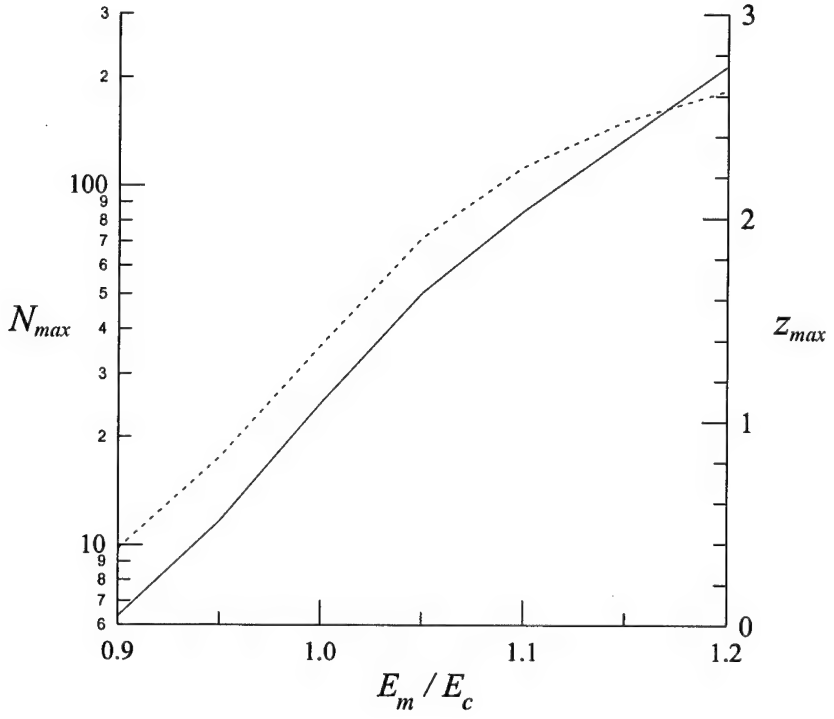

Fig.2.4. The dependence of maximal electron density N_{max} and the location of this maximum z_{max} on parameter E_m/E_c.

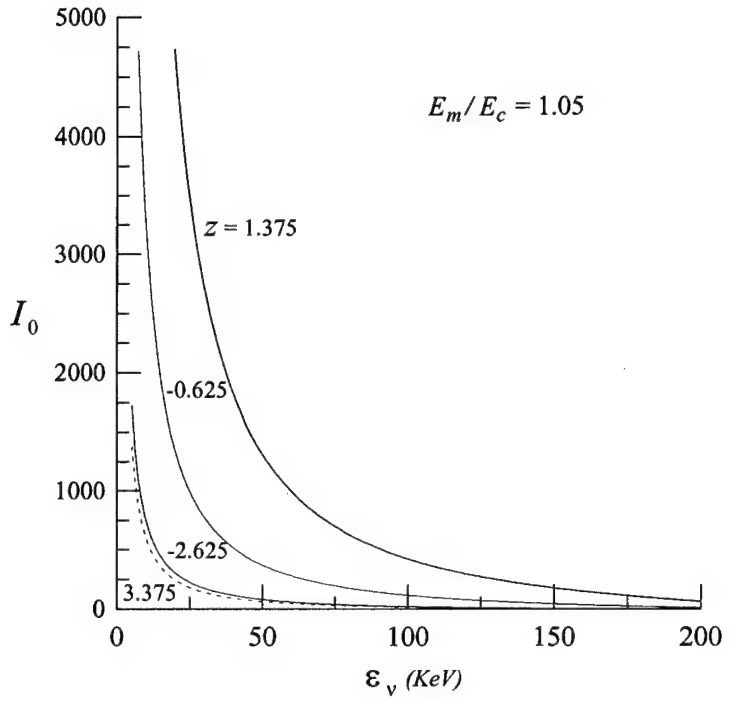

Fig.2.5. The dependence of local X-ray intensity I_0 generated by runaway electrons on photon energy ε_ν. I_0 – is a normalized flux proportional to j_ν

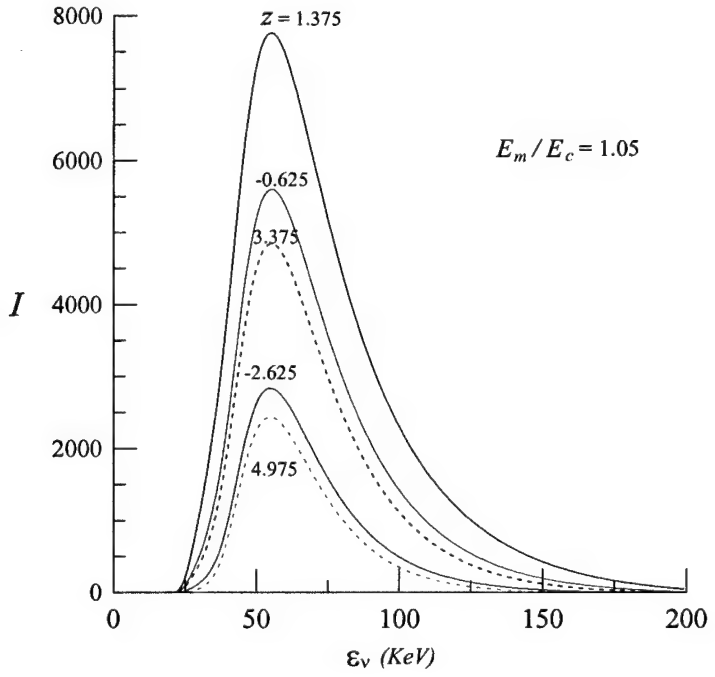

Fig.2.6. The spectrum of X - rays calculated for different position z. Parameter E_m/E_c=1.05

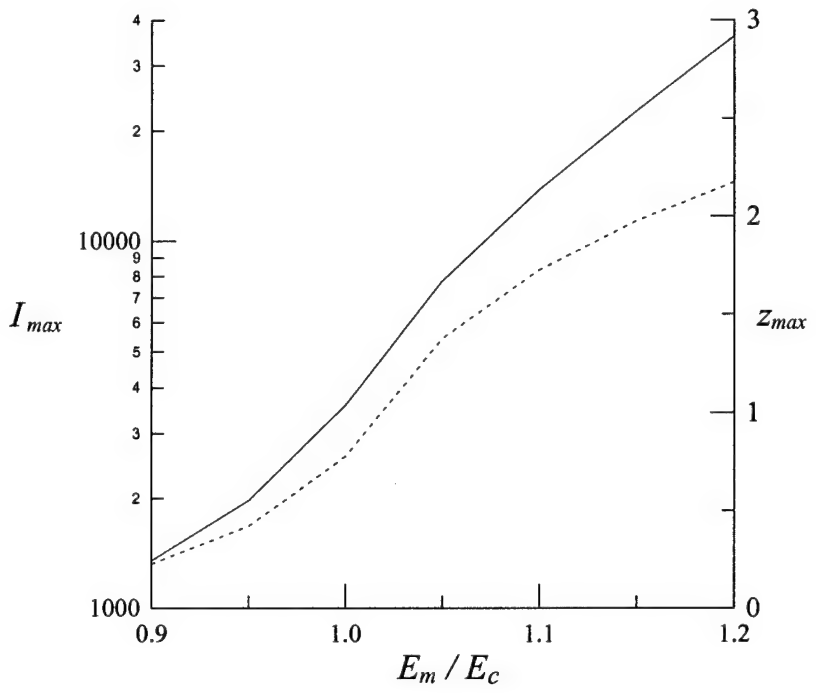

Fig.2.7. The dependence of maximal value of X-ray emission I_{max} and position of this maximum z_{max} on parameter E_m/E_c.

3. Investigation of runaway breakdown phenomena in laboratory installation in conditions of cyclotron resonance

Abstract

The microwave electron cyclotron resonance discgarge in air is sstudied in a magnetic mirror trap. The obtained experimental data demonstrate a rapid growth of the number of fast electrons with a wide energy spectrum (1–300 keV). The discharge begins with the strong X-ray emission, followed by the syncrotron emission at second and third cyclotron harmonics. The optic emission from a low energy energy part of electron spectrum (<100 eV) has a delay up to 80 ms with respect to the X-ray emission.

3.1 Setup description

The setup represented in Fig.3.1 includes a vacuum chamber 2 of quasispherical form, which has a the distance between a pair of opposite flanges 450 mm. The chamber is placed between two similar coaxial copper coils 1 of a static magnetic field. The magnetic field force line distribution inside the chamber has configuration of a bottle with two symmetric necks which forms a magnetic trap for collisionless electrons. The trapped electrons confinement time in the chamber is likely to be enough to confine a bulk of initial electrons of large energies during the time of run-away electrons breakdown in air. The magnitude of the static magnetic field at the center of chamber varies relative to value 875 Gs which corresponds to the ECR for the electric field frequency 2,45 GHz.

A magnetron 3 generates electromagnetic oscillations at the fixed frequency 2,45 GHz, with varying power up to 5 kW which creates the ECR accelerating field for electrons

caught inside the mirror trap. The microwave power is transmitted into the chamber through a waveguide system 6 which consists of the adapter with pyrex window insulating vacuum of the chamber from athmosphere, the horn antenna 7, the circular waveguide with travelling TE_{11} mode, the smooth waveguide transition from a rectangular cross section to circular one, the rectangular waveguide elbow, the water attenuator or ferrite circulator 4. For purpose of pulse periodic regime realization it was made mechanical waveguide cutter off. The maximum microwave electric field strength at the center of vacuum chamber under condition of travelling wave at maximum power is $E_0 \approx 150$ V/cm. In the vicinity of the ECR the microwave electric field is equivalent to a static electric accelerating field for electrons.
Following experimental techniques for study of x-ray bremmsstrahlung radiation and optical radiation produced by the run away electrons and microwave synchrotron radiation at the harmonics of the accelerating field were used:

- Scintillation x-ray transducer 14 (BYCRON, model 2.5M2.5/3LP-X).

The transducer consists of NaJ(Tl) scintillator covered with aluminium cup of 1 mm thickness and combined with a photomultiplier. The optical axis of the transducer placed in the chamber was perpendicularly directed to the trap axis. The operating quantum energy range of the x- ray transducer 100 keV ÷ 1 MeV. Its signal was registered at a monitor of the PC «Pentium» by means of an oscillograph card.

- Photomultiplier 16 for observing of visible air glow discharge under action of both ECR-discharge and run away electrons.
- Personal x-ray doze meter (not shown) for measurement of x-ray spectrum outside the chamber. The operating quantum energy range of the counter 0,05 ÷ 1,5 MeV. Its error of doze power measurements is ± 30%; exposition time is 36 s; the dependence of doze measurements over the operating energy range is no more 45%.
- Microwave spectrum analyser 13 over the frequency range of 2-nd and 3-d harmonics for the base frequency of the microwave generator. Signals for the analyser were received from loop antenna 12 at end of a coaxial feeder introduced along the trap axis.
- Detector 11 for monitoring incident MW power.

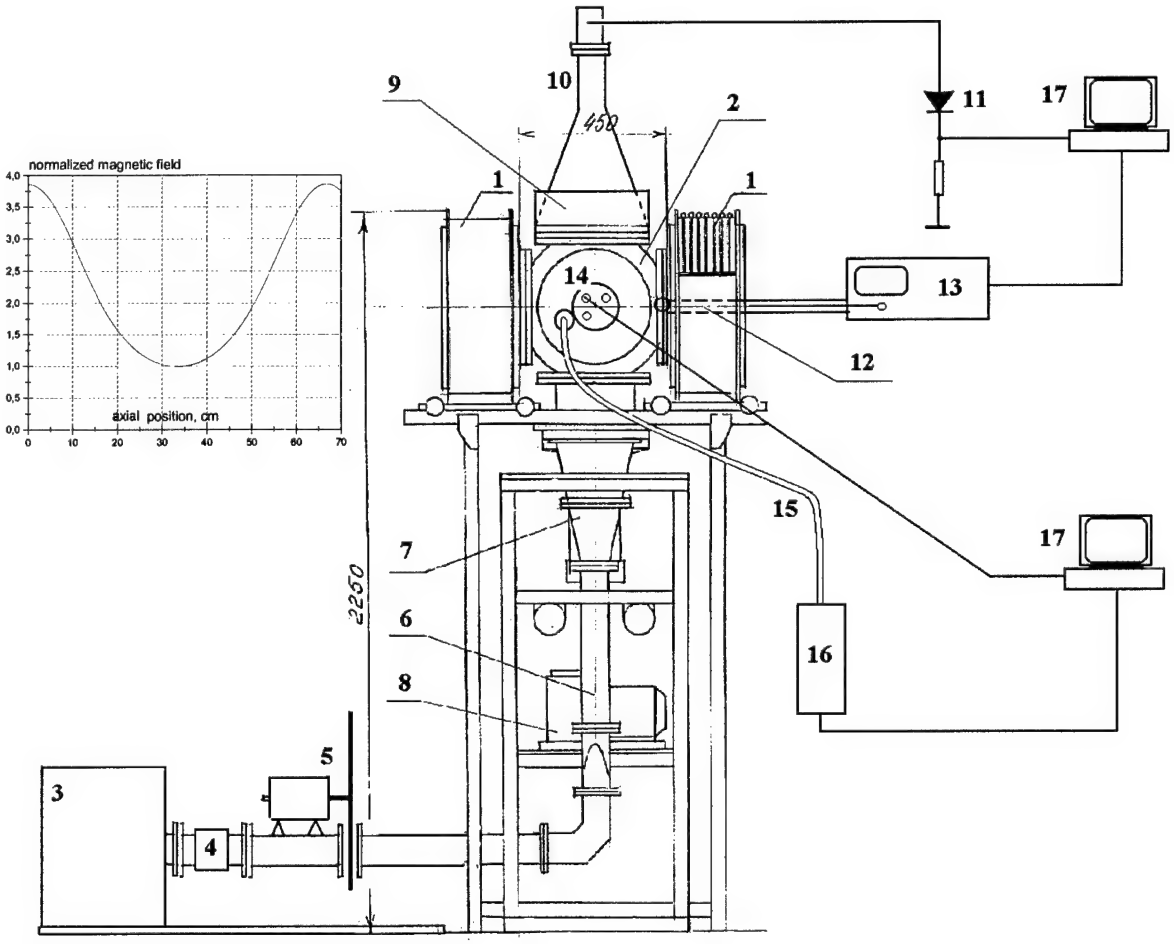

Fig.3.1. Scheme of the experimental setup: 1 – magnetic system; 2 – vacuum chamber; 3 – microwave generator; 4 – attenuator or isolator; 5 – obturator; 6 – waveguide components; 7 – horn coupler; 8 – vacuum pump; 9 – water attenuator section; 10 – horn antenna; 11 – detector; 12 – loop antenna; 13 – microwave receiver with spectrum analyzer; 14 – X-ray receiver; 15 – optic fiber; 16 – photomultiplier; 17 – data display system (computers).

The insertion demonstrates the magnetic field distribution in stationary state normalized to magnetic field in the center of vacuum chamber.

3.2 Experimental Results

In the experiments with the described setup the intense X-ray emission was found to be generated under ECR discharge at the pressure range $< 10^{-4}$ Torr due to bremmsstrahlung radiation of electrons accelerated in relatively weak electric field E=5÷20 V/cm up to subrelativistic energies 100÷300 keV. Simultaneously the MW synchrotron radiation at the second harmonic was observed. Its spectrum points out the presence bulk of electrons with energies ≤10 keV in the system. Specific feature was that the beginning of discharge visible emission owing to low energy part formation of electron spectrum (<100 eV) had a delay reaching 80 ms in respect to the appearance of X-ray and synchrotron signals. This allows to separate the whole process of the ECR breakdown into following two stages: first of which to be an initial stage of breakdown with participating of high energy run away electrons, and second one to be ordinary ECR discharge with participating of low energy electrons. Such separation is reasonable due to difference of physical processes resulting in the characteristic of electron distribution functions.It allows to find analogy of ECR breakdown with the model of runaway electron breakdown by Gurevich, Milikh and Roussel-Dupre applied for explanation of lightning mechanism in Earth atmosphere.

Recently interesting results were also observed in pulse mode of microwave power. Such mode can be achieved by regular cutting off the incident MW power with mechanical waveguide modulator. The preliminary results are shown in Fig.3.2.

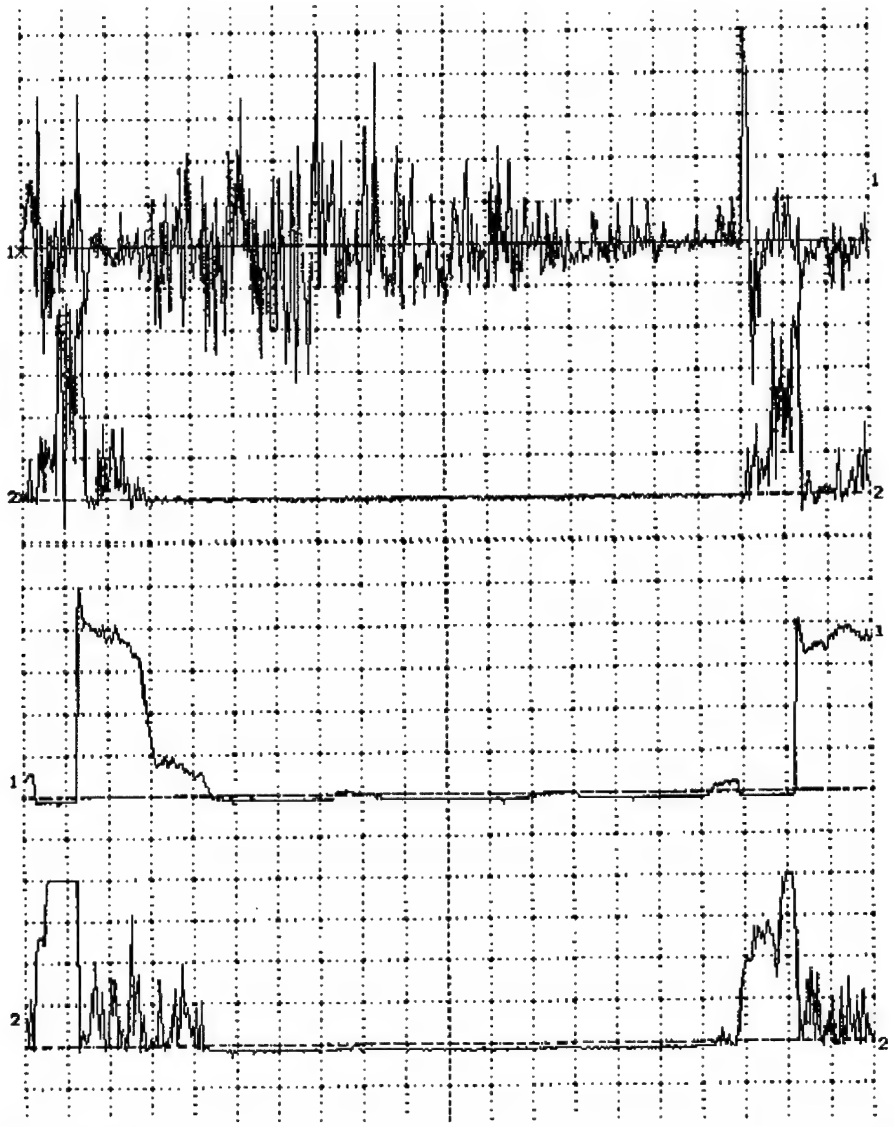

Fig.3.2. Oscillograms of pulse periodical mode operation: a – X-ray signal; b – II harmonic; c – visible light; d – transmitted MW power; $p = 5 \cdot 10^{-6}$ Torr.

Fig.3.3. The same as in Fig.3.2 but under air pressure 4 times more: $p = 2 \cdot 10^{-5}$ Torr.

One can see (Fig.3.2) that at air pressure $5 \cdot 10^{-6}$ Torr we always have a time delay visible light radiation of discharge in respect to the X-ray signal and the cut off transmitted MW radiation connected with that process of accumulation of low energy plasma with overcritical electron density.

The behavior of signals in Fig.3.3 corresponding to air pressure $2 \cdot 10^{-5}$ demonstrates the visible discharge is ahead in respect to the X-ray signal. However one can see the flickering of discharge when the incident microwave energy is redistributed between runaway electrons and low energy plasma.

The main objectives of our future work are detailed investigations of runaway electron breakdown taking into account its temporal and spatial dynamics, definition of energy characteristics of the process and energy balance, measurements of energy γ-quanta spectra depending on experimental conditions.

To study the dynamics of the discharge plasma density due to the RB a microwave interferometer (λ=8 mm) of opened resonator type will be constructed. The x-ray spectrometer in the energy range 30 keV - 1 MeV will be created with use of the X-ray scintillation detector (in our possession) and the μACE^{TM}-system (EG&G ORTEC) which consist of amplifier, multichannel analyzer plug-in card with emulation software(will be ordered to the ISTC). The averaged x-ray spectra depending on the regimes of the RB and optical spectra of the RB plasma will be studied. Both probe measurements and electron energy distribution function measurements with an electrostatic analizer for electrons leaving the magnetic trap will be carried out.

We intend to continue investigation with pulse mode of MW generation because it's reasonable to have the time limited action on the RB for study of its dynamics. For this purpose the waveguide modulator 5 (Fig.3.1) cutting off continuous microwave radiation was constructed. It allows to vary duration and period of pulses in wide range. The demands for the modulator was caused by the reason that MW generator is able to work in continuous mode generation, but not able to do it in pulse mode if to use pulse high voltage supply. Microwave pulses after the modulator have trapezoidal form with rise and fall time of order 1/3 of plateau. Owing to the pulse mode we hope to study lifetime of high energy electrons caught by the magnetic trap during a previous microwave pulse and their role as seed in the RB phenomenon during followed pulse.

4. Investigation of an influence of combined effects of runaway breakdown and cosmic rays on lightning processes in thunderstorm atmosphere

4.1 Abstract

The intensive X-ray emission during thunderstorms was studied at the height 3340 m above sea level. For the first time the short-time (1—5 min) bursts of X-ray emission were observed. The bursts are highly correlated at the wide space region (about 0.5 km). The main component of X-ray emission in bursts has the energy 50—80 keV. The observed bursts could be attributed to the bremsstrahlung determinated by the runaway breakdown (RB) effect in the thundercloud electric field. Ground based observations of RB open a wide opportunities for the studies of fundamental processes in thunderstorms.

4.2 Introduction

The new mechanism of lightning initiation in thunderstorm clouds based on a combined action of runaway breakdown (RB) and extensive atmospheric showers (EAS) was proposed in [1]. According to this theory in shower core the ionization of the air due to RB effect is growing strong enough to produce a local highly conductive plasma. The thunderstorm electric field is amplified strongly inside such region. That can serve to the triggering of a lightning discharge.

The Lebedev Physics Institute (LPI) group proposed an experimental program to study this mechanism. The program includes simultaneous observations of cosmic ray showers, runaway breakdown emission and lightning discharges at the mountain cosmic ray station (MCRS). The LPI MCRS is situated on a pass in Tien-Shan mountains at the height 3340 m above sea level (effective atmosphere depth 690 g/cm^2). The thunderstorm clouds go through the pass at the height about 0.1—1 km during of three months yearly. The installation can detect extensive air showers measuring simultaneously EAS electrons with energies 0.1÷10 MeV, muons with energies above 5 GeV and neutrons with energies above 100 MeV. The RB effect lead to a strong amplification of the X-ray emission inside and below the thunderclouds [2]–[6]. To observe RB emission a system of Geiger counters was installed in a wide region (approximately 500 m around MCRS). To fix the position of lightning discharge by its strong electromagnetic and acoustic radiation a group of special antennas together with directed microphones was established.

In the present work we inform about the first results of X-ray emission measurements. The strong amplification of emission during the whole thunderstorm period is found. For the first time the bursts — short time strong peaks of X-ray radiation were observed. The typical time length of such a burst is 1÷5 min and radiation increases are highly correlated in different points at the scales minimum of the order of several hundred meters.

4.3 Experimental Installation

The schematic layout of MCRS's detectors disposition is shown at Fig.4.1. The installation used in this experiment consists of the following main parts:

- The *shower system* on the base of scintillation detectors located nearly concentric circumferences on the flat part of the pass (the "Hadron" experiment installation [7]). The scintillators can detect the high energy (above 10 MeV) electrons and gamma quanta travelling through the installation within an extensive air shower fronts.
- The *NM64 type neutron supermonitor* [8] consisting of three independant units. Each unit has 3 m^2 sensitive area and includes six registration channels on the base of neutron counters SNM15. The supermonitor was designed for the registration of one-minute

intensity variations of cosmic ray hadrons with energy above 50—100 MeV. The electronics of neutron monitor's registration channels is designed to provide methodic error at the level of 0.01% in intensity measurements. The input threshold value for neutron counter's pulses is set to be equal to 10 mV, corresponding background pulse intensity being 2700 pulses per min (p.p.m.) for each unit.

- The boxies of *high threshould gamma ray and electron detector* are placed above supermonitor units as shown at Fig.4.1b. This detector is made on the base of Geiger-Mueller counter tubes of SI5G type which are capable to register hard X- and soft γ-ray emissions with nearly 1% efficiensy. Four detector boxies each of wich contains 20 counters with parallel outputs and corresponds to the one registration channel were mounted above each of three supermonitir units, their total sensetive area being equal to 8 m^2. Because the counters of this detector are operating in proportional regime it is necessary to decrease their dead times up to 5-10 mcs (which is 20 times shorter as for usual Geiger counters). To achive the charged particles registration efficiency as high as for Geiger regime (above 95%) the registration channel's threshould is set to 20 mV. The roof of the building where neutron supermonitor and high threshould γ-ray detector is situated is made of 0.8 mm thick iron, the wood ceiling has thikness about 15 cm and the detector's boxes are made of 2 mm thick aluminium. It provides the upper threshold about 25—30 MeV for relativistic charged particles registration. The main absorber above the detector is carbon with the effective thikness 13.6 g/cm^2. Thus, the threshold value for the photons is about 30 keV. The general count intensity for all channels is determinated mainly by the electron background flux and is equal to $3.2 \cdot 10^5$ p.p.m. The corresponding statistical error in 1-minute data is less than 0.2%.
- The *muon detector* made of SI5G type counters with common sensitive area 2.7 m^2 is placed under one of the supermonitor units (see Fig.4.1b). Output pulses from each of four lower detector boxies are switched to a coincidence scheme with the pulses coming from corresponding boxies, located above supermonitor unit. The thickness of matter above lower boxies is 15 g/cm^2 of carbon and 150 g/cm^2 of lead absorber. The latter exeeds 35 electromagnetic cascade units, excluding completly the registration of atmospheric photons and electrons with energies below 10 GeV. The detector registrates mainly the muons with energies above 220 MeV travelling through the unit in nearly vertical direction.The general count intensity is about $7 \cdot 10^4$ p.p.s. Hence, the fluctuations in one-minute data are about 0.5%. The registration channel's characteristics of muon detector are just the same as those for the high threshould gamma detector.
- The newly build *low threshould wide spread X-ray detector (WS)* created in Summer 1999 is designed to investigate the thunderstorm clouds low energy electromagnetic emission. It consists of four registration points situated perpendicular to the preferential direction of thunderstorm clouds motion over the cosmic ray station's pass (see Fig.4.1a). The distance between the extreme right and extreme left points is about 500 m. Each of the points has two layers of sixty SI5G counters. The outputs of the counters in each layer are combined in one registration channel. Hence, there are two registration channels in each point with sensitive square 2 m^2 each. The SI5G counters are put in Geiger-Mueller regime, and the threshold of registration channels is equal to 2—3 V. Electronic circuits in each detector point are based on vacuum tubes in order to protect them from the nearby lightning discharges. The powerfull vacuum tubes ensure the output pulse front length not worse then 2—3 mcs at output resistance of 240 Ohm and capacity about 20 mcF. Due to this distortion of the pulse form during its passage through 300—400 m long cable is negligible. The detectors of each registration points are placed within a little light house. The counters are separated from the atmosphere by the 0.8 mm (or 0.74 g/cm^2) thick iron roof.

All the detectors described above have the bouth independed power supply and data recording systems. Distant detectors are connected to a central registration system (located in the building with neutron supermonitor) by screened underground cables. The data are transfered to computer by the means of a CAMAC system. To avoid the danger of semiconductor electronics damage in the moment of lightning discharge, the cables are conjugated with CAMAC scaler blocks throughout vacuum tube based circuits.

The pulses coming from all of eight channels of low threshould WS X-ray detector were counted by CAMAC scalers during of one second time intervals and accumulated numbers of them were recorded by registration computer. Amounts of pulses obtained from other detectors were counted during of one minute intervals and registrated together with the clock indication, temperature and barometric pressure. The registration was perfomed continuously during of 4 monthes in July—October 1999.

We have tested the electric noise in all channels by switching off the high voltage power supply in registration points. In such a case the pulses from the channels were not registrated even in thunderstom conditions.

4.4 Experimental results

Intensity variations. During of July and up to the last days of August, 1999 there were no thunderstorms in the vicinity of mountain station. The typical measurements of pulse intensity, obtained from various detectors at this quiet period are presented at the 3.2. The shown data correspond to the total intensity registrated by all channels of each detector (i.e. the amounts of pulses obtained from 8 channels of low threshould X-ray detector, 12 channels of high threshould γ-ray detector, 3 neutron monitor units, 4 muon coincidence channels show the intensity curves at this figure).

One can see that both low and high threshould γ-ray detectors exhibit no significant changes in count velocity through the whole period shown (6 houres). The signals from neutron monitor and muon detector demonstrate the same stability (their slow trend is caused by variation of atmospheric pressure).

In the end of August 1999 we have observed five cases when at low heights over the MCRS were passing the thunderstorm cloud fronts accompanied by the strong lightning discharges. The same data as given at Fig.4.2 for a quiet day are presented at Fig.4.3a-e for typical thunderstorms events. Time scale at the bottom of the figure is centered relatively to the moment when thunderstorm beginning was fixed. This moment is marked by a vertical dotted line. Below we shall discuss the typical thunderstorm event on August, 31. Corresponding data are presented at Fig. 4.3.e.

It can be seen from the typical curves shown at Fig.4.3e, that each time after the moment of thunderstorm beginning a dramatic growths of emission intensity measured both by low and high threshould γ-ray detectors occures. We emphasize the significant difference between these two types of detectors: low threshold detectors measured practically free flux of X-rays, and high threshold detector that was *under the roof* having additional absorption equivalent to 13.6 g/cm^2 of carbon. One can see from the Fig.4.3.e, that the signals of the free (low threshould) and under the roof (high threshould) detectors are well correlated in time. These correlations are quite regular having the same character for every thunderstorm. The characteristic scale of long time emission increses is 2—3 houres after the moment when thunderstorm clouds begin to pass the MCRS.

At the same time the neutron monitor and muon detector (which are sensitive to energetic particles of cosmic radiation only) do not demonstrate any thunderstorm caused effect.

The results obtained for the all of five observed thunderstorms are quite analogous.

Space correlations. The γ-ray intensity increases during thunderstroms discussed above have been studied in data streams obtained separately from each of low threshould detector points shown at Fig.4.1a. The correlation coefficients between all available pairs of detector points were determined. The results — time dependences of correlation coefficients C_{ij} calculated for 100 sec. Length time periods for three detector points pairs — are presented at Fig.4.4 for one of the observed thunderstorms (the corresponding data obtained for all other detector pairs and of other thunderstorms are quite analogous). One can see from the Fig.4.4 that under the fine weather conditions the data at different observational points are practically noncorrelated. During the thunderstorm period the picture is absolutely different: correlation coefficients for all low threshold detector points pairs becomes very high — about 0.8 and even higher. This high correlation demonstrate that the observed of X-ray intensity strong growth is deeply connected with thunderstorm processes developing simultaneously at the wide space region of the order of 0.5 km, maybe even larger.

Short time emission bursts. The accompanying thunderstorm emission intensity variations are well correlated in time also. It can be seen from Fig.4.3.e for X-ray signals of the free (curve 1) and under the roof (curve 2) detectors. Analogous time correlations exist for the emission at different low threshold detector points. These correlations are quite regular, they have the same character for every thunderstorm. The characteristic timescale of this longtime emission variation is 30÷60 min. One can mention the following peculiarity of emission intensity — it has often a double or triple pike structure (see Fig.4.3.e).

An interesting new feature is short time bursts of X-ray emission. Characteristic length of the bursts is 1÷5 min. The typical short time bursts occured during of thunderstorm event of 31 August 1999 can be seen at Fig.4.3.e in time moments 0.2 (peak 1), 0.4 (peak 2), 1.4 (peak 3) houres after the beginning of thunderstorm. It is obvious good correlation between the intensity bursts of low and high threshould emission detectors. Any increases at corresponding time moments in the intensity of energetic cosmic ray components (i.e. neutrons and muons) are absent.

The one of the bursts data for low threshould detector intensities (peak 3) are shown in large scale at Fig.4.5 both for the sum of all channels and for each detector point separately. One can conclude from this figure, that emission intensity bursts are correlated strongly between various detectors separated with space distancies of the order of some hundreds of meters. According to statistical errors marked at Fig.4.5, the value of intensity increase during of a typical emission burst exeeds the level of statistical flluctuations by 15—30 times.

Absorption of emission. The two types of measurements of emission intensity were performed simultaneously: low threshold and high threshold, which demonstrate quite a good time correlation (Fig.4.3.e). The following main difference between these measurements exists. The low threshold detectors were separated from the atmosphere by the thin (0.8 mm) iron protector only. The high threshold detectors had the same protector, but they were installed inside the neutron supermonitor building, which has a roof with effective thickness 13.6 g/cm^2 of carbon. The roof gave a significant additional absorption. By the comparison of the data from free (low threshold) and under the roof (high threshold) detectors the characteristic absorption of emission could be found.

To perform comparison we determined first five-minute averaged background of both sets of data. As fast electrons determine the major part of the counts we have to eliminate the background and compare the excess, which is due to X-ray effect. The excess relation r for both sets of data is presented at Fig.4.6. One can see, that the typical value of excess relation of the free (low threshold) to the under roof (high threshold) data is 2÷4.

Such an absorption in 13.6 g/cm^2 carbon is characteristic for energy of γ-quanta 200÷500 keV [18].

It is important, that during short time bursts the value of r is always significantly higher, growing up to 8÷12 (Fig.4.6). That shows that the energy spectrum of X-rays during short bursts is essentially different from the main part of thunderstorm: its major component has *low energy X-rays* (≤ 50÷80keV) which are effectively absorbed by the roof. Note that peaks are more pronounced in absorption curves (Fig.4.6), than in intensity (Fig.4.3.e). It opens a possibility to use absorption as an effective method of X-ray burst detection.

Flux of X-ray quanta. To determine the flux of X-ray quanta we have first to average the excess counts of low threshold data and then takes into account absorption by the iron protector and sensitivity of Geiger-Muller counters SI5G for X-ray quanta. That gave an approximate value of flux in bursts 10÷20 photons/(cm^2 sec sr).

4.5 Discussion

The aim of this work is to study the influence of thunderstorms on the X-ray emission from atmosphere. Effective growth of the emission in all observed thunderstorms is definitely established.

In fine weather conditions weak disturbances of the emission (~ 1%) determined partly by the changes in atmospheric pressure are regularly observed (Fig.4.1) That agrees well with the previous statements [9] - [11]. During thunderstorm the picture changes fundamentally. The X-ray emission is strongly amplified for hours. The emission amplification in the thunderstorm period was studied previously in a number of papers (see [10]-[12]).

The main peculiarities of our observations are:

1. X-ray emission was studied at the ground, but high in the mountains (height 3340m). Analogous investigations were done previously only by Shaw [10] and Suszcynsky et al. [11] (mainly at lower heights).
2. For the first time the emission was observed simultaneously in several points with the large distance between them (Fig.4.1).
3. For the first time the free and partly screened emission was studied simultaneously.

Below we'll compare our observations with the previous studies. The new results will be discussed.

The main mechanisms of strong amplification of X-ray emission intensity during thunderstorm are:

1. Gamma ray emission from the beta decay of radon daughter-ion products.
2. Bremsstrahlung of accelerated electrons due to the action of a strong thunderstorm electric field.

Radon effect is determined by the precipitation of radon and its products to the ground during rainfall. Gamma ray emission from radon daughter-ion β decay has energies of quanta 0.2÷2 MeV. The decay processes and rainfall determine its main time characteristics: 20 ÷ 30 min growing up and about 50 min after washout [11,13].

Electric field effect is determined by the acceleration of electrons. Wilson [14] was the first who suggested that the secondary electrons generated by cosmic rays could be accelerated by the thunderstorm electric field. A new fundamental step was done in the runaway breakdown (RB) theory developed by Gurevich et al. [2]. It was shown that accelerated electrons could organize an exponentially growing avalanche in thunderstorm electric field. RB effect is supposed to determine maximal electric field reached in thunderclouds [2,15,16]. Directly RB process we discussed in the Introduction in connection with the

lightning triggering theory [1]. RB effect lead to the strong amplification of X-ray emission due to the bremsstrahlung.

Amplification of X-ray emission attributed to RB effect was observed in [3,4,17] during the measurements inside thunderclouds at the balloons. The main features of these observations could be summarized as follows:

a) The intensity of X-ray emission at the height ~ 4 km is sharply (in seconds time scale) growing up to 10^3 in the comparison with the standard level determined by cosmic rays. The maximum of observed emission bursts lays in the diapason 60÷90 keV, the maximal count rate is 40÷50 photon/(cm^2 sec sr) [4,17].
b) The horizontal scale of the region of emission amplification is of the order 1-km or more in agreement with the layered structure of thunderstorm clouds.
c) The time scale of X-ray bursts is of the order 1 min.
d) The intensity of bursts diminishes sharply (in second time scale) with the lightning. But in a 10-sec time scale it can grow up again.
e) Lightning was seen during all bursts. So, it is natural to suppose, that a correlation of lightning events with X-ray intensity bursts do exist.

Let us discuss now results of our observations, taking into account the main features of both considered mechanisms of X-ray emission amplification.

1. The general structure of a long time emission (Fig.4.3.e) agrees well with the radon source. A peculiarity, which could be mentioned, is the usual double pike structure of our intensity curves (Fig.4.3.e). The energy of gamma quanta (0.2÷0.5 MeV), determined by the absorption in the 13.6 g/cm^2 carbon for the main part of observed thunderstorm emission (Fig.4.6), agrees with radon source also.
2. Short time bursts of X-ray emission (Fig.4.3.e-4.6) are the main new result obtained in our measurements. The bursts are well correlated at the scales 0.5-km or more. Such correlated short time bursts in the ground-based measurements are observed for the first time. There exists a quite good correlation between the observations of free and partially absorbed bursts. The analysis of absorption effect shows, that the energy spectrum of X-rays in the bursts is essentially different from the main part of thunderstorm: its major part consists of the low energy X-rays ($E \leq 50 \div 80$ keV). Such type of energy spectrum is characteristic for RB effect only.

In Table 1 the main features of our observations of bursts are compared with the X-ray emission measured at balloons. We see that the features of the balloon measurements attributed to RB effect are rather close to the short burst observed on the ground in our measurements (Table 1). One can conclude that in short bursts the runaway breakdown bremsstrahlung was observed.

We note that this statement does not contradict to the other ground based studies, including the mostly comprehensive and detailed one made by Suschinskhy et al. [11]. As in [11], the main part of emission in our study definitely belongs to the radon. In the possibility to observe RB emission effect in our case essential role could be played by higher sensitivity of our system and observations of X-ray absorption. One should mention also a significant difference in heights: the main part of measurements in [11] were done at the height 2000 m, and our — at 3340 m. We emphasize that the mostly probable region of the high values of electric field which can lead to RB effect in thunderstorm clouds $E \sim E_c(z)$ according to multiple balloon measurements [15,16] lays at the heights 4÷8 km. The characteristic length of energetic photon $E \sim 30 \div 100$ keV propagation in atmosphere is $l_f \leq 1$ km [6]. So, the probability to observe RB emission is strongly diminishing with height below 3.5 km.

We see that though the RB emission is effectively screened by radon it could be brought to light in the ground based measurements as well. Of course more detailed ground based studies including higher heights and better energy spectrum and time resolution are needed.

4.6 Conclusion

In conclusion we will formulate briefly the main results of our observations.

1. X-ray emission during thunderstorm in mountains at the height 3340 m is studied for the first time simultaneously in several different places.
2. It is found that the emission is well correlated at the scale of the order 0.5 km or more.
3. For the first time well defined short bursts of X-ray emission are determined. The bursts are highly correlated at the whole studied space region (~0.5km).
4. The noticeable diminishing of emission intensity penetreating through the 13.6 g/cm^2 carbon layer is established. It means that the main component of X-rays observed in bursts has low energy (50÷80 keV).
5. The X-ray flux observed in bursts could be estimated as 10÷20 photon/(cm^2 sec sr).

The preliminary analysis of our measurements allows to suppose that the observed bursts of X-ray emission is the result of bremsstrahlung amplification determined by the runaway breakdown effect in thundercloud electric field.

4.7 Bibliography

1. A.V. Gurevich, K.P. Zybin, R. Roussel-Dupré, Phys.Lett.A **254** (1999) 79.
2. A.V. Gurevich, G.M. Milikh, R.Roussel-Dupré, Phys. Let. A **165** (1992), 463.
3. M.P. MacCarthy, G.K. Parks, Geophys. Res. Lett. **12** (1985) 393.
4. E.K. Eack, W.H. Beasley et al., J. Geophys. Res., **101** (1996) 29637.
5. A.V. Gurevich, G.M. Milikh, J.A. Valdivia, Phys.Lett.A **231** (1997) 402.
6. A.V.Gurevich, G.M.Milikh, Phys.Lett.A **262** (1999) 457.
7. S.F. Abrashitov et al. Izvestia AS USSR, **50** (1986) 2203.
8. V.M. Aushev et al. Izvestia RAS, **60** (1997) 488.
9. A.E. Sandrstrom, Cosmic Ray Physycs, chapter 6, North-Holland, N.Y., (1965).
10. G.E. Shaw, J.Geophys.Res., **72** (1967) 4623.
11. D.M. Suszcynsky, R. Roussel-Dupré, G.E. Shaw, J. Geophys. Res., **101** (1996) 23505.
12. N. D`Angelo, Ann.Geophysique Ser.B, **5** (1987) 119.
13. P. Bhandari, Rama, J.Geophys. Res., 68 (1963) 3813.
14. C.T.R. Wilson, Proc. Phys. Soc. London, **37** (1925) 320.
15. T.C. Marshall, M.P. McCarthy, W.D. Rust, J. Geophys. Res., **100** (1995) 7097.
16. D.R. MacGorman, W.D. Rust, The electrical nature of storms, NY 1998.
17. E.K. Eack, Rev.Sci.Instr., **67** (1996) 2005.
18. Particle Physics Booklet, Springer, 1998, p. 193.

Table 1

	Ground	Balloon
Time duration	1 ÷ 5 min	≥ 1 min
Space correlation	≥ 0.5 km	≥ 1 km
Characteristic energy	50 ÷ 80 keV	60 ÷ 90 keV
Characteristic intensity	10 ÷ 20 photons/cm^2 sec sr	40 ÷ 50 photons/cm^2 sec sr
Heights	3340 m	3500 ÷ 4000 m

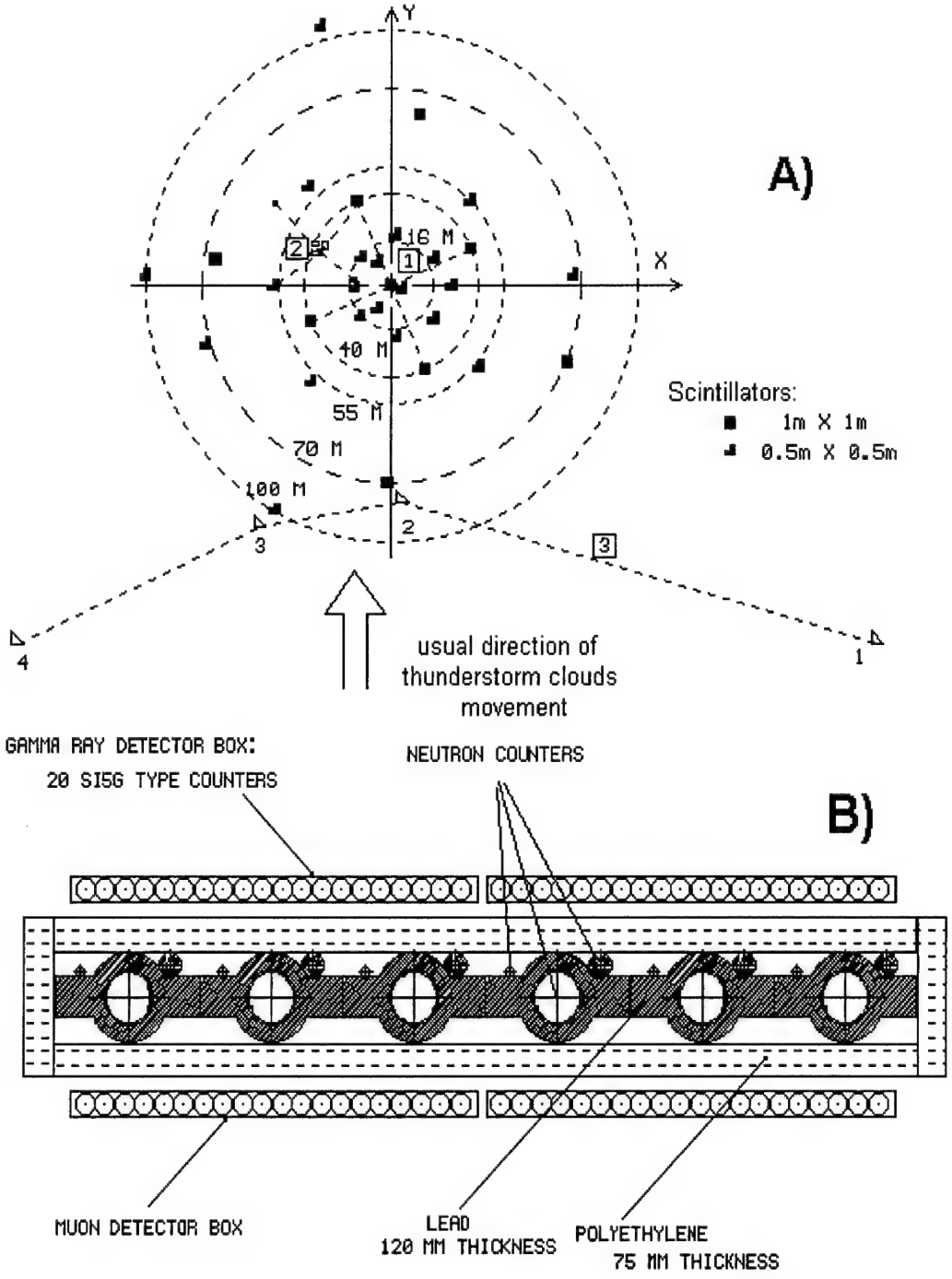

Figure 4.1. Disposition layout of mountain cosmic ray station's detectors (A): 1– the center of shower scincillation system, 2– neutron monitor and high-threshould gamma detectors, 3 – the system of four WS low-threshould gamma- and X-ray detector points, (B): the cross-section of a neutron monitor unit together with high-threshould and muon detectors.

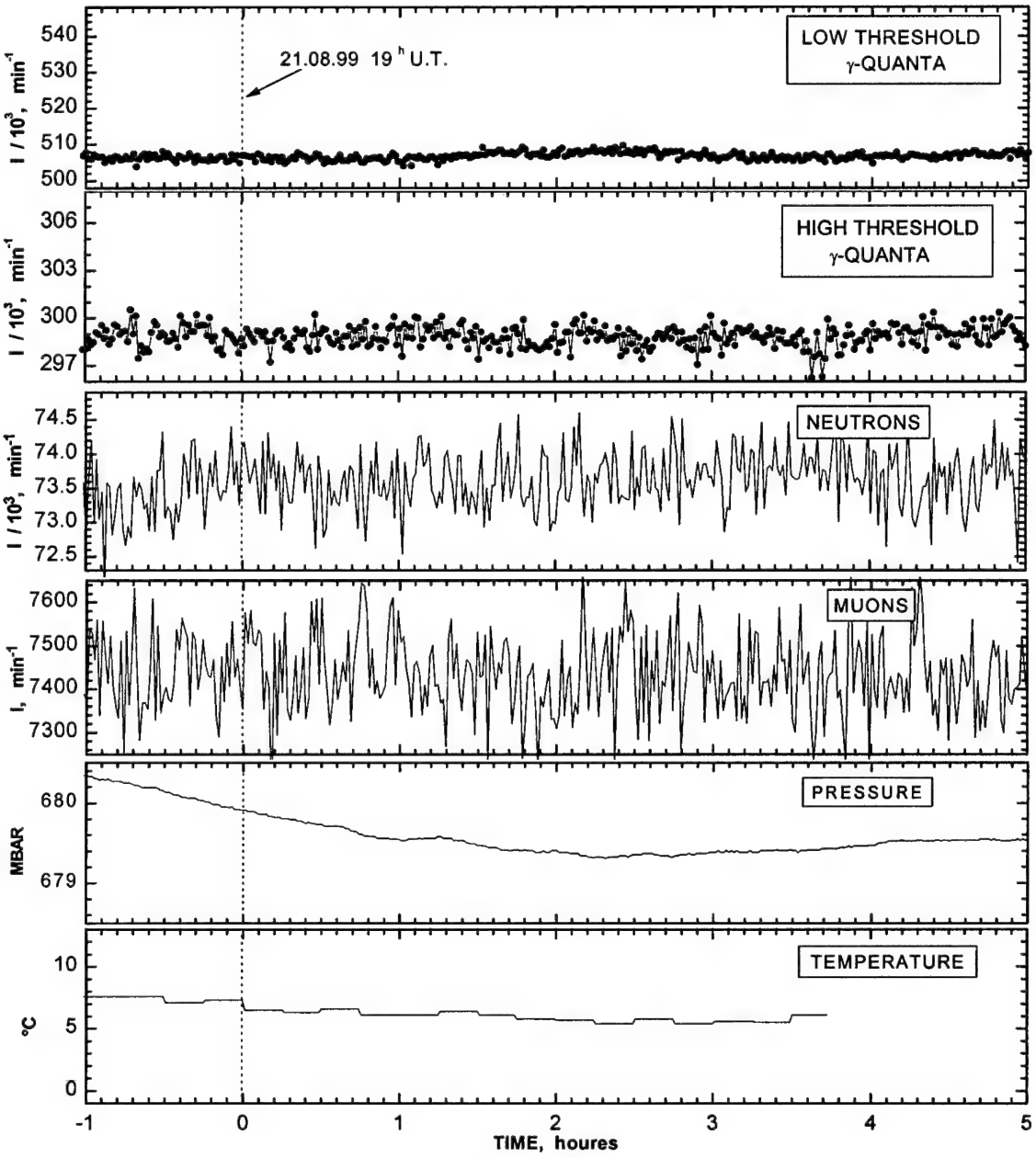

Figure 4.2. Typical behaviour of various cosmic ray components and atmospheric parameters in the absence of thunderstorm.

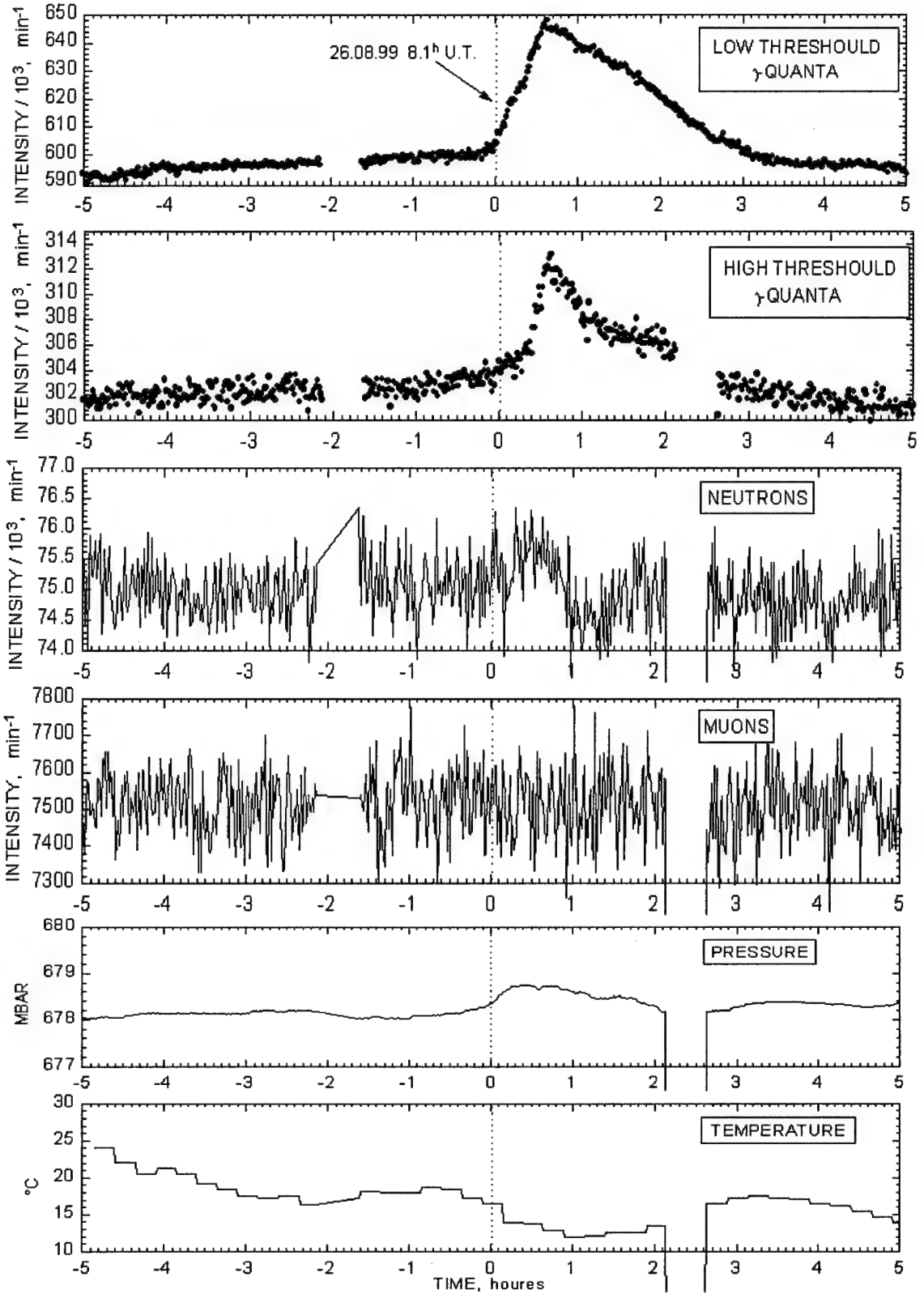

Figure 4.3a. The behaviour of various cosmic ray components and atmospheric parameters during of the thunderstorm at 26 August 1999.

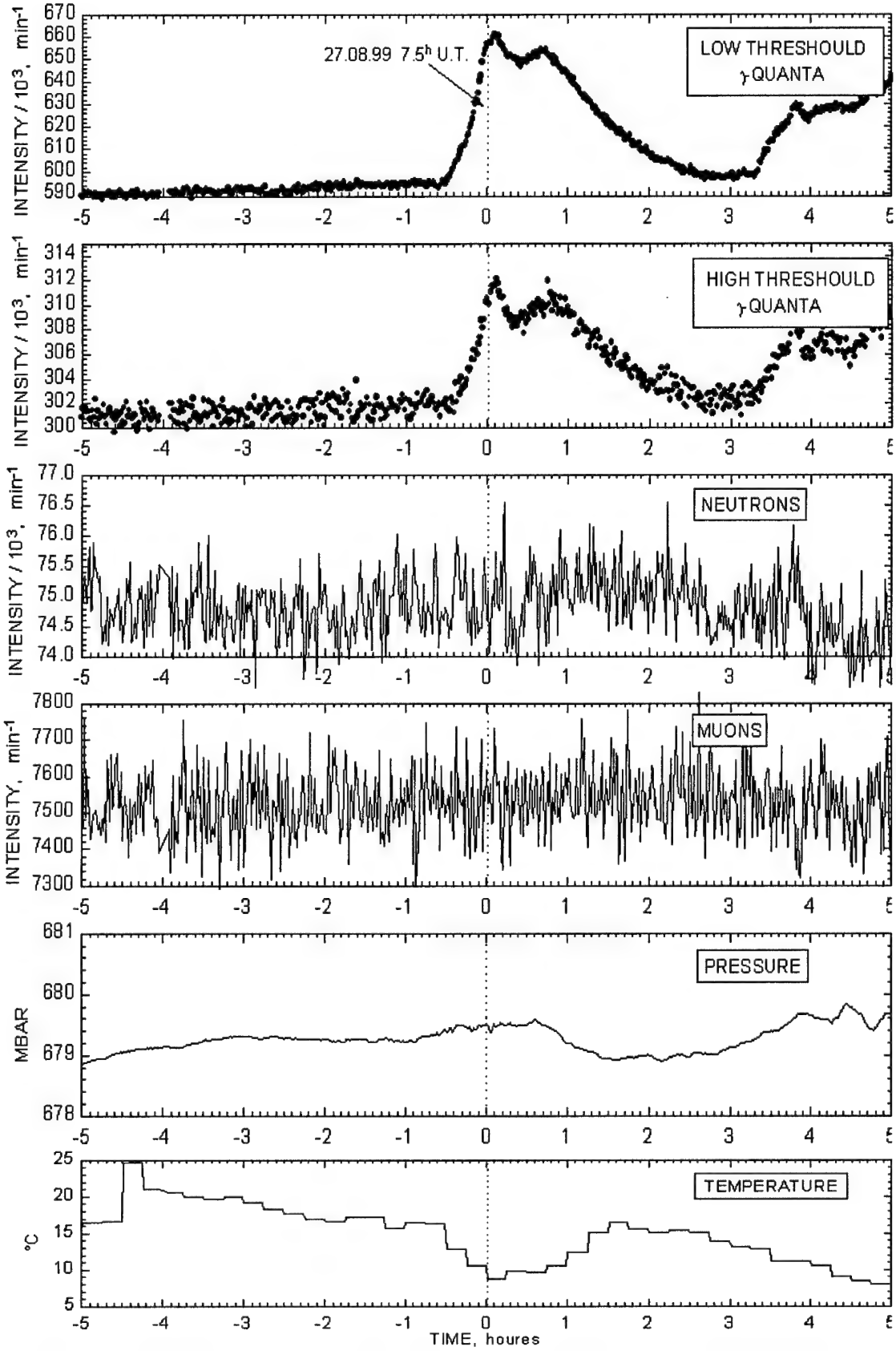

Figure 4.3b. The behaviour of various cosmic ray components and atmospheric parameters during of the thunderstorm at 27 August 1999.

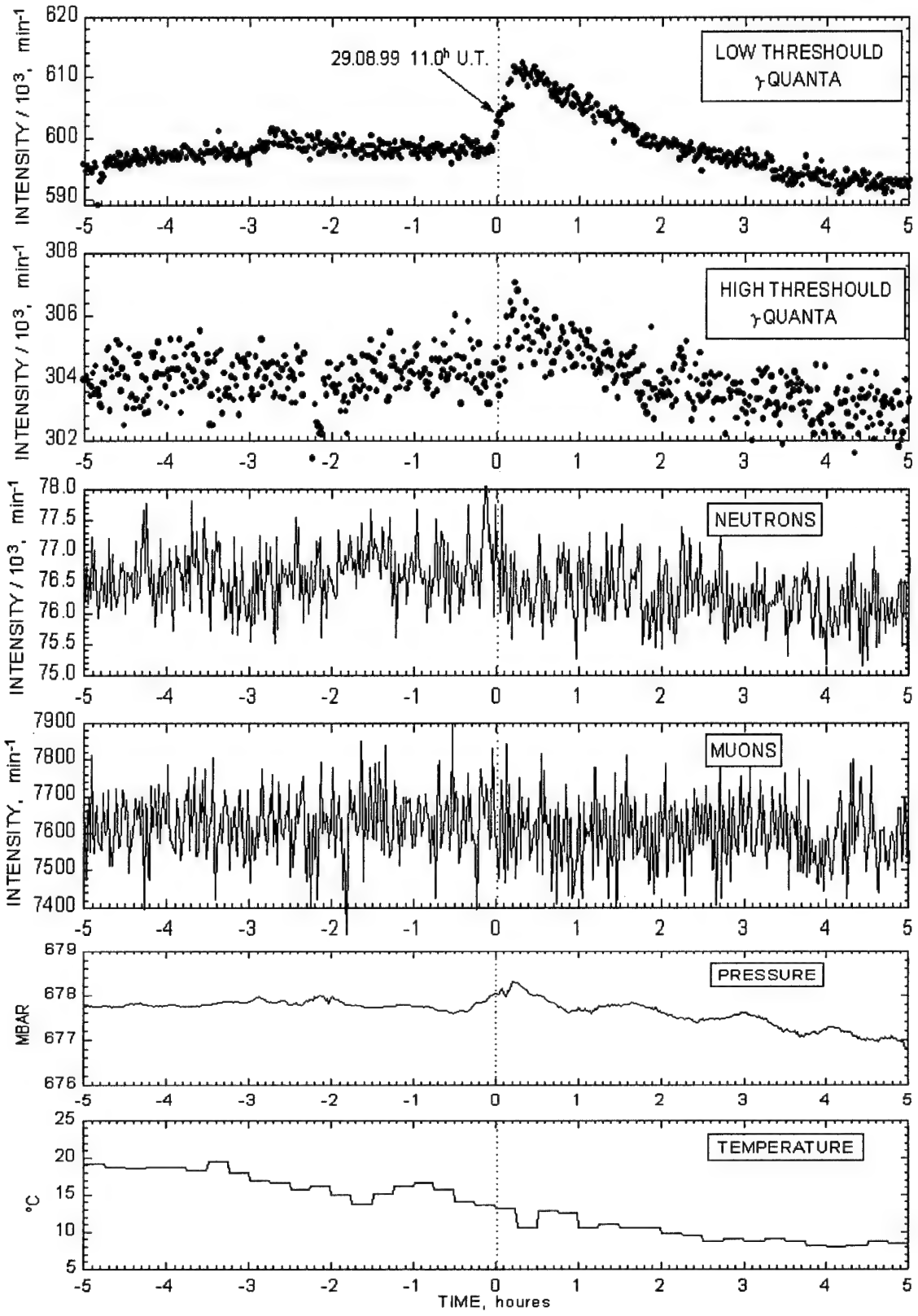

Figure 4.3c. The behaviour of various cosmic ray components and atmospheric parameters during of the thunderstorm at 29 August 1999.

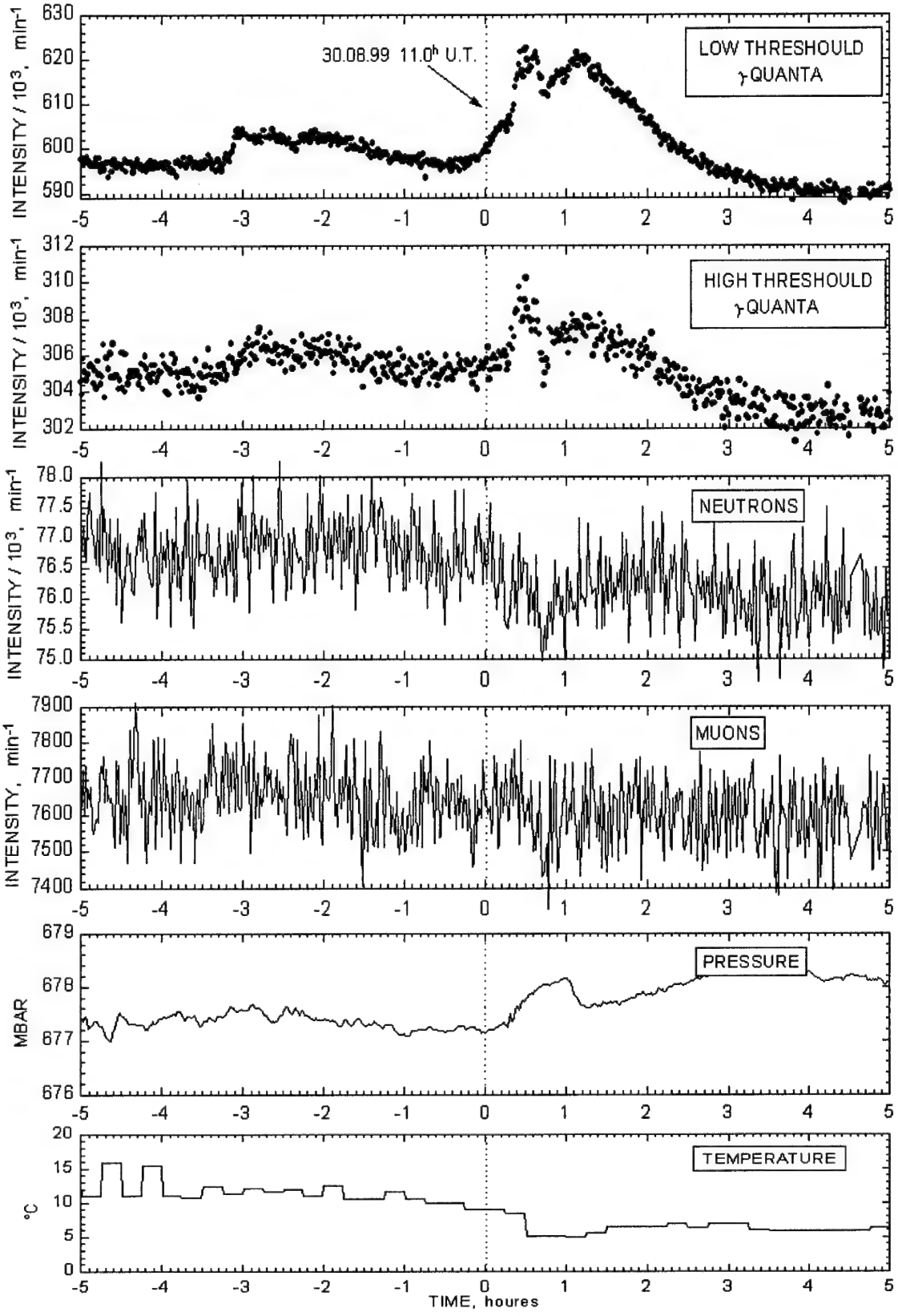

Figure 4.3d. The behaviour of various cosmic ray components and atmospheric parameters during of the thunderstorm at 29 August 1999.

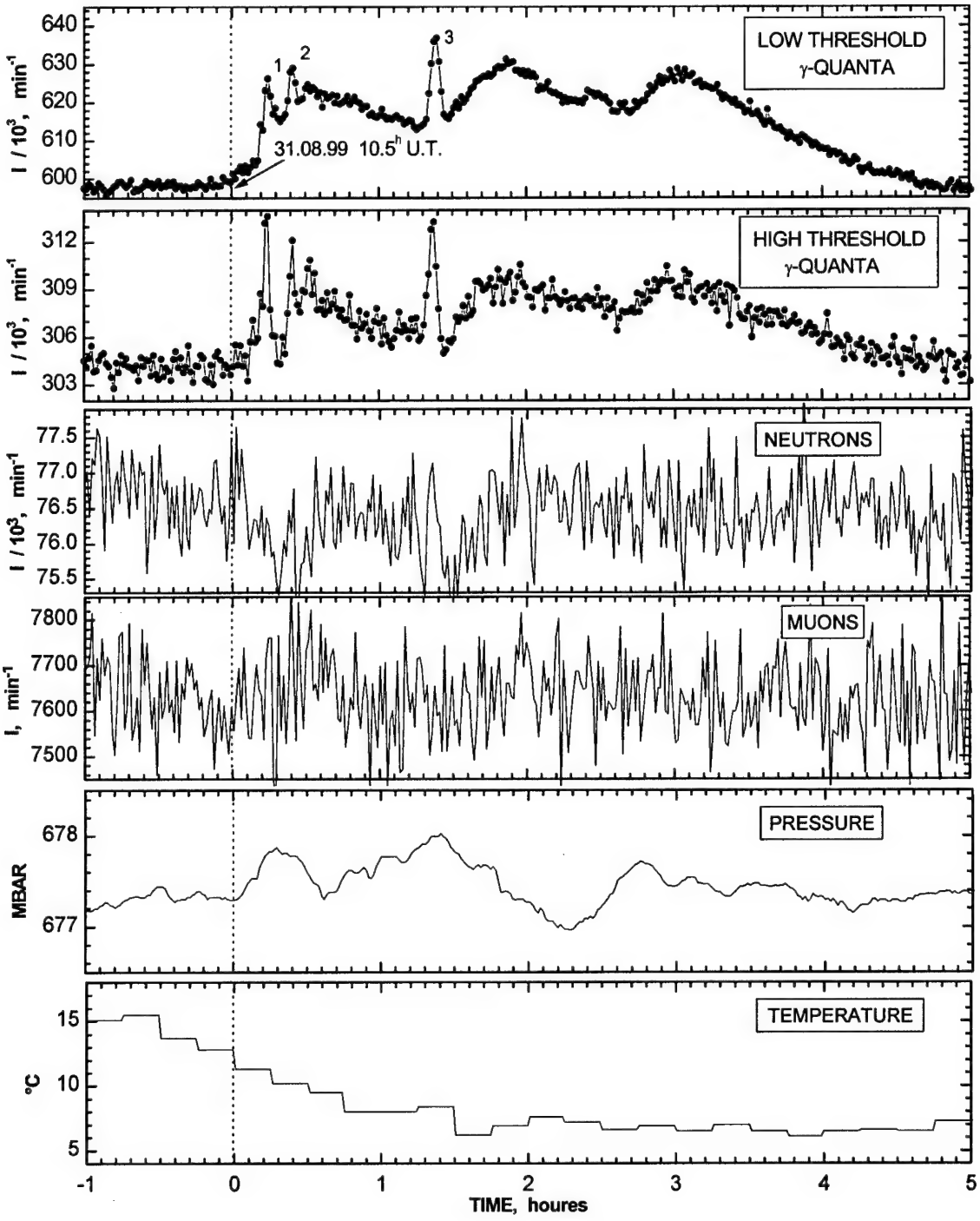

Figure 4.3.e. The behaviour of various cosmic ray components and atmospheric parameters during the thunderstorm on 31 August 1999.

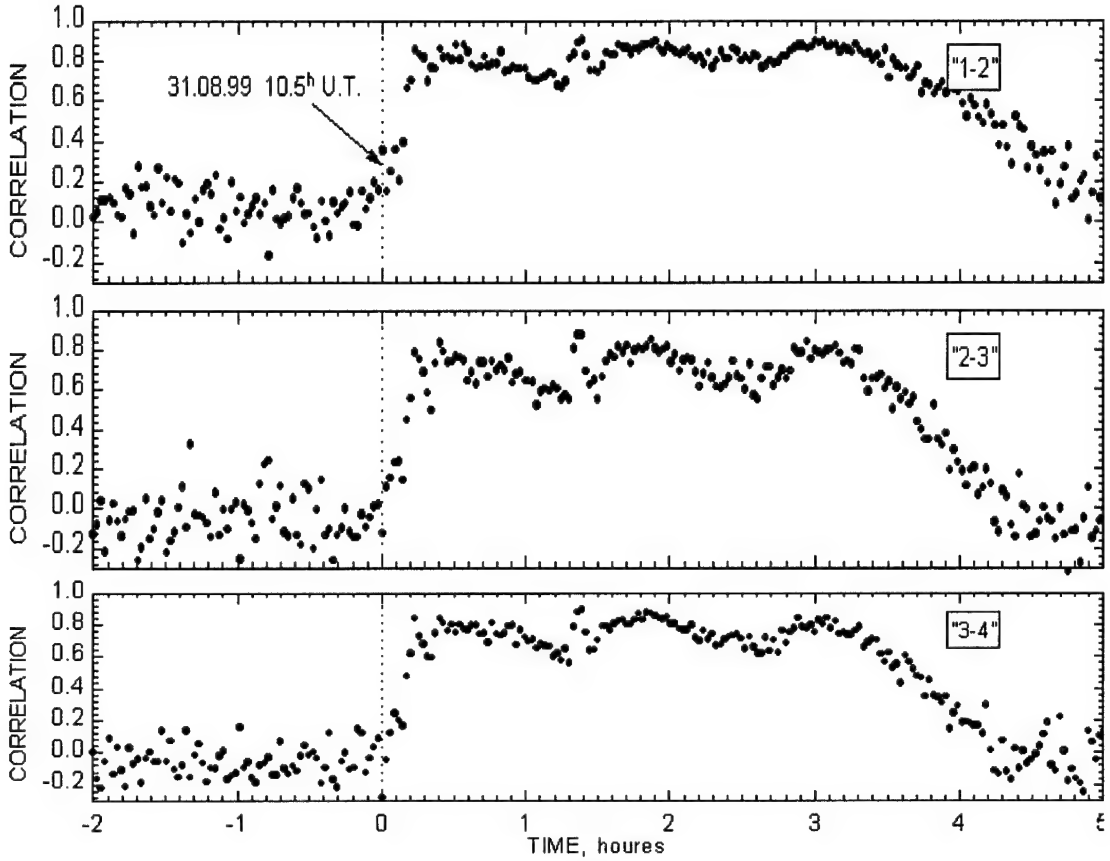

Figure 4.4. Time dependences of correlation coefficients C_{ij} for three detector pairs during the thunderstorm on 31 August 1999.

$$C_{ij} = \frac{\sum (n_i - < n_i >)(n_j - < n_j >)}{\sqrt{\sum (n_i - < n_i >)} \cdot \sqrt{\sum (n_j - < n_j >)}} ,$$

where each of i and j indices designates one of the low threshould detector points (i, j=1÷4, i≠j), n_i and n_j mean amounts of pulses obtained from bouth registration channels of i-th and j-th detector during of 1 sec intensity counting, $<n_i>$ and $<n_j>$ are the corresponding average values defined over the measurements immediately preceding thunderstorm moment. Summation in the above formulae was carried out during of 100 second length time periods.

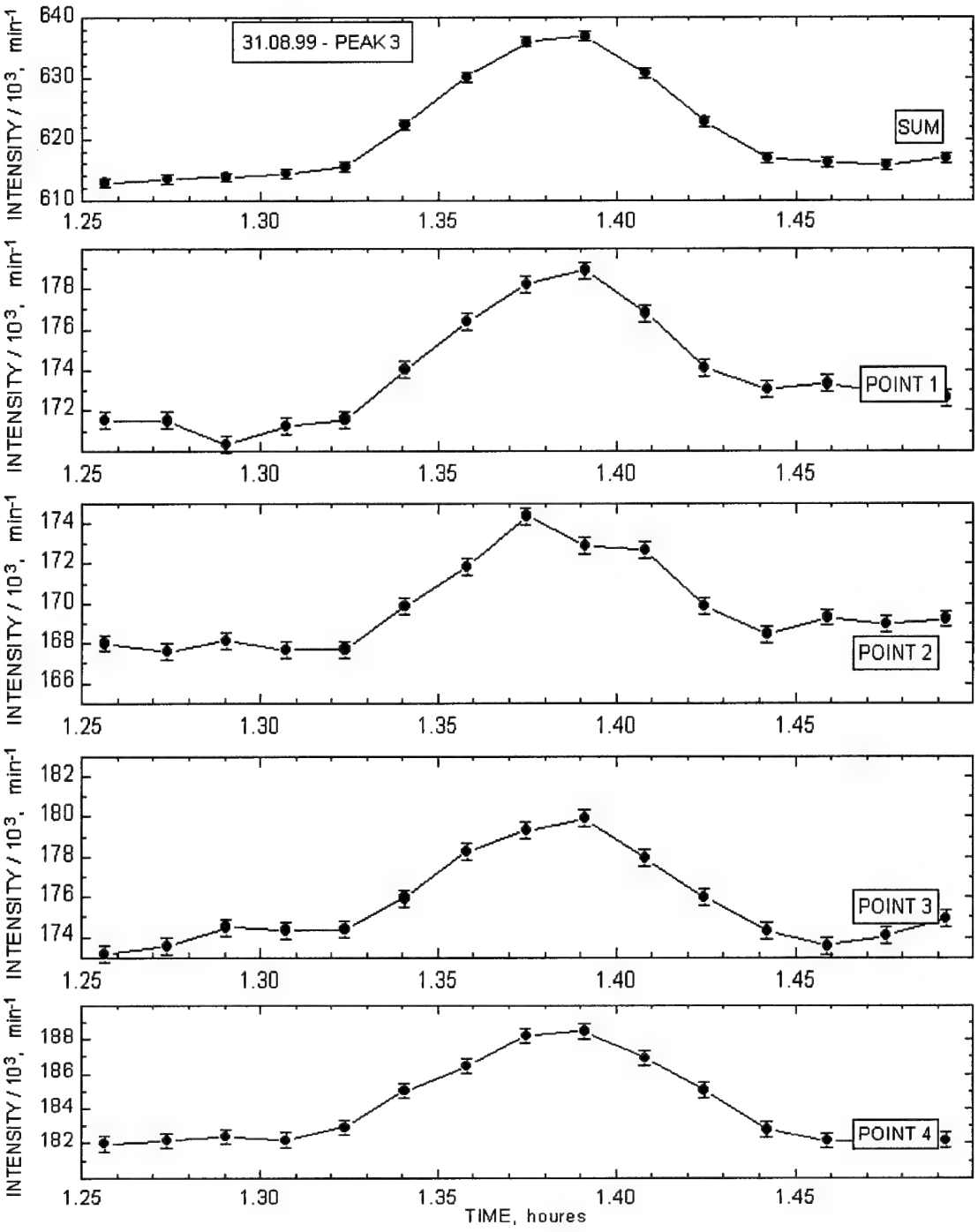

Figure 4.5. Short time low threshould emission intensity burst (peak 3) observed at different points during the thunderstorm on 31 August 1999.

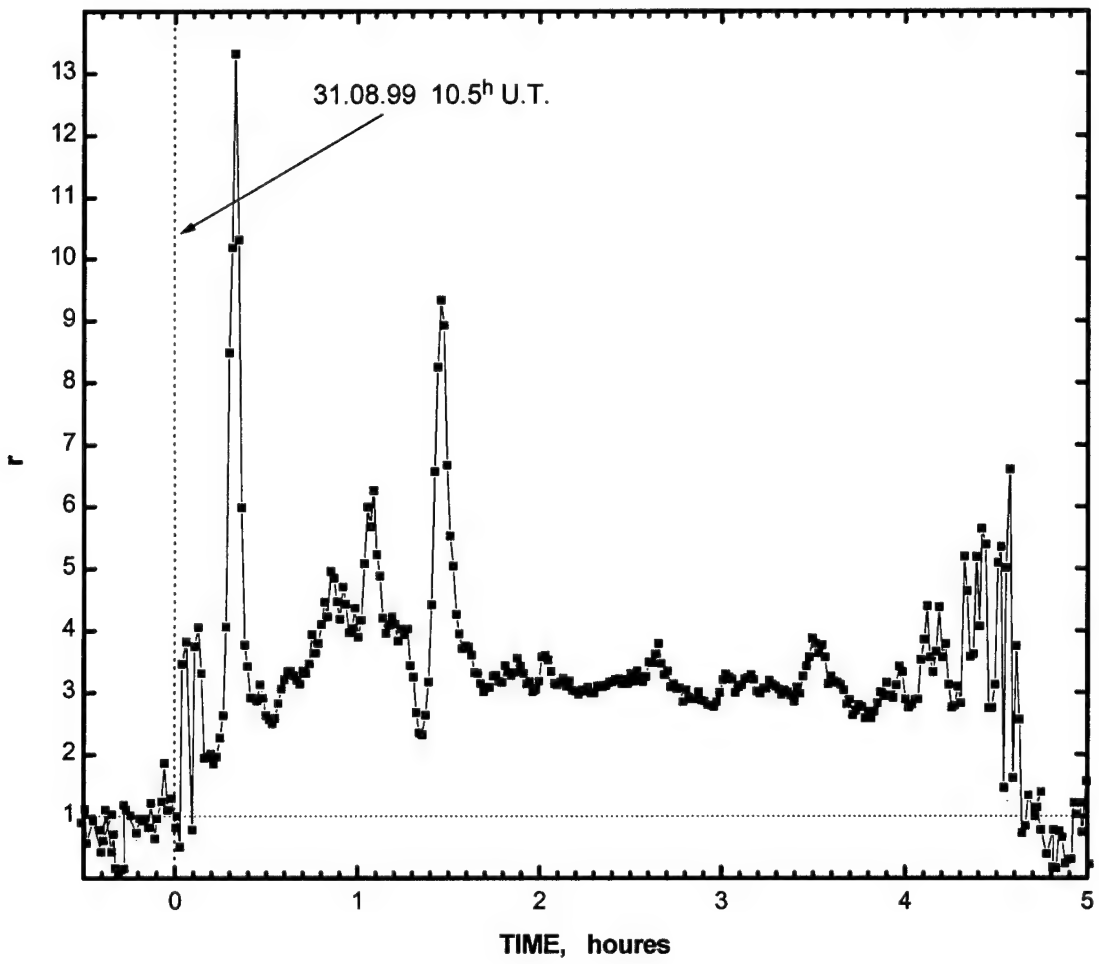

Figure 4.6. The excess relation of low threshold to high threshold data during the thunderstorm on 31 August 1999.

$$r = \left(\frac{I_{\text{low}}}{I_{\text{lowbackgr}}} - 1 \right) \Big/ \left(\frac{I_{\text{high}}}{I_{\text{highbackgr}}} - 1 \right)$$

Grant SPC 00-4040

Interum Report

Studies of Intensive X, γ and Optic Emission in Runaway Breakdown Process

This work is driven by intersection of two lines of activities in studying of the electromagnetic emission generated by the suprathermal electrons. We have addressed the following advanced problems in the grant proposal:

1. Theoretical investigation of runaway breakdown process in stationary electric field.
2. Investigation of runaway breakdown phenomena in laboratory installation in conditions of cyclotron resonance.
3. Investigation of an influence of combined effects of runaway breakdown and cosmic rays on lightning processes in thunderstorm atmosphere.

The following papers with the results of the investigations are prepared for publication:

1. Gurevich A.V., H.C. Carlson, Yu.V.Medvedev and K.P.Zybin "Generation of electron - positron pairs in runaway breakdown".
2. Sergeichev K.F., I.A.Sychov "Pecularities of ICR air breakdown in mirror magnetic trap."
3. Chubenko A.P., Antonova V.P., Kryukov S.Yu., Piskal V.V., Ptitsyn M.O., Shepetov A.L., Vildanova L.I., Zybin K.P., Gurevich A.V. "Intensive X-ray Emission Bursts During Thunderstorm"

1. Theoretical investigation of runaway breakdown process in stationary electric field

1.1 Abstract

The full kinetic theory of runaway breakdown for electrons at high energy range is developed. The theory takes into account both ionization and bremsstrahlung processes. The electron–positron pairs generation is studied. The possibility to observe e^+e^- annihilation line during intensive discharges in atmosphere is predicted.

1.2 Introduction

Runaway breakdown is a new phenomena determined by the effect of constant electric field at high energy ($\varepsilon \geq 100$ Kev) electrons [1]. Its physical mechanism is deeply related to the Coulomb character of neutral molecules ionization by high energy electrons: collisional crossection σ in nonrelativistic region drops rapidly with energy increase $\sigma \propto 1/\varepsilon^2$. Thus fast electrons in the presence of electric field $E > E_c$ (E_c – critical field) are able to become runaways: in other words they can be accelerated by the electric field. Accelerated electrons produce a number of low energy electrons by ionization of neutral molecules. In addition, a small number of high energy electrons may be generated. These electrons become runaways also if their energy exceeds critical value $\varepsilon_c \sim mc^2(E_c/E)$. Being accelerated, they produce another generation of fast runaway electrons and the process is ongoing, i.e. as a result an avalanche of runaway electrons starts. Exactly this process is called "runaway breakdown". It is determined by multiplication and acceleration of fast electrons. The exponential growth of the runaway electrons number characterizes the development of the avalanche and absorption of electromagnetic energy by discharge.

The kinetic theory of runaway breakdown was developed previously [2-5]. In these papers electrons with not very high energies ($\varepsilon \leq 5$ MeV) were considered. The goal of the present work to provide the full kinetic description of runaway breakdown effect for high energies also. We will demonstrate that at high energies the main role in runaway breakdown process is played not by ionization Coulomb collisions, but by much more stronger bremsstrahlung effect. The structure of electron distribution function at high energies would be determined. The role of energy distribution of initial fast electrons triggering the runaway avalanche will be examined in details. The generation of electron - positron pairs during runaway breakdown will be studied as well. It would be demonstrated, that the last process is quite effective what allows to predict the possibility to observe e^+e^- annihilation γ-line during powerfull atmospheric discharges.

1.3 Kinetic theory of runaway breakdown at high energies

At high energies to describe the runaway breakdown it is necessary in addition to ionization effect take into account bremsstrahlung processes for electrons, additional ionization by high energy photons and Compton effect for photons. To estimate the influence of all these processes let us first discuss kinetic equations for electrons and photons in a simple "τ" approximation

$$\frac{dn_{ph}}{dx} = -\frac{n_{ph}}{l_c} + \frac{n_e}{l_{br}} \qquad (1)$$

$$\frac{dn_e}{dx} = -\frac{n_e}{l_I} + \frac{n_{ph}}{l_c} \qquad (2)$$

$$\frac{1}{l_c} \approx \pi N_m r_0^2 \frac{1}{\gamma} \ln(2\gamma) \qquad \frac{1}{l_I} \approx 2\pi N_m Z r_0^2 mc^2 \ln\left[\frac{\gamma^2 (mc^2)^2}{I^2(Z)}\right] \qquad (3)$$

$$\frac{1}{l_{br}} \approx 4\pi\alpha Z^2 r_0^2 \ln(2\gamma)$$

Here n_e and n_{ph} – number densities of electrons and photons, N_m and Z – number density of molecules and full charge of their nucleas, $\alpha = e^2/\hbar c$ is a fine structure constant, $r_0 = e^2/mc^2$ – classical radius of electron. The first term in (1) describes the absorbtion of photons because of Compton effect, l_c is Compton absorption length, the second term in (1) describes the photon generation due to bremsstrahlung (l_{br} is the length of generation of photon). The first term in (2) describes the ionization of neutral moleculas by fast electrons (l_I – ionization length, $I(Z)$=13.5 Z eV), and the second one by photons.

Let us first compare the ionization and Compton terms (3). Analyzing the equations (1) and (2) it is possible to show, that in conditions

$$\gamma \ln^2(2\gamma) << (\pi/\alpha Z) \ln^2[2^{1/2} mc^2/I(Z)] \qquad (4)$$

the avalanche is determined mostly by ionization process. In this work condition (4) is supposed to be fulfilled always.

The full kinetic equation describing the runaway breakdown process takes inconditions

(4) the following form [6].

$$\frac{\partial f}{\partial t} = \mathrm{e}\,\mathrm{E}\left\{\mu\frac{\partial f}{\partial p} + \frac{1-\mu^2}{p}\frac{\partial f}{\partial \mu}\right\} = St(f) + S_I(f)$$

$$St(f) = \frac{1}{p^2}\frac{\partial}{\partial p}\left(p^2\left(F_D + F_{br}\right)f(p,\mu)\right) + \upsilon(p)\frac{\partial}{\partial \mu}\left[\left(1-\mu^2\right)\frac{\partial f(p,\mu)}{\partial \mu}\right] \qquad (5)$$

$$\mathrm{F_D} = \frac{4\pi Z e^4 N_m}{mc^2}\frac{\gamma^2}{\gamma^2 - 1}a \qquad \upsilon(p) = \mathrm{F_D}\frac{\xi}{4\gamma p} \qquad \xi = \sum_{i=1}\frac{Z_i^2}{Z} \qquad a \approx 11$$

$$S_I = N_m v \frac{2\pi Z c^4}{mc^2}\int_{\varepsilon}^{\infty}\frac{\gamma'^2}{\gamma^2 - 1}\left[\frac{1}{\varepsilon^2} + \frac{1}{\left(W + mc^2\right)^2}\right]\int\frac{d\phi}{2\pi}\int f(W,\mu',\phi)\delta(\mu_1 - \mu_0)d\mu_1 dW$$

$$\mu' = \frac{\mu\mu_1 \pm (1-\mu_1^2)^{1/2}\sin\phi\sqrt{\mu_1^2 - \mu^2 + (1-\mu_1^2)\sin^2\phi}}{\mu_1^2 + (1-\mu_1^2)\sin^2\phi}$$

$$\mu_0 = \left[\varepsilon(W + 2mc^2)/W(\varepsilon + 2mc^2)\right]^{1/2}$$

Here $f(p,\mu,t)$ is the electron distribution function, p – electron momentum, E – electric field, $\mu = (\boldsymbol{E}\,\boldsymbol{p})/(E\,p)$ – cosine of pitch angle. The integral St describes collision of fast electrons with atomic electrons and nucleus. F_D and F_{br} is friction forces of electron determining energy losses due to ionization and bremsstrahlung:

$$F_{br} = \left\langle \frac{d\varepsilon}{dt} \right\rangle = -4\alpha N_m Z_i^2 \frac{e^4}{m^2c^4} \varepsilon v \{\ln(2\gamma) - 1/3\} \qquad (6)$$

Here Z_i is nucleus charge.

The second term in (5) describes pitch angle scattering of runaway electrons. Term S_I describes appearance of a new born runaway electrons, γ – Lorentz factor of electron, ε and W – kinetic energy of fast electron $\varepsilon = mc^2(\gamma - 1)$, $W = mc^2(\gamma' - 1)$.

At Fig.1.1 the full friction force is demonstrated. One can see, that the ionization plays the main role at low energies $\varepsilon \leq 5$ MeV. At $\varepsilon \geq 5$ MeV the dominant role belongs to bremsstrahlung force. The basic relation of the theory which determines the runaway boundaries $eE = F$ now has two roots. The first root $\gamma = \gamma_1$ determines as usual critical electron energy ε_c [1]. The runaway region lays between γ_1 and γ_2 . The second root is determined mainly by bremsstrahlung force. The runaway boundaries energies $\varepsilon_c = mc^2(\gamma_1 - 1)$ and $\varepsilon_{c2} = mc^2(\gamma_2 - 1)$ depend on relation E/E_c

$$\varepsilon_c \approx mc^2 \frac{E_c}{E} \qquad \varepsilon_{c2} \approx mc^2 \frac{\pi a}{\alpha Z_i \ln(2\gamma_2)} \frac{E}{E_c} \qquad E > E_c \qquad (7)$$

where

$$E_c = \frac{F_{\min}}{e} = \frac{4\pi Z_i e^3}{mc^2} a \qquad (8)$$

F_{min} is the minimal drag force of electrons [1]. One can see from (7), that the width of runaway region

$$\Delta\varepsilon_r = \varepsilon_{c2} - \varepsilon_c \approx \varepsilon_{c2} \approx mc^2 \frac{\pi a}{\alpha Z_i \ln(2\gamma_2)} \frac{E}{E_c}$$

The highest energy ε_{c2} which can be reached by runaway electron is growing with E/E_c approximately linearly: at $E/E_c = 5$ it reaches the value *430 MeV*, *at* $E/E_c = 10$ – the value *850 MeV*. This values are fully determined by bremsstrahlung force. We note, that in previous papers the term (6) was omitted. It means that kinetic theory was considered in [1] for low energy diapason $\varepsilon << \varepsilon_{c2}$ only.

Analyzing collision integral we see that pitch angle scattering due to relativistic growth of electron mass with energy increase falls down more efficient than drag force. So, it could be neglected if conditions

$$\frac{\xi}{4\gamma} << 1 \qquad (9)$$

are fulfilled. At such conditions pitch angle scattering is not significant and due to this the distribution function becomes strongly directed along electric field (see [7]). Thus one can consider one dimensional – integrated over angles distribution function.

$$f_0(\gamma) = \frac{1}{2}\int_{-1}^{1} f(\gamma,\mu)d\mu$$

Introducing dimensionless variables γ t^*,

$$\gamma = \sqrt{\left(\frac{p}{mc}\right)^2 + 1}, \qquad t^* = \frac{t}{t_0}, \qquad t_0 = \frac{m^2c^3}{4\pi e^4 Z N_m a} \qquad (10)$$

we finaly obtain:

$$\frac{\partial}{\partial\gamma}\left\{\left[\left(\gamma^2-1\right)\left(\phi_D+\kappa_{br}\right)-\delta_E\right]f_0\right\}=\gamma\sqrt{\gamma^2-1}\frac{\partial f_0}{\partial t}-S_I(f_0) \qquad (11)$$

$$\phi_D=\frac{1}{a}\frac{\gamma^2}{\gamma^2-1}\left[8.4+\frac{1}{2}\ln(\gamma^2-1)+\frac{1}{2}\ln(\gamma-1)-0.347\left(\frac{2}{\gamma}-\frac{1}{\gamma^2}\right)+\frac{1}{2\gamma^2}+\frac{(\gamma-1)^2}{16\gamma^2}\right]$$

Here $\delta_E=E/E_c$ is electric field parameter, function φ_D:
determines dimensionless ionization losses and:

$$\kappa_{br}=\frac{\alpha Z\gamma}{\pi a}\left(\ln(2\gamma)-\frac{1}{3}\right)$$

– bremsstrahlung losses.
The ionization term takes a simple form:

$$S_I=N_m v\frac{2\pi Ze^4}{mc^2}\int_{\varepsilon}^{\infty}\frac{\gamma'^2}{\gamma^2-1}\left\{\frac{1}{\varepsilon^2}+\frac{1}{\left(W+mc^2\right)^2}\right\}f_0(W)dW \qquad (12)$$

Thus in a high energy range due to relativistic growth of the electron mass its scattering by atomic neucleus is weak enough and the distribution function of energetic electrons became strongly alongated along electric field. It allows to use kinetic equation in a more simple form (11), (12).

1.4 Time development of distribution function

The threshold field for runaway breakdown E_c is usually much less than for conventional breakdown E_t. As an example for air and for hydogenium $E_c/E_{th} \sim 0.1$. On the other hand to excite runaway breakdown one needs fast electrons with energies $\varepsilon > \varepsilon_c$. That determines an important difference between runaway and conventional breakdown. How the time development of distribution function depends on the existance of fast electrons or more generally on initial function $f_0(\gamma)$? The problem was studied numerically. The numerical soutions were obtained in runaway region ($\gamma < \gamma_{c2}$) by predictor – corrector and Crank – Nickolson methods with boundary condition $f(\gamma_{c2})=0$. Both methods demonstrates identical results. To determine the dependance of runaway process on the energy of seed electrons the initial function $f_0(\gamma)$ was taken usually close to delta function $f_0(\gamma) \propto \delta(\gamma-\gamma^*)$.

Results of numerical calculations of equation (11) are demonstrated at the Fig.1.2 – Fig.1.5. We see from Fig.1.2, that at $\gamma^* < \gamma_1$ (or $\varepsilon^* < \varepsilon$) independing on the value of electric field ($E > E_c$), the initial distribution function dissapears in time and initial number density of electrons N_e falls down exponentially. So, without seed fast electrons runaway breakdown does not exist.

On the contrary, if $\gamma^* > \gamma_1$ the runaway breakdown is effectively developing. Its main features seen from Fig.1.3: independently on the value γ^* the distribution function at low energies develops very fast to its quasistationary state

$$f(\gamma,t)=F_0(\gamma)\, e^{\lambda t} \qquad (13)$$

The typical time of this process

$$t_1 \sim \lambda^{-1} \qquad (14)$$

At the high energy range ($\gamma \geq \gamma^*$) the establishing of quasistationary solution is much more slow and takes time

$$t_2 \sim (\gamma_2-\gamma^*)/(\delta_E-1) \qquad \delta_E > 1.2 \qquad (15)$$

Note that the time t_2 is diminishing with the growth of γ^* and at $\gamma^* \geq \gamma_2$ its became an order of t_1.

The established asympthotic solution takes the exponential form (13) quite analogous to the conventional breakdown. It is natural, because runaway breakdown is described by linear equation. Stationary asympthotic distribution function $F_0(\gamma)$ is shown at Fig.1.4. for different values of parameter δ_E. One can see, that function F_0 falls down monotonically with γ, sharply increasing at small energies $\varepsilon = mc^2(\gamma-1)$ and disappearing at the second runaway boundary $F_0(\gamma_2) = 0$. The behaviour of asympthotic solution F_0 could be studied analytically. The analytical analysis of equation (5) shows that ionization integral and friction term are most essential at small energies. The balance of these terms gives asymptotics at $\varepsilon \to 0$

$$f \propto \varepsilon^{-1+1/a}.$$

In intermediate energy range $\gamma_1 << \gamma << \gamma_2$ the distribution function falls down exponentially

$$f \propto \exp\left\{-\frac{\lambda}{\delta_E} u\right\} \qquad u = \sqrt{1-\frac{1}{\gamma^2}}$$

To determine cutoff the distribution function near right stationary point γ_2 we can neglect the ionization term. Expanding friction force near this point we can find the solution

$$f \propto \left(1-\frac{q}{\delta_E}\mu p\right)^{\frac{\lambda}{q}-3} \qquad 1-\frac{q}{\delta_E}\mu p > 0 \qquad p = mc\gamma$$

Here $q = \left.\frac{dF_D}{d\gamma}\right|_{\gamma=\gamma_2}$. These results are in agreement with numerical simulation.

1.5 The avalanche rate

One of the most important parameter of breakdown is the avalanche rate. The increasing of number density of electrons N(t) is shown for different beam energies γ^* at Fig.1.5. We see that the asympthotic solution demonstrates exponential growth with parameter λ:

$$N(t) = N_0 e^{\lambda t}$$

We investigated the dependence of avalanche rate λ on dimensionless electric field δ. The results are shown at Fig.1.6. For high enough values of δ this behavior is well fitted by the law:

$$\lambda = 0.064\ \delta^{3/2} \qquad (16)$$

Note that as seen from Fig.1.5. the asympthotic time behaviour of electron density does not depend on on the initial distribution function (if $\gamma^* > \gamma_c$) in agreement with (13). Some small difference in $N(t)$ is seen in the begining of the process at time scale of the order of t_1 (14). We see, that the full time of establishment of distribution function (15) is not significant — electron density growth is going with the same avalanche rate from the very begining. It means that the avalanche process practically does not depend on the established distribution function $F_0(\gamma)$ in the whole breakdown region. The dominant role is played by its initial part in the vicinity of the left stationary point — the first root γ_1. In

other words, only the region near critical energy ε_c determines the avalanche rate. This fact is in agreement with qualitative theory [1].

Basing on this analysis we can estimate analytically the avalanche rate. Really, near left stationary point it is possible to consider nonrelativistic approximation. In this approximation the kinetic equation (5) is reduced to the form:

$$\frac{\partial f_0}{\partial t} = \delta_E \frac{1}{u^2}\frac{\partial}{\partial u}\left(u^2 f_0\right) = \frac{1}{u^2}\frac{\partial f}{\partial u} + \frac{1}{au^5}\int_u^\infty f_0(w)w dw, \qquad w = \sqrt{1-\frac{1}{\gamma^2}} \tag{17}$$

There is an important property of the equation (17) – it allower to eliminate the electric field δ_E. Introducing variables

$$\tau = 2t\delta_E^{3/2}, \qquad v = u\sqrt{\delta_E}$$

one can find

$$\frac{\partial f_0}{\partial \tau} + \frac{1}{v^2}\frac{\partial}{\partial v}\left(v^2 f_0\right) = \frac{1}{v^2}\frac{\partial f}{\partial v} + \frac{1}{av^5}\int_v^\infty f_0(w)w dw \tag{18}$$

Searching exponential solution of equation (18) $f_0 = f e^{2\tau\sigma/a}$ we reduce it to the form:

$$(1-y)\Phi'' - \left(\frac{\sigma}{a}\sqrt{y}+1\right)\Phi' - \frac{\Phi}{4ay^2} = 0 \tag{19}$$

Here $\Phi = \int_u^\infty f(w)w dw$, and variable $y = v^2 = u^2\delta_E$.

Note, that parameter a determined by (5) could be cosidered in equation (19) as a large parameter. For $a \to \infty$ we have from (19)

$$(1-y)\Phi'' - \Phi' = 0 \qquad \Phi = C_0 \ln(y-1) + C_1$$

This solution is not valid for $y \to \infty$ and $y \to 1$. To match this solution let us return to the finite big values of parameter a and use an expanding variables introducing z as $y = a^2 z$.
The equation (19) takes the form:

$$\frac{1}{a^2}(1-a^2 z)\Phi_{zz} - (\sigma\sqrt{z}+1)\Phi_z - \frac{\Phi}{4a^3 z^2} = 0$$

For $a \to \infty$ its solution is

$$\Phi_z = A_0 \frac{e^{-2\sigma z}}{z}$$

Using a procedure of matching solution [8] we find "combined" solution which is good with exponential accuracy everywhere except the vicinity of point $y=1$:

$$\Phi_y = \frac{e^{-2\sigma\sqrt{y}/a}}{y-1} \tag{20}$$

In the vicinity of $y=1$, introducing x: $y = 1 + x\,a^{-1}$ we find the solution

$$\Phi = e^{-\frac{x}{4}}$$

It means that solution (20) is cut at $u_*^2 = 1 + 4/a$. As we shall see below this cutting defines the avalanche rate with logarithmic accuracy. Integrating (18) from u_* to ∞, one can find:

$$\sigma \ln\left(\frac{a^3}{16\sigma^2}\right) = \frac{1}{2}\ln\left[\frac{a}{2}\left(1+\frac{2}{a}+\sqrt{1+\frac{4}{a}}\right)\right] + \left(1+\frac{4}{a}\right)^{-\frac{1}{2}} + O\left(\sigma/a\right) \tag{21}$$

This algebraic equation defines parameter $\lambda=2\sigma\delta^{3/2}/a$. For $a=11$ the solution of (21) gives

$$\lambda \approx 0.055\ \delta^{3/2}$$

This result is in a good agreement with numerical calculations (16). More than that it is in agreement with previous numerical solution of kinetic equation in the low energy limit [2-5] and with approximate qualitative theory [1]. The reason of this agreement is in the fact that main role in ranaway breakdown process plays the low energy runaway boundary ε_c.

1.6 e^+ e^- generation

The distribution function of runaway electrons falls down rather slow (see(20)). It means that fast electrons generates intensive flux of X and γ photons due to bremsstrahlung process. The high energy photons can generate electron - positron pairs.

The process of X and γ generation by fast electrons in neutral gas is well known. The total number of photons could be estimated using emissivity q_γ [9]

$$\frac{dN_\gamma}{dt}=\frac{q_\gamma}{\varepsilon}cN_mN_\varepsilon \qquad q_\gamma \approx 4Z^2\alpha r_0\varepsilon$$

Here N_e – the number density of fast electrons which generate bremsstrahlung emission and N_m – density of neutrals.

The crossection of $e^\pm$ generation is quite analogous to Bethe and Heitler bremsstrahlung crossection [9]

$$d\sigma=-\frac{Z^2\alpha r_0}{2\pi}\frac{m^2p_+p_-d\varepsilon}{\omega^3q^4}\sin\theta_+d\theta_+\sin\theta_-d\theta_-d\phi\times D \qquad (22)$$

$$D=\frac{p_+^2}{\kappa_+^2}(4\varepsilon_-^2-q^2)\sin\theta_+ +\frac{p_-^2}{\kappa_-^2}(4\varepsilon_+^2-q^2)\sin\theta_- -\frac{2\omega^2}{\kappa_+\kappa_-}(p_+^2\sin^2\theta_+ + p_-^2\sin^2\theta_-)-$$

$$-\frac{2p_+p_-}{\kappa_+\kappa_-}(2\varepsilon_+^2+2\varepsilon_-^2q^2)\sin\theta_+\sin\theta_-\cos\phi$$

Here

$$\kappa_\pm=\varepsilon_\pm-p_\pm\cos\theta_\pm, \qquad q^2=(\boldsymbol{p}_+ + \boldsymbol{p}_- - \boldsymbol{k})^2, \qquad \varepsilon_+ + \varepsilon_- = \omega$$

Integrating this crossection we can estimate the $e^\pm$ production

$$\frac{dN_{e\pm}}{dt}=\sigma_\pm cN_mN_\gamma \qquad \sigma_\pm \approx \frac{22}{9}Z^2\alpha r_0$$

Taking into account that N_e grows exponentially with t, we find :

$$\frac{N_{e\pm}}{N_\gamma}\approx\frac{7}{9}\frac{N_\gamma}{N_e} \qquad (23)$$

This relation determines the number of generated e^+e^- pairs.

To estimate the emission intensity of the e^+e^- annihilation line intensity generated during thunderstorm it is natural to compare with the results of observations γ - burst from high altitude lightning at "Compton" observatory. According to Fishman et al [10] and Nemiroff et al. [11] the flux of gamma quants in energy diapason 300 ÷ 1000 KeV observed by BATSE at the heights 500 km was of the order of 100 photons/cm^{2}s. Using relation (23) and taking into account that $N_\gamma/N_e \sim \alpha \sim 10^{-2}$ one can estimate the flux of photons from e^+e^- annihilation at the distance 100 km from the source as 20 photons/cm^{2}s. Taking into account that the width of unihilation line is narrow one can suppose that the γ-quants generated during thunderstorm could be detected in experiments.

1.7 References

[1] A.V.Gurevich, G.M.Milikh and R.Roussel-Dupre Phys.Lett.A **165** (1992), 463 – 468.

[2] R.A.Roussel - Dupre, A.V.Gurevich, T. Tunnell, G.M.Milikh Phys.Rev.E **v.49**, N3, 1994 (2257 – 2271)

[3] N.G.Lehtinen, T.E.Bell V.P.Pasko, U.S. Inan GRL **24**, 2639, 1997

[4] L.P.Babich, I.M.Kutsyk, E.N.Donskoy, A.Yu.Kondratiev Phys.Lett.A **245**, 460, 1998

[5] E.Symbalisty, R.Roussel - Dupre, L.Babich, I.Kutsyk, E.Donskoy, A.Kudryavtsev EOS Trans. AGU, **46**, 4760, 1997

[6] A.V.Gurevich R.A.Roussel - Dupré and K.P.Zybin Phys.Lett.A Phys.Lett.A **237**, 240, 1998.

[7] A.V.Gurevich Sov.Phys. JETP **12**, 904, 1961.

[8] A.H.Najfe Introduction to Perturbation Techniques, Wiley-Interscience Publication NY 1980.

[9] L.D.Landau, E.M.Lifshits Quantum Electrodynamics Moscow Nauka 1980.

[10] J.Fishman et al. Science, **264**, 1313,1994.

[11] J.Nemiroff, J.Bounell, J.Norris JGR, **102**, 9659, 1997.

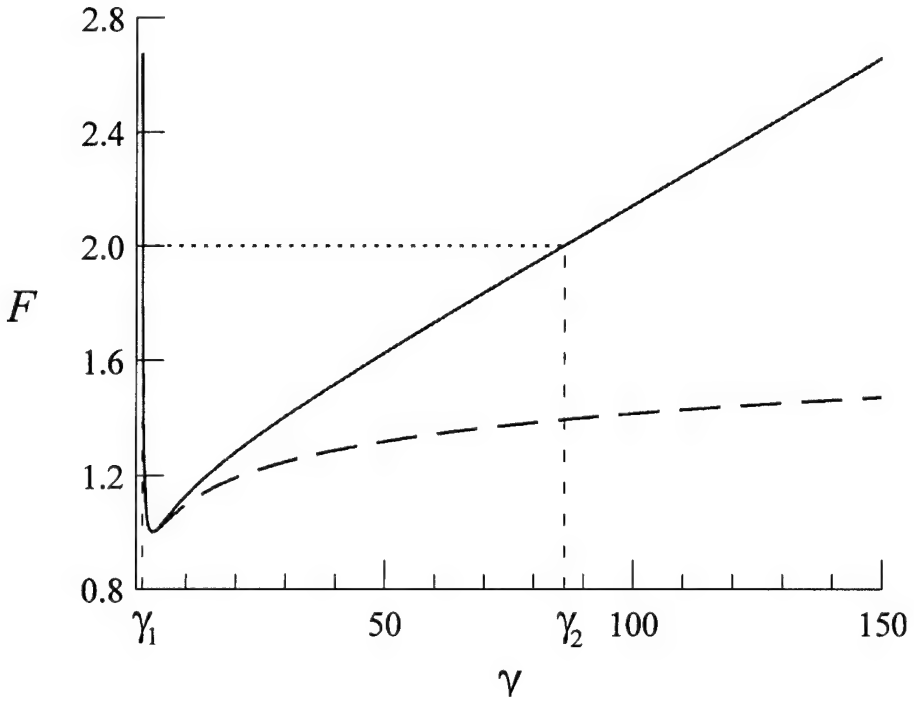

Figure 1.1 Dependence of the full friction force F on γ (solid curve). The dashed curev presents the friction force without accounting bremsstrahlung.

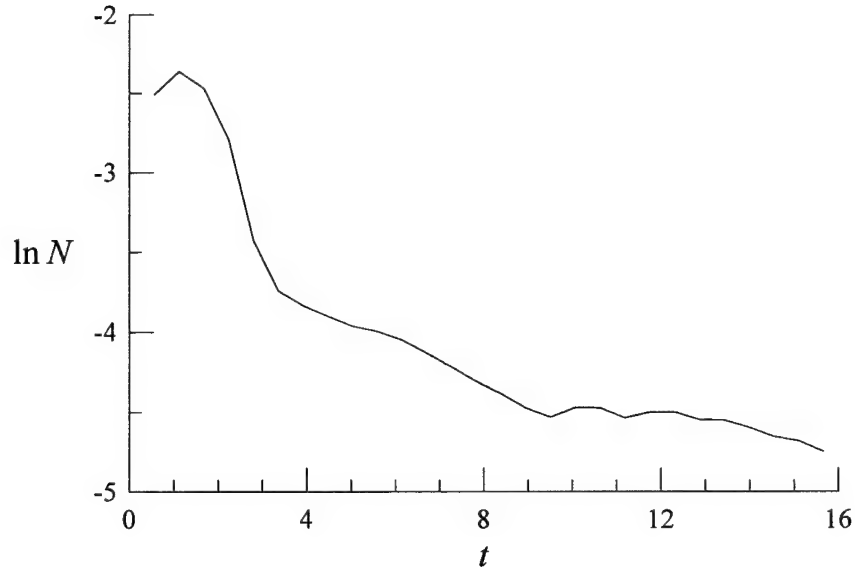

Figure 1.2 Logarithm of the full number of electrons N as a function of time in the case of $\gamma_b<\gamma_1$.

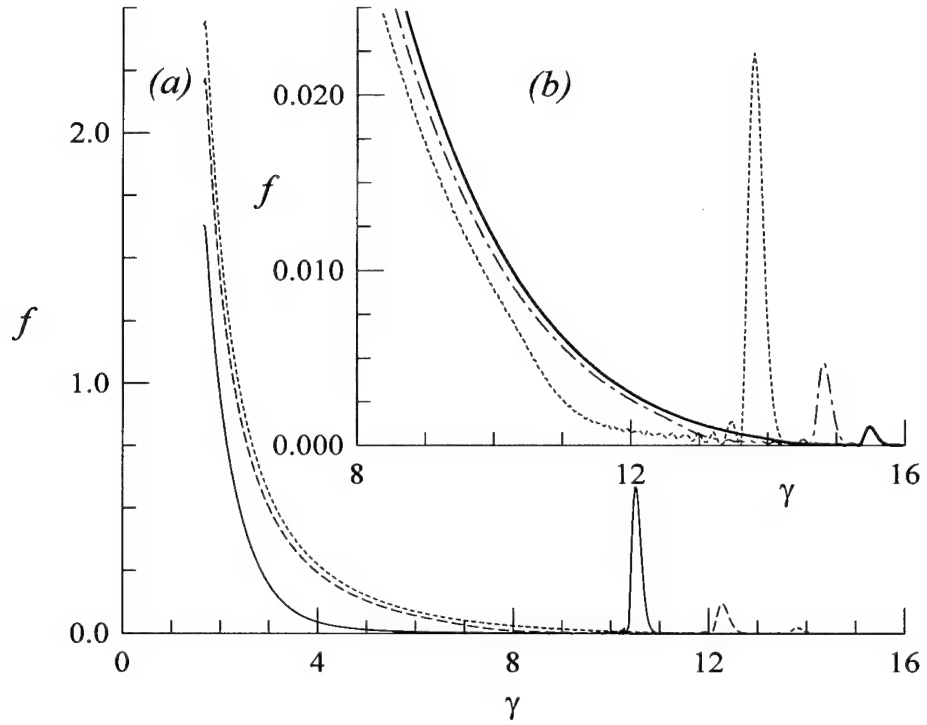

Figure 1.3 Distribution function $f(\gamma)$ at t=5.6 (solid), 28 (dashed), 56 (dotted), 84 (dot-dashed) and 112 (double solid) in the case of γ_b=10, δ=1.21.

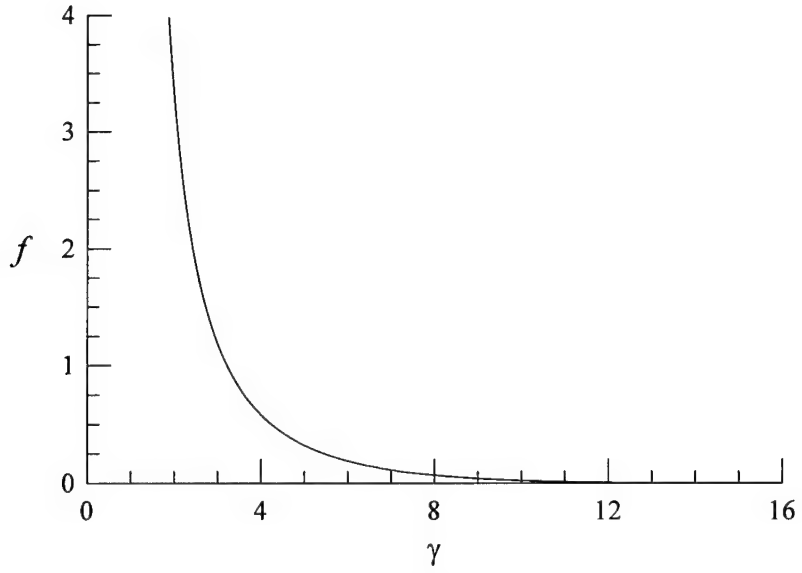

Figure 1.4 Stationary distibution function $f(\gamma)\exp(-\lambda t)$.

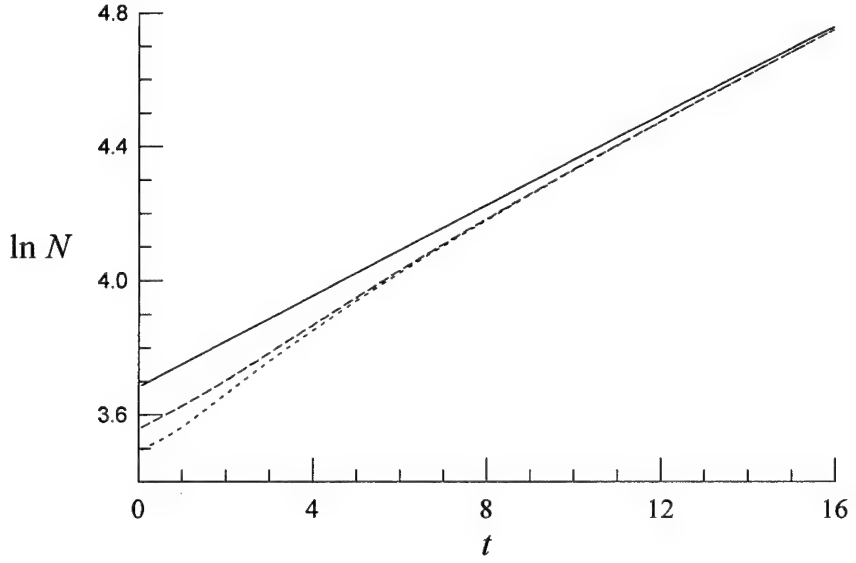

Figure 1.5 Logarithm of the full number of electrons N as a function of time for different positions of the beam of seed electrons $\gamma_b = 5$ (dotted), 10 (dashed) and 15 (solid)

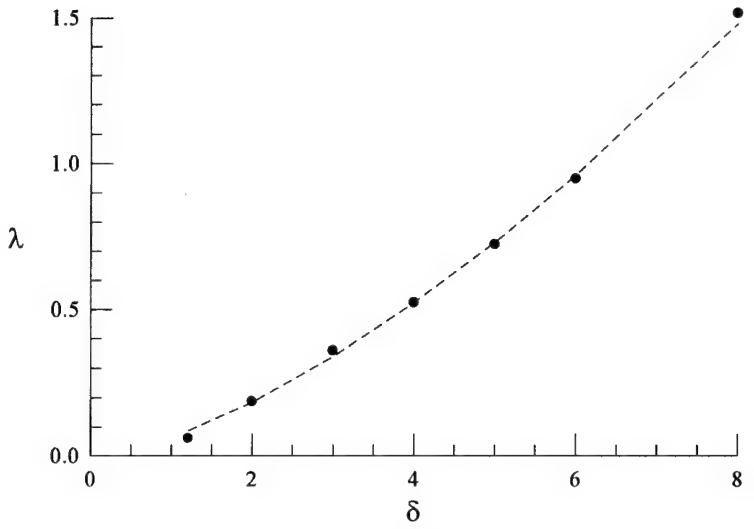

Figure 1.6 Dependence of λ on δ (symbols) in comparision with the fitting curve $\lambda=0.0654\delta^{3/2}$ (dashed curve)

2. Investigation of runaway breakdown phenomena in laboratory installation in conditions of cyclotron resonance

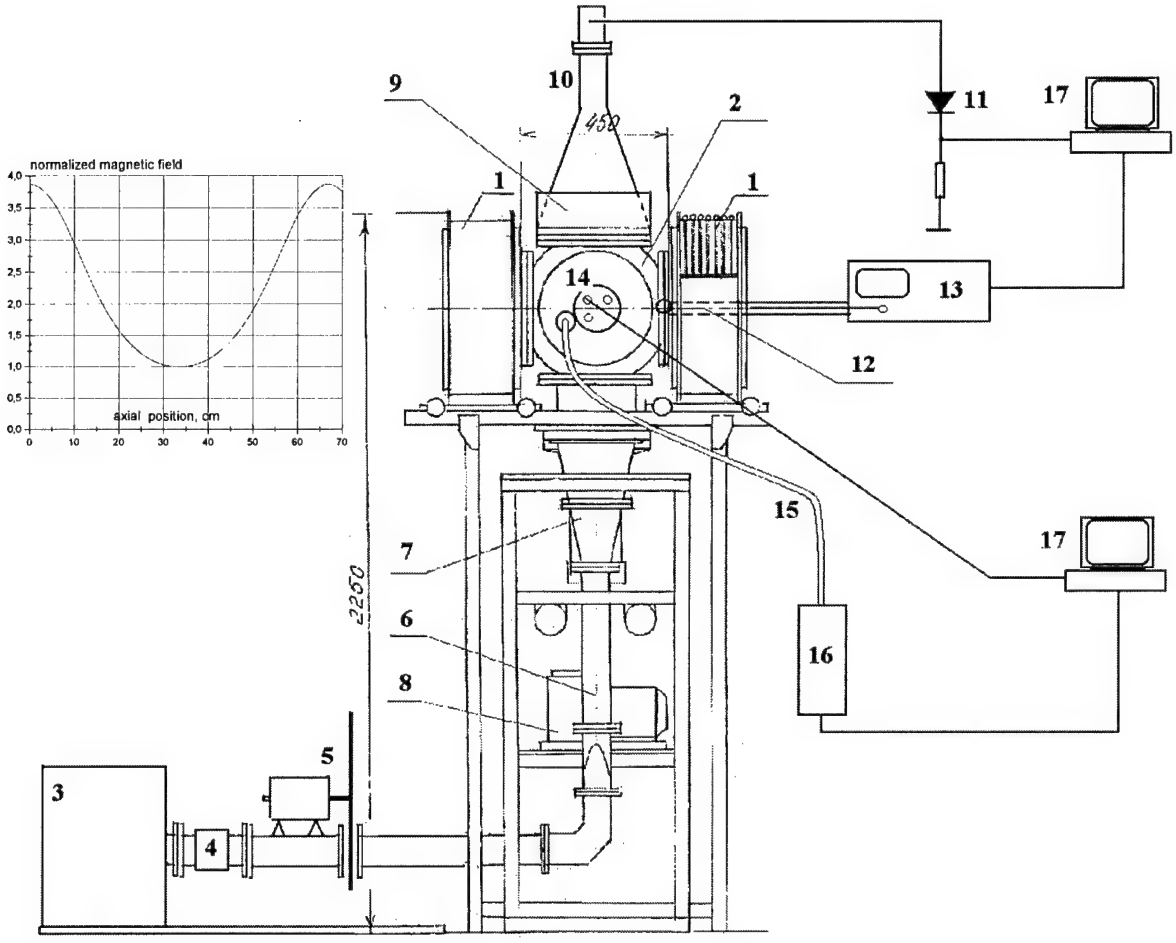

Fig.2.1. Scheme of the experimental setup: 1 – magnetic system; 2 – vacuum chamber; 3 – microwave generator; 4 – attenuator or isolator; 5 – obturator; 6 – waveguide components; 7 – horn coupler; 8 – vacuum pump; 9 – water attenuator section; 10 – horn antenna; 11 – detector; 12 – loop antenna; 13 – microwave receiver with spectrum analyzer; 14 – X-ray receiver; 15 – optic fiber; 16 – photomultiplier; 17 – data display system (computers).

The insertion demonstrates the magnetic field distribution in stationary state normalized to magnetic field in the center of vacuum chamber.

2.1 Setup description

The setup represented in Fig.2.1 includes a vacuum chamber 2 of quasispherical form, which has a the distance between a pair of opposite flanges 450 mm. The chamber is placed between two similar coaxial copper coils 1 of a static magnetic field. The magnetic field force line distribution inside the chamber has configuration of a bottle with two symmetric necks which forms a magnetic trap for collisionless electrons. The trapped electrons confinement time in the chamber is likely to be enough to confine a bulk of initial electrons of large energies during the time of run-away electrons breakdown in air. The magnitude of the static magnetic field at the center of chamber varies relative to value 875 Gs which corresponds to the ECR for the electric field frequency 2,45 GHz.

A magnetron 3 generates electromagnetic oscillations at the fixed frequency 2,45 GHz, with varying power up to 5 kW which creates the ECR accelerating field for electrons caught inside the mirror trap. The microwave power is transmitted into the chamber through a waveguide system 6 which consists of the adapter with pyrex window insulating vacuum of the chamber from athmosphere, the horn antenna 7, the circular waveguide with travelling TE_{11} mode, the smooth waveguide transition from a rectangular cross section to circular one, the rectangular waveguide elbow, the water attenuator or ferrite circulator 4. For purpose of pulse periodic regime realization it was made mechanical waveguide cutter off. The maximum microwave electric field strength at the center of vacuum chamber under condition of travelling wave at maximum power is $E_0 \approx 150$ V/cm. In the vicinity of the ECR the microwave electric field is equivalent to a static electric accelerating field for electrons.
Following experimental techniques for study of x-ray bremmsstrahlung radiation and optical radiation produced by the run away electrons and microwave synchrotron radiation at the harmonics of the accelerating field were used:

- Scintillation x-ray transducer 14 (BYCRON, model 2.5M2.5/3LP-X).

The transducer consists of NaJ(Tl) scintillator covered with aluminium cup of 1 mm thickness and combined with a photomultiplier. The optical axis of the transducer placed in the chamber was perpendicularly directed to the trap axis. The operating quantum energy range of the x- ray transducer 100 keV ÷ 1 MeV. Its signal was registered at a monitor of the PC «Pentium» by means of an oscillograph card.

- Photomultiplier 16 for observing of visible air glow discharge under action of both ECR-discharge and run away electrons.
- Personal x-ray doze meter (not shown) for measurement of x-ray spectrum outside the chamber. The operating quantum energy range of the counter 0,05 ÷ 1,5 MeV. Its error of doze power measurements is ± 30%; exposition time is 36 s; the dependence of doze measurements over the operating energy range is no more 45%.
- Microwave spectrum analyser 13 over the frequency range of 2-nd and 3-d harmonics for the base frequency of the microwave generator. Signals for the analyser were received from loop antenna 12 at end of a coaxial feeder introduced along the trap axis.
- Detector 11 for monitoring incident MW power.

2.2 Experimental Results

In the experiments with the described setup the intense X-ray emission was found to be generated under ECR discharge at the pressure range $< 10^{-4}$ Torr due to bremmsstrahlung radiation of electrons accelerated in relatively weak electric field E=5÷20 V/cm up to

subrelativistic energies 100÷300 keV. Simultaneously the MW synchrotron radiation at the second harmonic was observed. Its spectrum points out the presence bulk of electrons with energies ≤10 keV in the system. Specific feature was that the beginning of discharge visible emission owing to low energy part formation of electron spectrum (<100 eV) had a delay reaching 80 ms in respect to the appearance of X-ray and synchrotron signals. This allows to separate the whole process of the ECR breakdown into following two stages: first of which to be an initial stage of breakdown with participating of high energy run away electrons, and second one to be ordinary ECR discharge with participating of low energy electrons. Such separation is reasonable due to difference of physical processes resulting in the characteristic of electron distribution functions.It allows to find analogy of ECR breakdown with the model of runaway electron breakdown by Gurevich, Milikh and Roussel-Dupre applied for explanation of lightning mechanism in Earth atmosphere.
Recently interesting results were also observed in pulse mode of microwave power. Such mode can be achieved by regular cutting off the incident MW power with mechanical waveguide modulator. The preliminary results are shown in Fig.2.2.

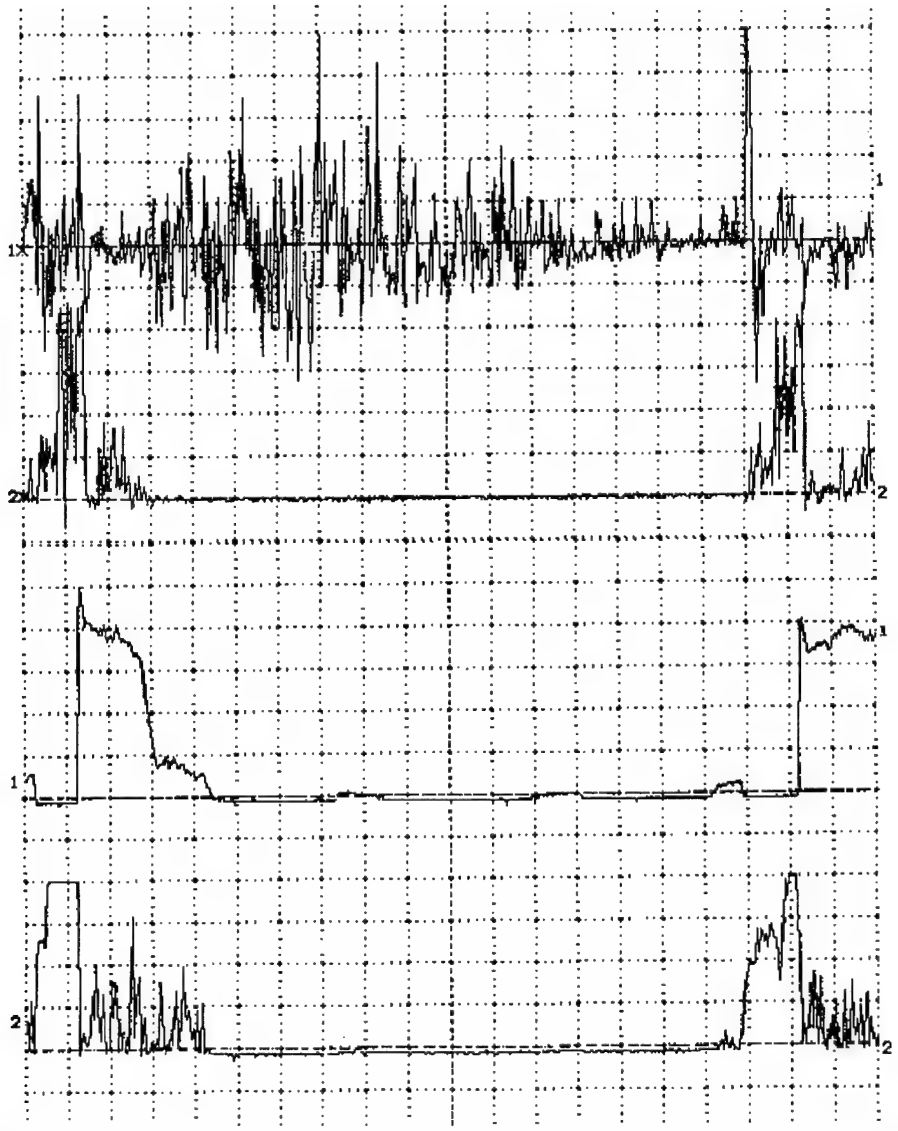

Fig.2.2. Oscillograms of pulse periodical mode operation: a – X-ray signal; b – II harmonic; c – visible light; d – transmitted MW power; $p = 5 \cdot 10^{-6}$ Torr.

Fig.2.3. The same as in Fig.2.2 but under air pressure 4 times more: $p = 2 \cdot 10^{-5}$ Torr.

One can see (Fig.2.2) that at air pressure $5 \cdot 10^{-6}$ Torr we always have a time delay visible light radiation of discharge in respect to the X-ray signal and the cut off transmitted MW radiation connected with that process of accumulation of low energy plasma with overcritical electron density.

The behavior of signals in Fig.2.3 corresponding to air pressure $2 \cdot 10^{-5}$ demonstrates the visible discharge is ahead in respect to the X-ray signal. However one can see the flickering of discharge when the incident microwave energy is redistributed between runaway electrons and low energy plasma.

The main objectives of our future work are detailed investigations of runaway electron breakdown taking into account its temporal and spatial dynamics, definition of energy characteristics of the process and energy balance, measurements of energy γ-quanta spectra depending on experimental conditions.

To study the dynamics of the discharge plasma density due to the RB a microwave interferometer (λ=8 mm) of opened resonator type will be constructed. The x-ray spectrometer in the energy range 30 keV - 1 MeV will be created with use of the X-ray scintillation detector (in our possession) and the μACE^{TM}-system (EG&G ORTEC) which consist of amplifier, multichannel analyzer plug-in card with emulation software(will be ordered to the ISTC). The averaged x-ray spectra depending on the regimes of the RB and optical spectra of the RB plasma will be studied. Both probe measurements and electron energy distribution function measurements with an electrostatic analizer for electrons leaving the magnetic trap will be carried out.

We intend to continue investigation with pulse mode of MW generation because it's reasonable to have the time limited action on the RB for study of its dynamics. For this purpose the waveguide modulator 5 (Fig.2.1) cutting off continuous microwave radiation was constructed. It allows to vary duration and period of pulses in wide range. The demands for the modulator was caused by the reason that MW generator is able to work in continuous mode generation, but not able to do it in pulse mode if to use pulse high voltage supply. Microwave pulses after the modulator have trapezoidal form with rise and fall time of order 1/3 of plateau. Owing to the pulse mode we hope to study lifetime of high energy electrons caught by the magnetic trap during a previous microwave pulse and their role as seed in the RB phenomenon during followed pulse.

3. Investigation of an influence of combined effects of runaway breakdown and cosmic rays on lightning processes in thunderstorm atmosphere

3.1 Abstract

The intensive X-ray emission during thunderstorms was studied at the height 3340 m above sea level. For the first time the short-time (1—5 min) bursts of X-ray emission were observed. The bursts are highly correlated at the wide space region (about 0.5 km). The main component of X-ray emission in bursts has the energy 50—80 keV. The observed bursts could be attributed to the bremsstrahlung determinated by the runaway breakdown (RB) effect in the thundercloud electric field. Ground based observations of RB open a wide opportunities for the studies of fundamental processes in thunderstorms.

3.2 Introduction

The new mechanism of lightning initiation in thunderstorm clouds based on a combined action of runaway breakdown (RB) and extensive atmospheric showers (EAS) was proposed in [1]. According to this theory in shower core the ionization of the air due to RB effect is growing strong enough to produce a local highly conductive plasma. The thunderstorm electric field is amplified strongly inside such region. That can serve to the triggering of a lightning discharge.

The Lebedev Physics Institute (LPI) group proposed an experimental program to study this mechanism. The program includes simultaneous observations of cosmic ray showers, runaway breakdown emission and lightning discharges at the mountain cosmic ray station (MCRS). The LPI MCRS is situated on a pass in Tien-Shan mountains at the height 3340 m above sea level (effective atmosphere depth 690 g/cm^2). The thunderstorm clouds go through the pass at the height about 0.1—1 km during of three months yearly. The installation can detect extensive air showers measuring simultaneously EAS electrons with energies 0.1÷10 MeV, muons with energies above 5 GeV and neutrons with energies above 100 MeV. The RB effect lead to a strong amplification of the X-ray emission inside and below the thunderclouds [2]–[6]. To observe RB emission a system of Geiger counters was installed in a wide region (approximately 500 m around MCRS). To fix the position of lightning discharge by its strong electromagnetic and acoustic radiation a group of special antennas together with directed microphones was established.

In the present work we inform about the first results of X-ray emission measurements. The strong amplification of emission during the whole thunderstorm period is found. For the first time the bursts — short time strong peaks of X-ray radiation were observed. The typical time length of such a burst is 1÷5 min and radiation increases are highly correlated in different points at the scales minimum of the order of several hundred meters.

3.3 Experimental Installation

The schematic layout of MCRS's detectors disposition is shown at Fig.3.1. The installation used in this experiment consists of the following main parts:

- The *shower system* on the base of scintillation detectors located nearly concentric circumferences on the flat part of the pass (the "Hadron" experiment installation [7]). The scintillators can detect the high energy (above 10 MeV) electrons and gamma quanta travelling through the installation within an extensive air shower fronts.
- The *NM64 type neutron supermonitor* [8] consisting of three independant units. Each unit has 3 m^2 sensitive area and includes six registration channels on the base of neutron counters SNM15. The supermonitor was designed for the registration of one-minute

intensity variations of cosmic ray hadrons with energy above 50—100 MeV. The electronics of neutron monitor's registration channels is designed to provide methodic error at the level of 0.01% in intensity measurements. The input threshold value for neutron counter's pulses is set to be equal to 10 mV, corresponding background pulse intensity being 2700 pulses per min (p.p.m.) for each unit.

- The boxies of *high threshould gamma ray and electron detector* are placed above supermonitor units as shown at Fig.3.1b. This detector is made on the base of Geiger-Mueller counter tubes of SI5G type which are capable to register hard X- and soft γ-ray emissions with nearly 1% efficiensy. Four detector boxies each of wich contains 20 counters with parallel outputs and corresponds to the one registration channel were mounted above each of three supermonitir units, their total sensetive area being equal to 8 m^2. Because the counters of this detector are operating in proportional regime it is necessary to decrease their dead times up to 5-10 mcs (which is 20 times shorter as for usual Geiger counters). To achive the charged particles registration efficiency as high as for Geiger regime (above 95%) the registration channel's threshould is set to 20 mV. The roof of the building where neutron supermonitor and high threshould γ-ray detector is situated is made of 0.8 mm thick iron, the wood ceiling has thikness about 15 cm and the detector's boxes are made of 2 mm thick aluminium. It provides the upper threshold about 25—30 MeV for relativistic charged particles registration. The main absorber above the detector is carbon with the effective thikness 13.6 g/cm^2. Thus, the threshold value for the photons is about 30 keV. The general count intensity for all channels is determinated mainly by the electron background flux and is equal to $3.2 \cdot 10^5$ p.p.m. The corresponding statistical error in 1-minute data is less than 0.2%.
- The *muon detector* made of SI5G type counters with common sensitive area 2.7 m^2 is placed under one of the supermonitor units (see Fig.3.1b). Output pulses from each of four lower detector boxies are switched to a coincidence scheme with the pulses coming from corresponding boxies, located above supermonitor unit. The thickness of matter above lower boxies is 15 g/cm^2 of carbon and 150 g/cm^2 of lead absorber. The latter exeeds 35 electromagnetic cascade units, excluding completly the registration of atmospheric photons and electrons with energies below 10 GeV. The detector registrates mainly the muons with energies above 220 MeV travelling through the unit in nearly vertical direction.The general count intensity is about $7 \cdot 10^4$ p.p.s. Hence, the fluctuations in one-minute data are about 0.5%. The registration channel's characteristics of muon detector are just the same as those for the high threshould gamma detector.
- The newly build *low threshould wide spread X-ray detector (WS)* created in Summer 1999 is designed to investigate the thunderstorm clouds low energy electromagnetic emission. It consists of four registration points situated perpendicular to the preferential direction of thunderstorm clouds motion over the cosmic ray station's pass (see Fig.3.1a). The distance between the extreme right and extreme left points is about 500 m. Each of the points has two layers of sixty SI5G counters. The outputs of the counters in each layer are combined in one registration channel. Hence, there are two registration channels in each point with sensitive square 2 m^2 each. The SI5G counters are put in Geiger-Mueller regime, and the threshold of registration channels is equal to 2—3 V. Electronic circuits in each detector point are based on vacuum tubes in order to protect them from the nearby lightning discharges. The powerfull vacuum tubes ensure the output pulse front length not worse then 2—3 mcs at output resistance of 240 Ohm and capacity about 20 mcF. Due to this distortion of the pulse form during its passage through 300—400 m long cable is negligible. The detectors of each registration points are placed within a little light house. The counters are separated from the atmosphere by the 0.8 mm (or 0.74 g/cm^2) thick iron roof.

All the detectors described above have the bouth independed power supply and data recording systems. Distant detectors are connected to a central registration system (located in the building with neutron supermonitor) by screened underground cables. The data are transfered to computer by the means of a CAMAC system. To avoid the danger of semiconductor electronics damage in the moment of lightning discharge, the cables are conjugated with CAMAC scaler blocks throughout vacuum tube based circuits.

The pulses coming from all of eight channels of low threshould WS X-ray detector were counted by CAMAC scalers during of one second time intervals and accumulated numbers of them were recorded by registration computer. Amounts of pulses obtained from other detectors were counted during of one minute intervals and registrated together with the clock indication, temperature and barometric pressure. The registration was perfomed continuously during of 4 monthes in July—October 1999.

We have tested the electric noise in all channels by switching off the high voltage power supply in registration points. In such a case the pulses from the channels were not registrated even in thunderstom conditions.

3.4 Experimental results

Intensity variations. During of July and up to the last days of August, 1999 there were no thunderstorms in the vicinity of mountain station. The typical measurements of pulse intensity, obtained from various detectors at this quiet period are presented at the 3.2. The shown data correspond to the total intensity registrated by all channels of each detector (i.e. the amounts of pulses obtained from 8 channels of low threshould X-ray detector, 12 channels of high threshould γ-ray detector, 3 neutron monitor units, 4 muon coincidence channels show the intensity curves at this figure).

One can see that both low and high threshould γ-ray detectors exhibit no significant changes in count velocity through the whole period shown (6 houres). The signals from neutron monitor and muon detector demonstrate the same stability (their slow trend is caused by variation of atmospheric pressure).

In the end of August 1999 we have observed five cases when at low heights over the MCRS were passing the thunderstorm cloud fronts accompanied by the strong lightning discharges. The same data as given at Fig.3.2 for a quiet day are presented at Fig.3.3a-e for typical thunderstorms events. Time scale at the bottom of the figure is centered relatively to the moment when thunderstorm beginning was fixed. This moment is marked by a vertical dotted line. Below we shall discuss the typical thunderstorm event on August, 31. Corresponding data are presented at Fig. 3.3.e.

It can be seen from the typical curves shown at Fig.3.3e, that each time after the moment of thunderstorm beginning a dramatic growths of emission intensity measured both by low and high threshould γ-ray detectors occures. We emphasize the significant difference between these two types of detectors: low threshold detectors measured practically free flux of X-rays, and high threshold detector that was *under the roof* having additional absorption equivalent to 13.6 g/cm^2 of carbon. One can see from the Fig.3.3.e, that the signals of the free (low threshould) and under the roof (high threshould) detectors are well correlated in time. These correlations are quite regular having the same character for every thunderstorm. The characteristic scale of long time emission increses is 2—3 houres after the moment when thunderstorm clouds begin to pass the MCRS.

At the same time the neutron monitor and muon detector (which are sensitive to energetic particles of cosmic radiation only) do not demonstrate any thunderstorm caused effect.

The results obtained for the all of five observed thunderstorms are quite analogous.

Space correlations. The γ-ray intensity increases during thunderstroms discussed above have been studied in data streams obtained separately from each of low threshould detector points shown at Fig.3.1a. The correlation coefficients between all available pairs of detector points were determined. The results — time dependences of correlation coefficients C_{ij} calculated for 100 sec. Length time periods for three detector points pairs — are presented at Fig.3.4 for one of the observed thunderstorms (the corresponding data obtained for all other detector pairs and of other thunderstorms are quite analogous). One can see from the Fig.3.4 that under the fine weather conditions the data at different observational points are practically noncorrelated. During the thunderstorm period the picture is absolutely different: correlation coefficients for all low threshold detector points pairs becomes very high — about 0.8 and even higher. This high correlation demonstrate that the observed of X-ray intensity strong growth is deeply connected with thunderstorm processes developing simultaneously at the wide space region of the order of 0.5 km, maybe even larger.

Short time emission bursts. The accompanying thunderstorm emission intensity variations are well correlated in time also. It can be seen from Fig.3.3.e for X-ray signals of the free (curve 1) and under the roof (curve 2) detectors. Analogous time correlations exist for the emission at different low threshold detector points. These correlations are quite regular, they have the same character for every thunderstorm. The characteristic timescale of this longtime emission variation is 30÷60 min. One can mention the following peculiarity of emission intensity — it has often a double or triple pike structure (see Fig.3.3.e).

An interesting new feature is short time bursts of X-ray emission. Characteristic length of the bursts is 1÷5 min. The typical short time bursts occured during of thunderstorm event of 31 August 1999 can be seen at Fig.3.3.e in time moments 0.2 (peak 1), 0.4 (peak 2), 1.4 (peak 3) houres after the beginning of thunderstorm. It is obvious good correlation between the intensity bursts of low and high threshould emission detectors. Any increases at corresponding time moments in the intensity of energetic cosmic ray components (i.e. neutrons and muons) are absent.

The one of the bursts data for low threshould detector intensities (peak 3) are shown in large scale at Fig.3.5 both for the sum of all channels and for each detector point separately. One can conclude from this figure, that emission intensity bursts are correlated strongly between various detectors separated with space distancies of the order of some hundreds of meters. According to statistical errors marked at Fig.3.5, the value of intensity increase during of a typical emission burst exeeds the level of statistical flluctuations by 15—30 times.

Absorption of emission. The two types of measurements of emission intensity were performed simultaneously: low threshold and high threshold, which demonstrate quite a good time correlation (Fig.3.3.e). The following main difference between these measurements exists. The low threshold detectors were separated from the atmosphere by the thin (0.8 mm) iron protector only. The high threshold detectors had the same protector, but they were installed inside the neutron supermonitor building, which has a roof with effective thickness 13.6 g/cm^2 of carbon. The roof gave a significant additional absorption. By the comparison of the data from free (low threshold) and under the roof (high threshold) detectors the characteristic absorption of emission could be found.

To perform comparison we determined first five-minute averaged background of both sets of data. As fast electrons determine the major part of the counts we have to eliminate the background and compare the excess, which is due to X-ray effect. The excess relation r for both sets of data is presented at Fig.3.6. One can see, that the typical value of excess relation of the free (low threshold) to the under roof (high threshold) data is 2÷4.

Such an absorption in 13.6 g/cm^2 carbon is characteristic for energy of γ-quanta 200÷500 keV [18].

It is important, that during short time bursts the value of r is always significantly higher, growing up to 8÷12 (Fig.3.6). That shows that the energy spectrum of X-rays during short bursts is essentially different from the main part of thunderstorm: its major component has *low energy X-rays* (≤ 50÷80keV) which are effectively absorbed by the roof. Note that peaks are more pronounced in absorption curves (Fig.3.6), than in intensity (Fig.3.3.e). It opens a possibility to use absorption as an effective method of X-ray burst detection.

Flux of X-ray quanta. To determine the flux of X-ray quanta we have first to average the excess counts of low threshold data and then takes into account absorption by the iron protector and sensitivity of Geiger-Muller counters SI5G for X-ray quanta. That gave an approximate value of flux in bursts 10÷20 photons/(cm^2 sec sr).

3.5 Discussion

The aim of this work is to study the influence of thunderstorms on the X-ray emission from atmosphere. Effective growth of the emission in all observed thunderstorms is definitely established.

In fine weather conditions weak disturbances of the emission (~ 1%) determined partly by the changes in atmospheric pressure are regularly observed (Fig.3.1) That agrees well with the previous statements [9] - [11]. During thunderstorm the picture changes fundamentally. The X-ray emission is strongly amplified for hours. The emission amplification in the thunderstorm period was studied previously in a number of papers (see [10]-[12]).

The main peculiarities of our observations are:

1. X-ray emission was studied at the ground, but high in the mountains (height 3340m). Analogous investigations were done previously only by Shaw [10] and Suszcynsky et al. [11] (mainly at lower heights).
2. For the first time the emission was observed simultaneously in several points with the large distance between them (Fig.3.1).
3. For the first time the free and partly screened emission was studied simultaneously.

Below we'll compare our observations with the previous studies. The new results will be discussed.

The main mechanisms of strong amplification of X-ray emission intensity during thunderstorm are:

1. Gamma ray emission from the beta decay of radon daughter-ion products.
2. Bremsstrahlung of accelerated electrons due to the action of a strong thunderstorm electric field.

Radon effect is determined by the precipitation of radon and its products to the ground during rainfall. Gamma ray emission from radon daughter-ion β decay has energies of quanta 0.2÷2 MeV. The decay processes and rainfall determine its main time characteristics: 20 ÷ 30 min growing up and about 50 min after washout [11,13].

Electric field effect is determined by the acceleration of electrons. Wilson [14] was the first who suggested that the secondary electrons generated by cosmic rays could be accelerated by the thunderstorm electric field. A new fundamental step was done in the runaway breakdown (RB) theory developed by Gurevich et al. [2]. It was shown that accelerated electrons could organize an exponentially growing avalanche in thunderstorm electric field. RB effect is supposed to determine maximal electric field reached in thunderclouds [2,15,16]. Directly RB process we discussed in the Introduction in connection with the

lightning triggering theory [1]. RB effect lead to the strong amplification of X-ray emission due to the bremsstrahlung.

Amplification of X-ray emission attributed to RB effect was observed in [3,4,17] during the measurements inside thunderclouds at the balloons. The main features of these observations could be summarized as follows:

a) The intensity of X-ray emission at the height ~ 4 km is sharply (in seconds time scale) growing up to 10^3 in the comparison with the standard level determined by cosmic rays. The maximum of observed emission bursts lays in the diapason 60÷90 keV, the maximal count rate is 40÷50 photon/(cm^2 sec sr) [4,17].
b) The horizontal scale of the region of emission amplification is of the order 1-km or more in agreement with the layered structure of thunderstorm clouds.
c) The time scale of X-ray bursts is of the order 1 min.
d) The intensity of bursts diminishes sharply (in second time scale) with the lightning. But in a 10-sec time scale it can grow up again.
e) Lightning was seen during all bursts. So, it is natural to suppose, that a correlation of lightning events with X-ray intensity bursts do exist.

Let us discuss now results of our observations, taking into account the main features of both considered mechanisms of X-ray emission amplification.

1. The general structure of a long time emission (Fig.3.3.e) agrees well with the radon source. A peculiarity, which could be mentioned, is the usual double pike structure of our intensity curves (Fig.3.3.e). The energy of gamma quanta (0.2÷0.5 MeV), determined by the absorption in the 13.6 g/cm^2 carbon for the main part of observed thunderstorm emission (Fig.3.6), agrees with radon source also.
2. Short time bursts of X-ray emission (Fig.3.3.e-3.6) are the main new result obtained in our measurements. The bursts are well correlated at the scales 0.5-km or more. Such correlated short time bursts in the ground-based measurements are observed for the first time. There exists a quite good correlation between the observations of free and partially absorbed bursts. The analysis of absorption effect shows, that the energy spectrum of X-rays in the bursts is essentially different from the main part of thunderstorm: its major part consists of the low energy X-rays ($E \leq 50 \div 80$ keV). Such type of energy spectrum is characteristic for RB effect only.

In Table 1 the main features of our observations of bursts are compared with the X-ray emission measured at balloons. We see that the features of the balloon measurements attributed to RB effect are rather close to the short burst observed on the ground in our measurements (Table 1). One can conclude that in short bursts the runaway breakdown bremsstrahlung was observed.

We note that this statement does not contradict to the other ground based studies, including the mostly comprehensive and detailed one made by Suschinskhy et al. [11]. As in [11], the main part of emission in our study definitely belongs to the radon. In the possibility to observe RB emission effect in our case essential role could be played by higher sensitivity of our system and observations of X-ray absorption. One should mention also a significant difference in heights: the main part of measurements in [11] were done at the height 2000 m, and our — at 3340 m. We emphasize that the mostly probable region of the high values of electric field which can lead to RB effect in thunderstorm clouds $E \sim E_c(z)$ according to multiple balloon measurements [15,16] lays at the heights 4÷8 km. The characteristic length of energetic photon $E \sim 30 \div 100$ keV propagation in atmosphere is $l_f \leq 1$ km [6]. So, the probability to observe RB emission is strongly diminishing with height below 3.5 km.

We see that though the RB emission is effectively screened by radon it could be brought to light in the ground based measurements as well. Of course more detailed ground based studies including higher heights and better energy spectrum and time resolution are needed.

3.6 Conclusion

In conclusion we will formulate briefly the main results of our observations.

1. X-ray emission during thunderstorm in mountains at the height 3340 m is studied for the first time simultaneously in several different places.
2. It is found that the emission is well correlated at the scale of the order 0.5 km or more.
3. For the first time well defined short bursts of X-ray emission are determined. The bursts are highly correlated at the whole studied space region (~0.5km).
4. The noticeable diminishing of emission intensity penetreating through the 13.6 g/cm^2 carbon layer is established. It means that the main component of X-rays observed in bursts has low energy (50÷80 keV).
5. The X-ray flux observed in bursts could be estimated as 10÷20 photon/(cm^2 sec sr).

The preliminary analysis of our measurements allows to suppose that the observed bursts of X-ray emission is the result of bremsstrahlung amplification determined by the runaway breakdown effect in thundercloud electric field.

3.7 Bibliography

1. A.V. Gurevich, K.P. Zybin, R. Roussel-Dupré, Phys.Lett.A **254** (1999) 79.
2. A.V. Gurevich, G.M. Milikh, R.Roussel-Dupré, Phys. Let. A **165** (1992), 463.
3. M.P. MacCarthy, G.K. Parks, Geophys. Res. Lett. **12** (1985) 393.
4. E.K. Eack, W.H. Beasley et al., J. Geophys. Res., **101** (1996) 29637.
5. A.V. Gurevich, G.M. Milikh, J.A. Valdivia, Phys.Lett.A **231** (1997) 402.
6. A.V.Gurevich, G.M.Milikh, Phys.Lett.A **262** (1999) 457.
7. S.F. Abrashitov et al. Izvestia AS USSR, **50** (1986) 2203.
8. V.M. Aushev et al. Izvestia RAS, **60** (1997) 488.
9. A.E. Sandrstrom, Cosmic Ray Physycs, chapter 6, North-Holland, N.Y., (1965).
10. G.E. Shaw, J.Geophys.Res., **72** (1967) 4623.
11. D.M. Suszcynsky, R. Roussel-Dupré, G.E. Shaw, J. Geophys. Res., **101** (1996) 23505.
12. N. D`Angelo, Ann.Geophysique Ser.B, **5** (1987) 119.
13. P. Bhandari, Rama, J.Geophys. Res., 68 (1963) 3813.
14. C.T.R. Wilson, Proc. Phys. Soc. London, **37** (1925) 320.
15. T.C. Marshall, M.P. McCarthy, W.D. Rust, J. Geophys. Res., **100** (1995) 7097.
16. D.R. MacGorman, W.D. Rust, The electrical nature of storms, NY 1998.
17. E.K. Eack, Rev.Sci.Instr., **67** (1996) 2005.
18. Particle Physics Booklet, Springer, 1998, p. 193.

Table 1

	Ground	Balloon
Time duration	1 ÷ 5 min	≥ 1 min
Space correlation	≥ 0.5 km	≥ 1 km
Characteristic energy	50 ÷ 80 keV	60 ÷ 90 keV
Characteristic intensity	10 ÷ 20 photons/cm^2 sec sr	40 ÷ 50 photons/cm^2 sec sr
Heights	3340 m	3500 ÷ 4000 m

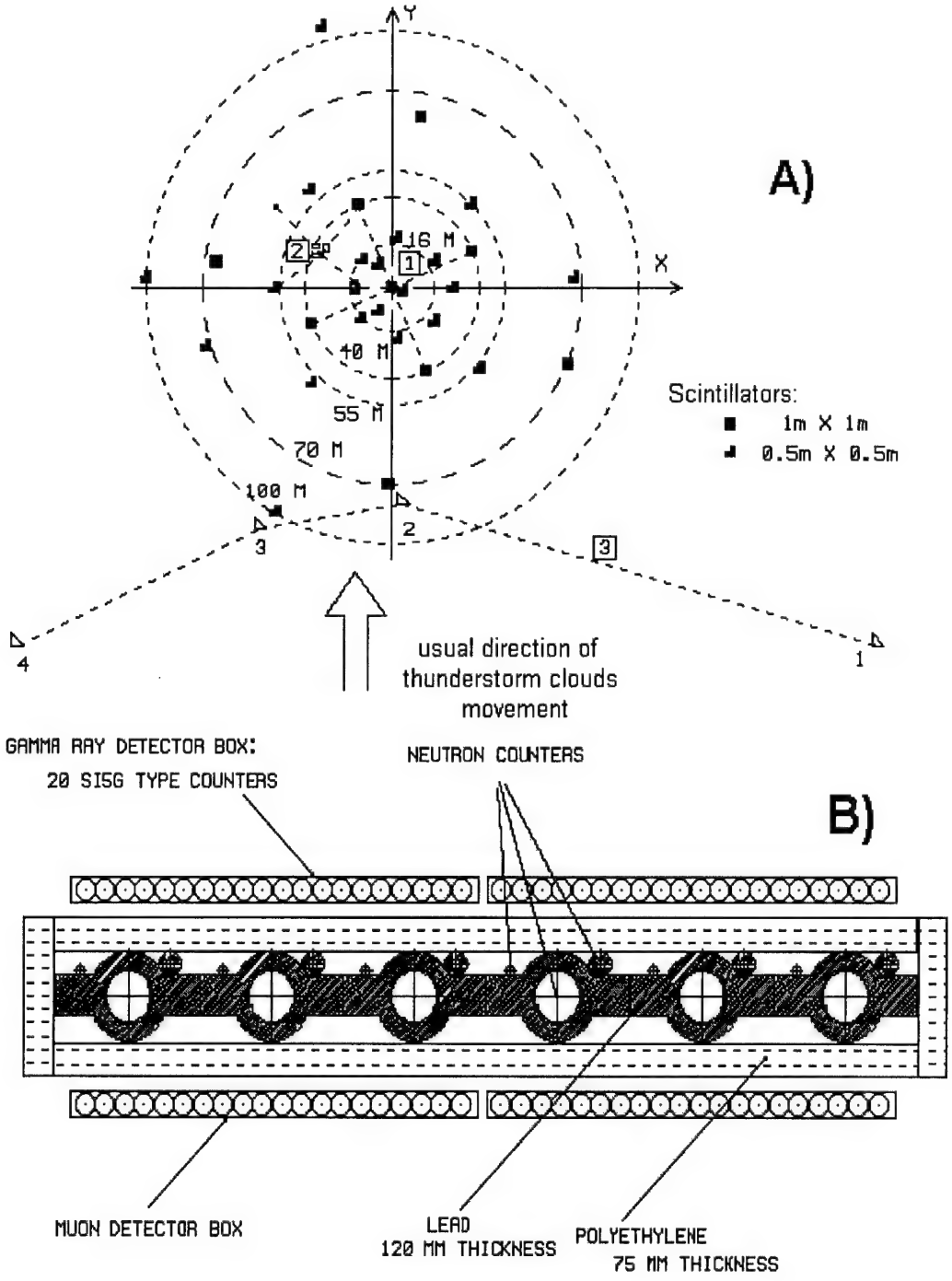

Figure 3.1. Disposition layout of mountain cosmic ray station's detectors (A): 1– the center of shower scincillation system, 2– neutron monitor and high-threshould gamma detectors, 3 – the system of four WS low-threshould gamma- and X-ray detector points, (B): the cross-section of a neutron monitor unit together with high-threshould and muon detectors.

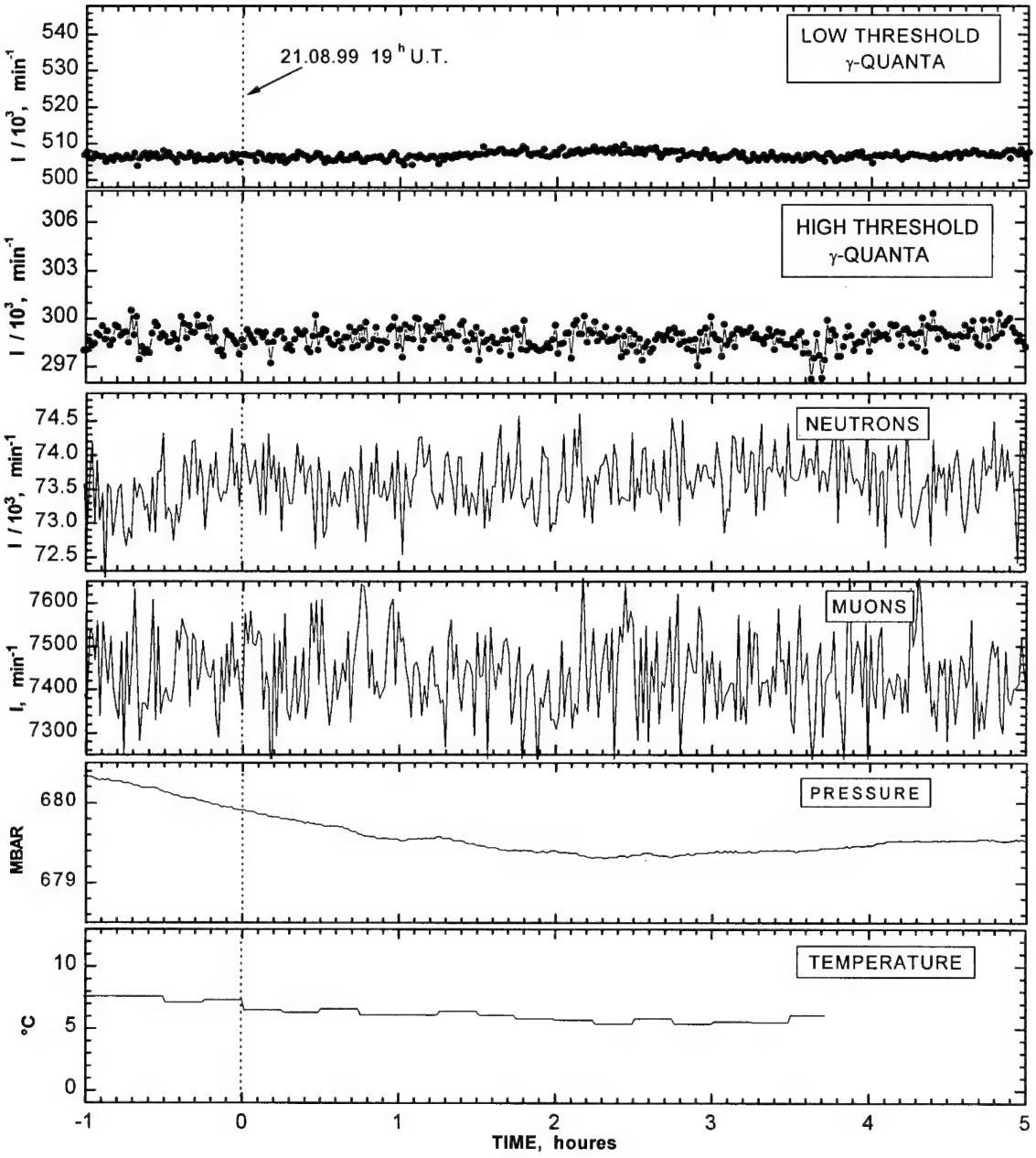

Figure 3.2. Typical behaviour of various cosmic ray components and atmospheric parameters in the absence of thunderstorm.

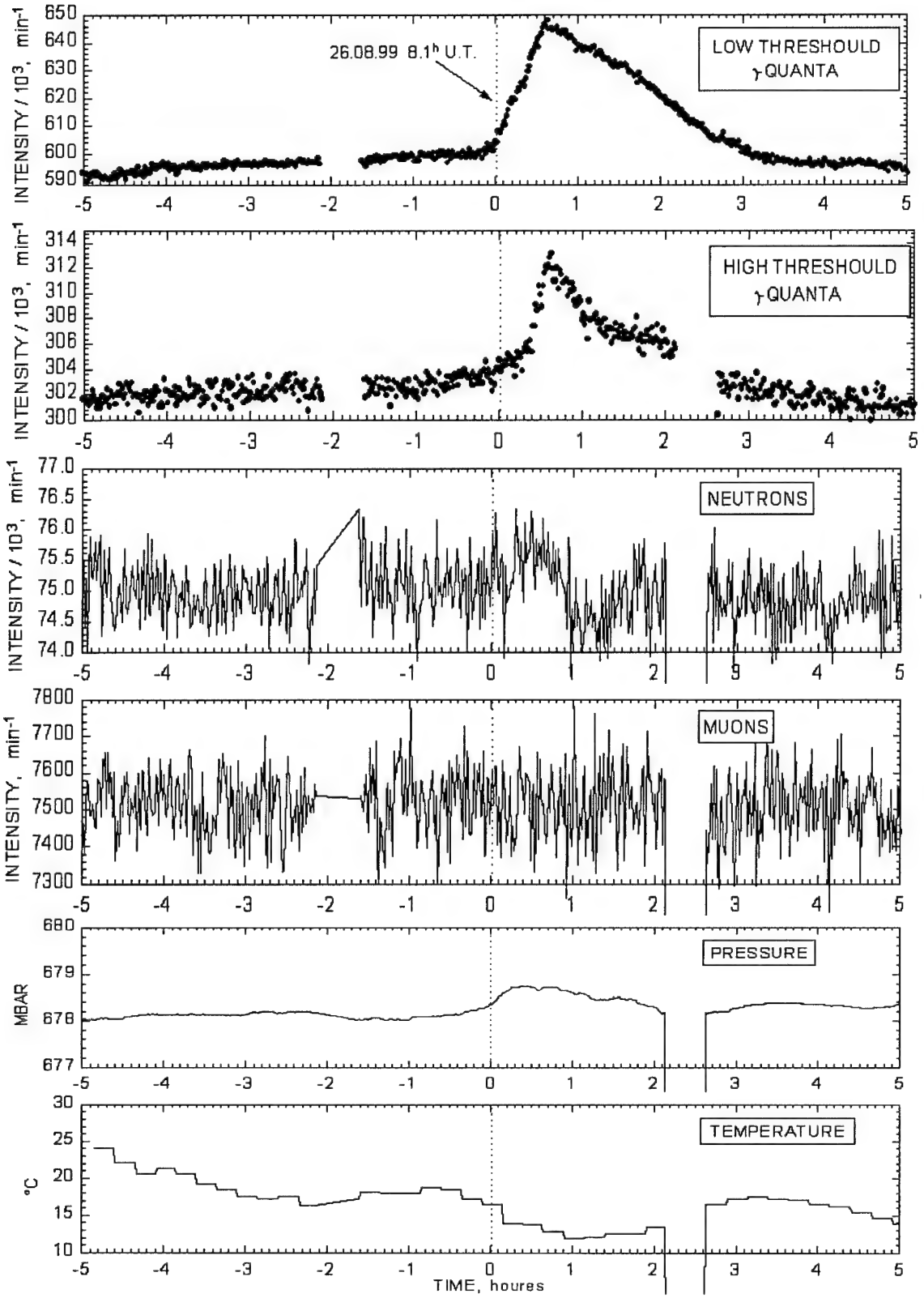

Figure 3.3a. The behaviour of various cosmic ray components and atmospheric parameters during of the thunderstorm at 26 August 1999.

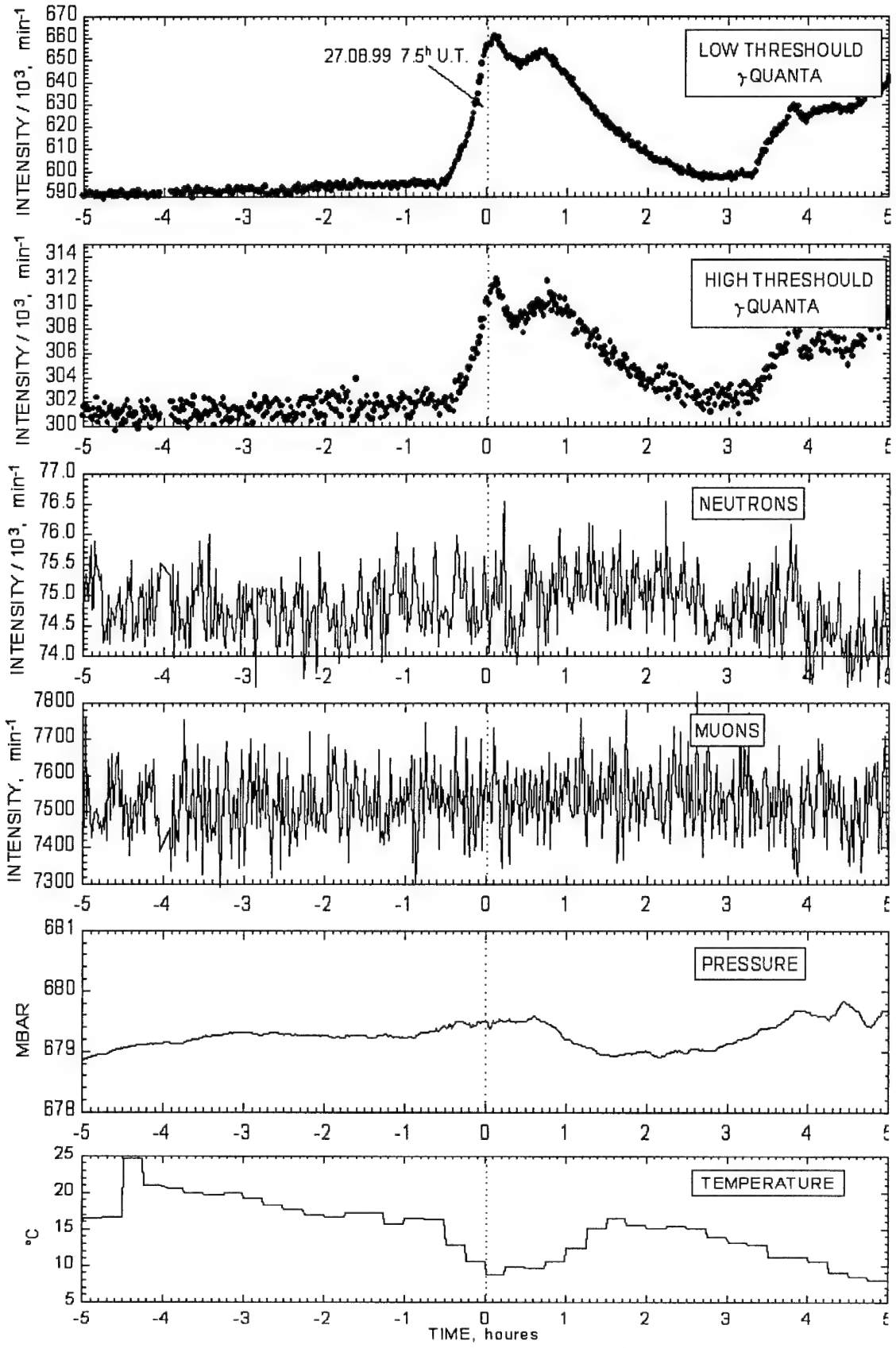

Figure 3.3b. The behaviour of various cosmic ray components and atmospheric parameters during of the thunderstorm at 27 August 1999.

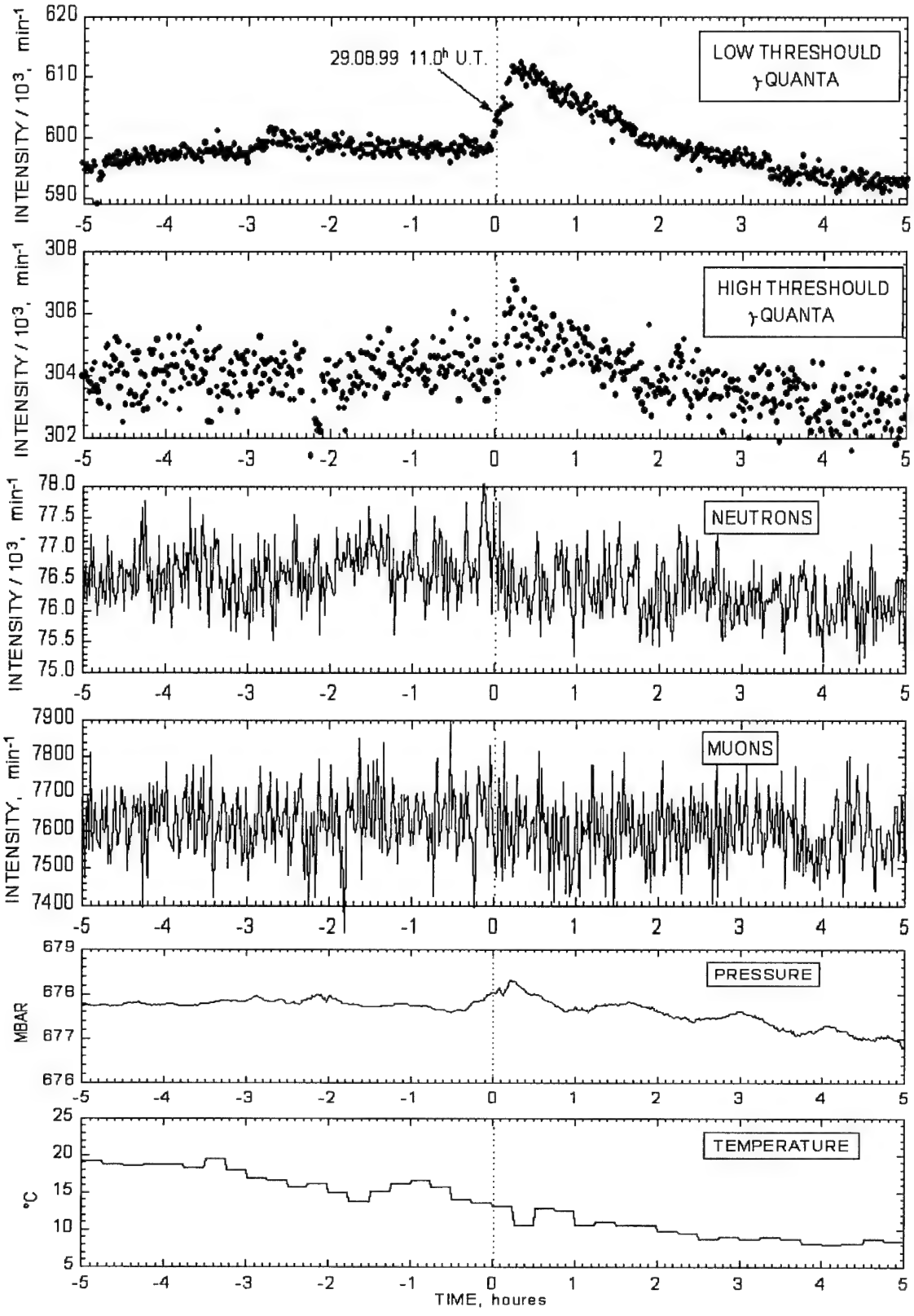

Figure 3.3c. The behaviour of various cosmic ray components and atmospheric parameters during of the thunderstorm at 29 August 1999.

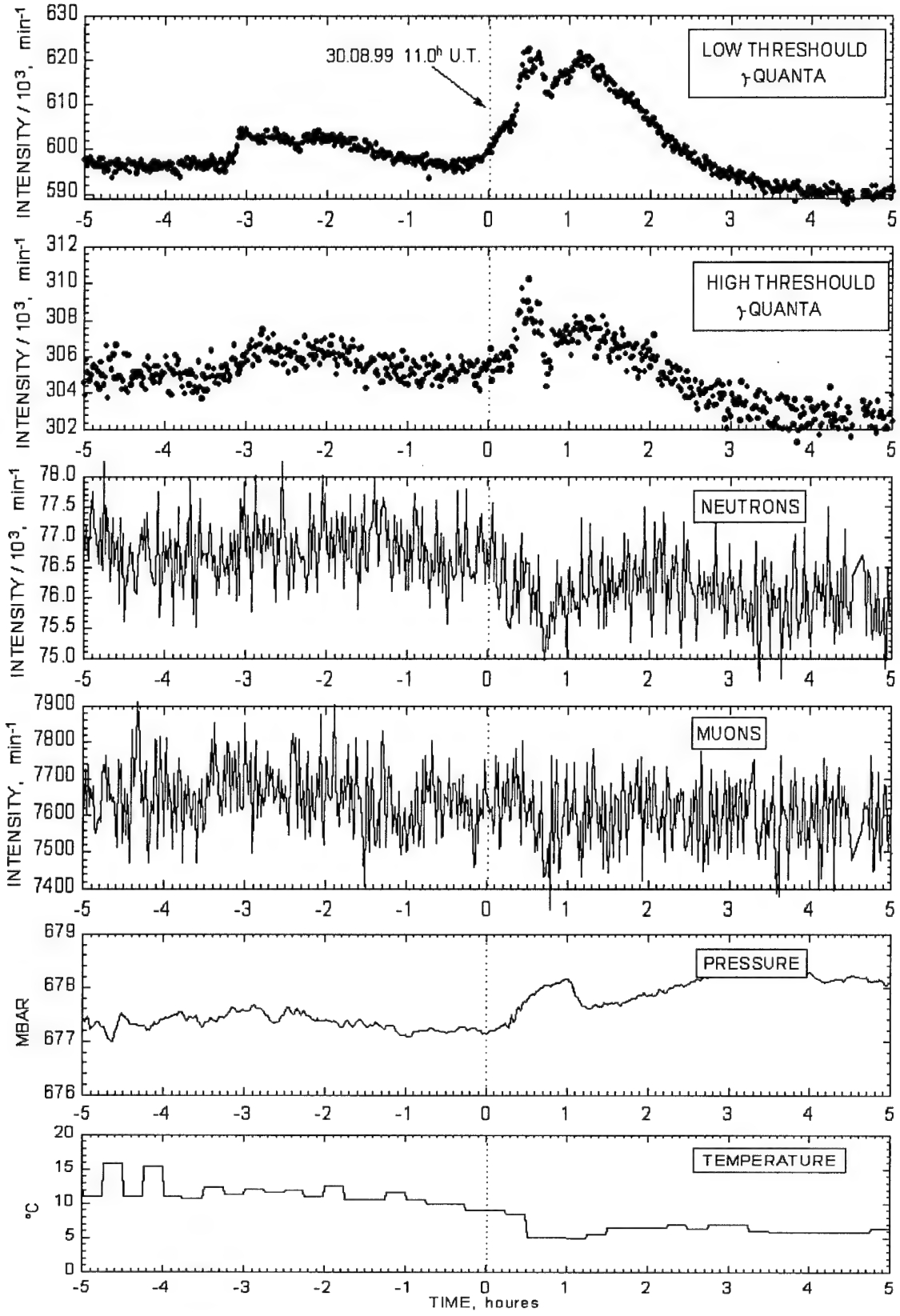

Figure 3.3d. The behaviour of various cosmic ray components and atmospheric parameters during of the thunderstorm at 29 August 1999.

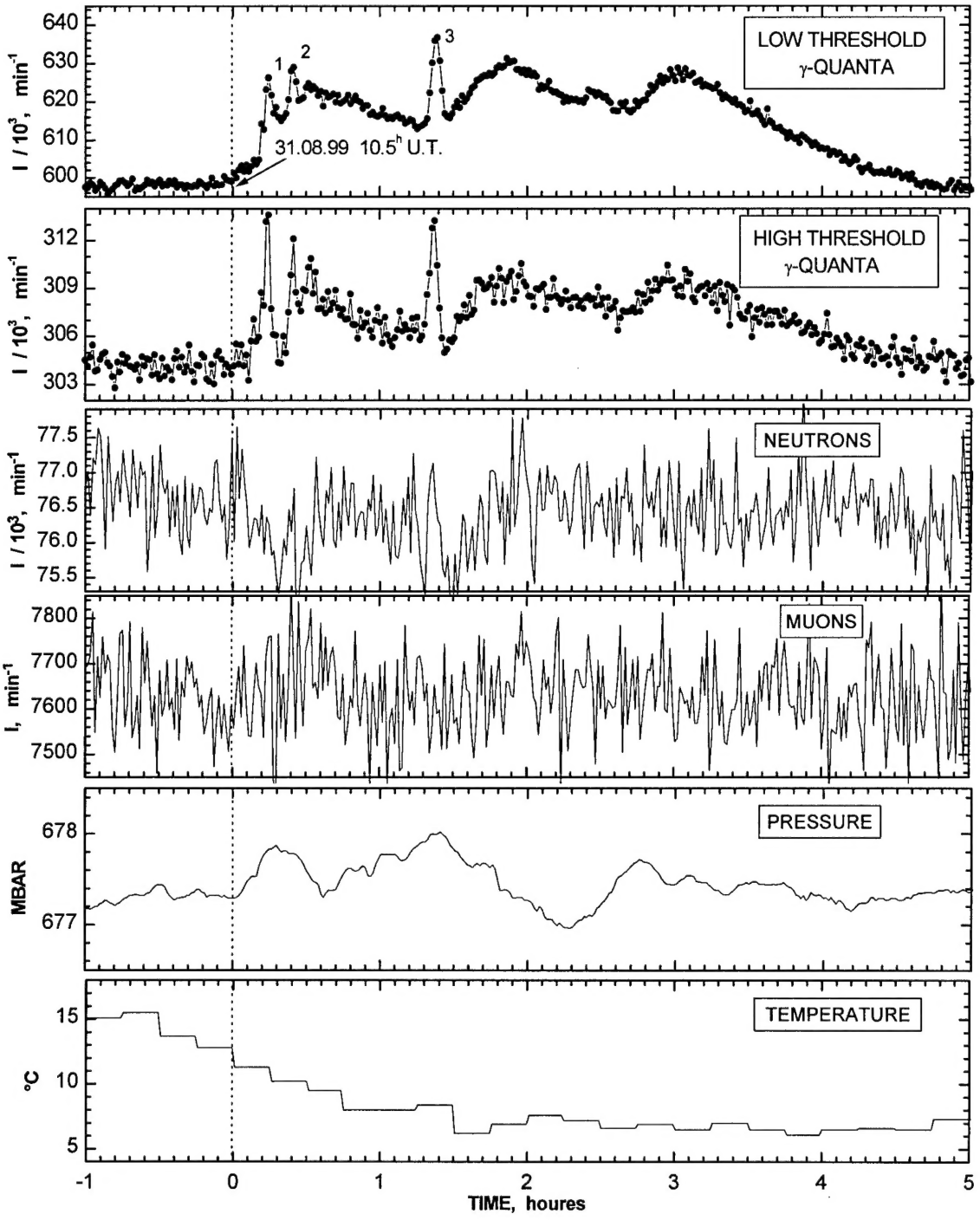

Figure 3.3.e. The behaviour of various cosmic ray components and atmospheric parameters during the thunderstorm on 31 August 1999.

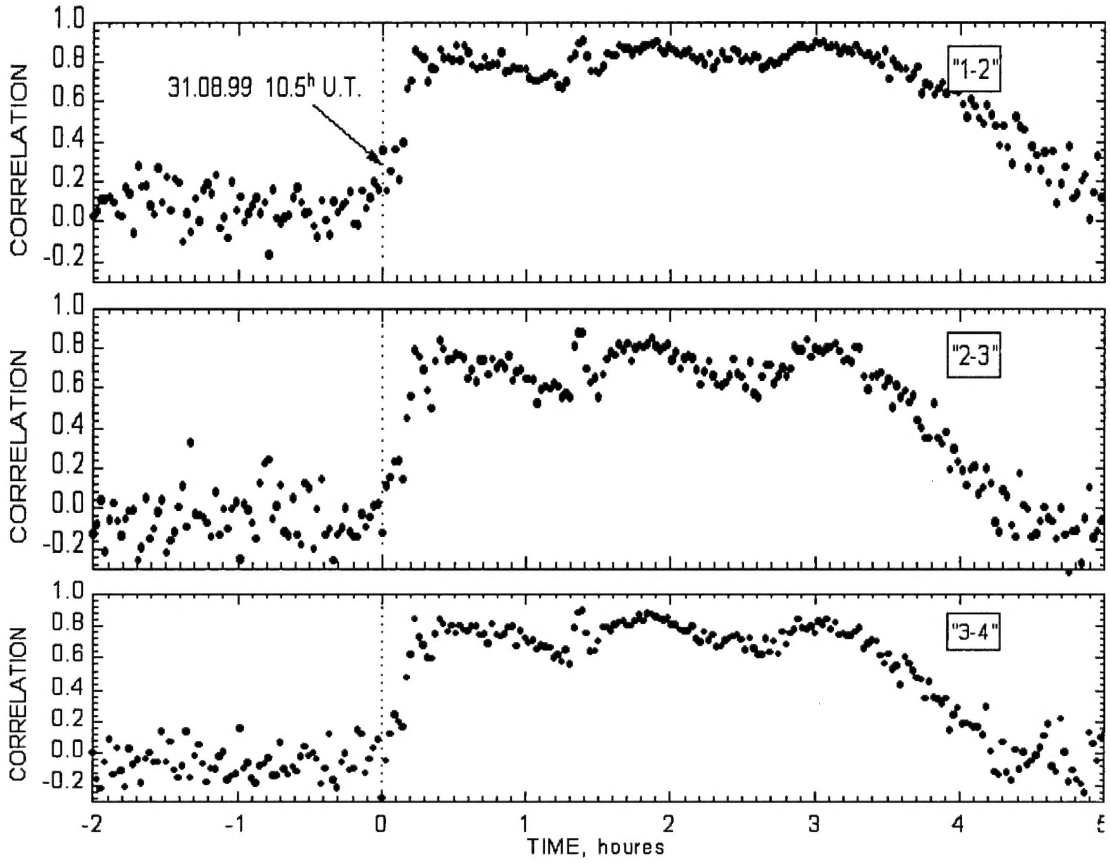

Figure 3.4. Time dependences of correlation coefficients C_{ij} for three detector pairs during the thunderstorm on 31 August 1999.

$$C_{ij} = \frac{\sum (n_i - < n_i >)(n_j - < n_j >)}{\sqrt{\sum (n_i - < n_i >)} \cdot \sqrt{\sum (n_j - < n_j >)}},$$

where each of i and j indices designates one of the low threshould detector points (i, j=1÷4, i≠j), n_i and n_j mean amounts of pulses obtained from bouth registration channels of i-th and j-th detector during of 1 sec intensity counting, $<n_i>$ and $<n_j>$ are the corresponding average values defined over the measurements immediately preceding thunderstorm moment. Summation in the above formulae was carried out during of 100 second length time periods.

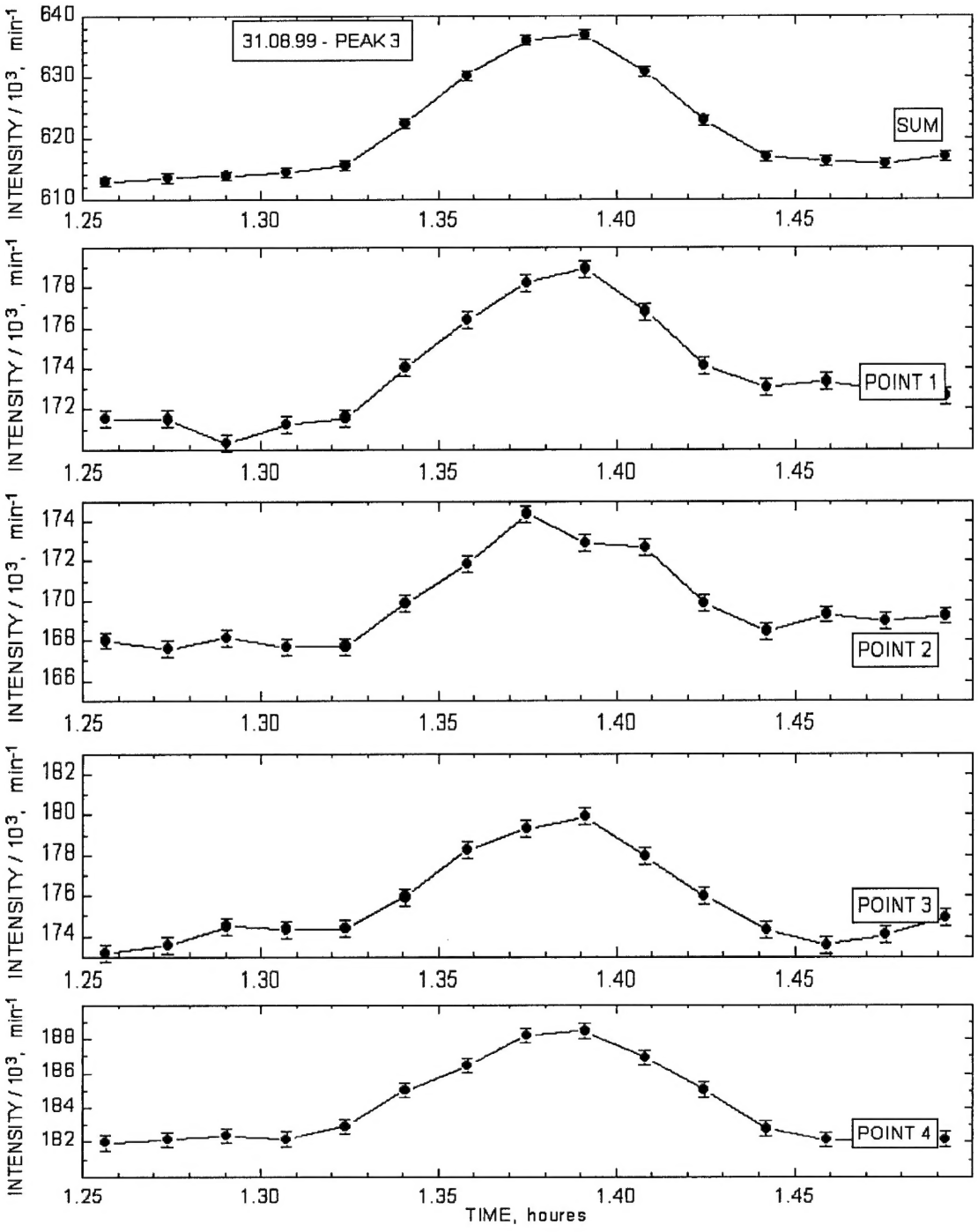

Figure 3.5. Short time low threshould emission intensity burst (peak 3) observed at different points during the thunderstorm on 31 August 1999.

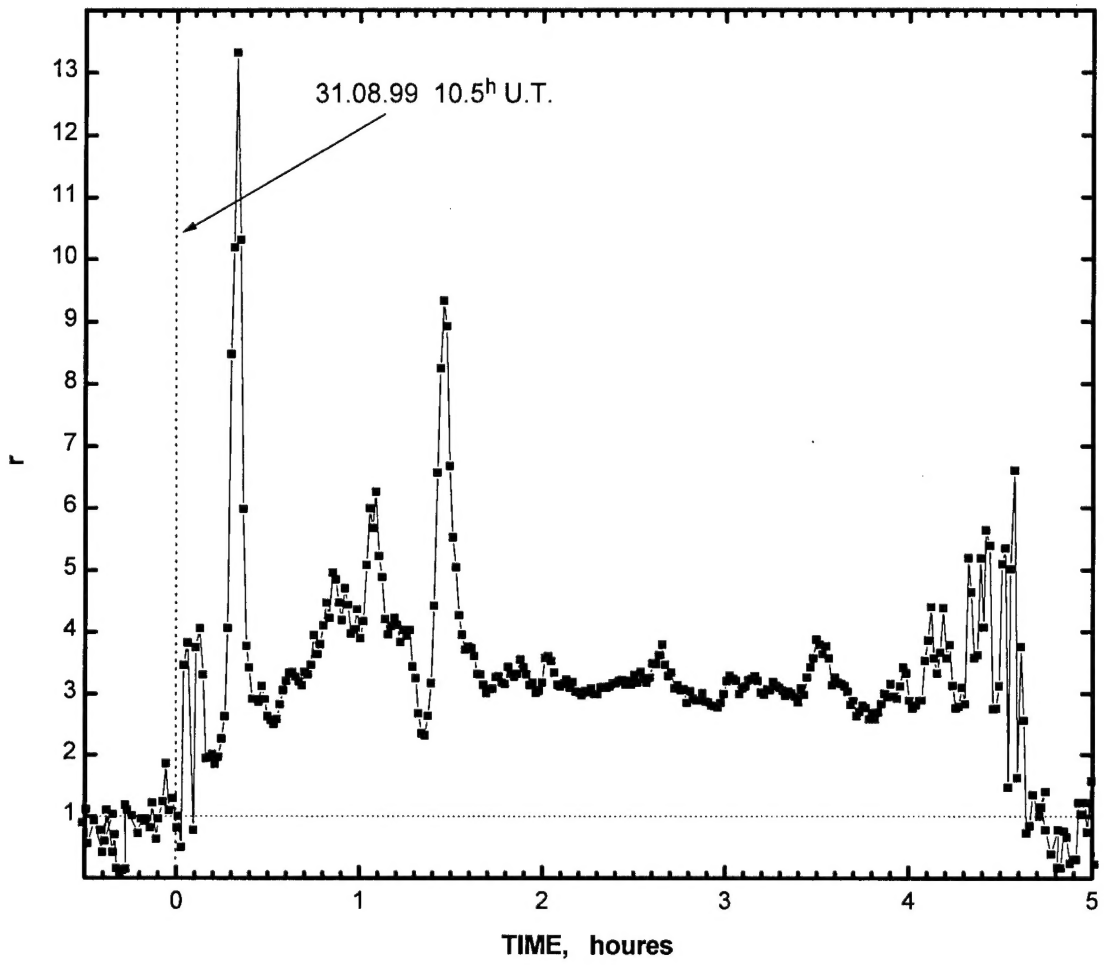

Figure 3.6. The excess relation of low threshold to high threshold data during the thunderstorm on 31 August 1999.

$$r = \left(\frac{I_{\text{low}}}{I_{\text{low}\_\text{backgr}}} - 1 \right) \Big/ \left(\frac{I_{\text{high}}}{I_{\text{high}\_\text{backgr}}} - 1 \right)$$